Photocatalytic activity of supported TiO_2 nanocrystals

Thandiwe Crystal Totito

B-Tech Chemistry (Cape Peninsula University of Technology)

A thesis submitted in fulfillment of the requirements for the degree of

Magister Scientiae in Chemistry.

Department of Chemistry

University of the Western Cape

November 2013

Supervisor: Prof. Leslie F. Petrik

Photocatalytic activity of supported TiO_2 nanocrystals

Thandiwe Crystal Totito

KEY WORDS

Photocatalysis

Sol gel

TiO_2

Nanofibres

Nanocrystals

Calcination

Decomposition

Electrospinning

Coating

Immobilised

Stainless steel mesh

In recent times, the occurrence and presence of complex recalcitrant toxic contaminants in water and wastewater is increasing and consequently contributes to the non-availability of clean and safe drinking water. Water treatment is complex, time demanding and energy intensive due to the physico-chemical structural complexity and diversity of the pollutants. Non-availability of good drinking water has negatively affected human health and the ecosystem. Over the years, numerous conventional treatment techniques were used to degrade and remove these pollutants, but investigations indicated that some of the pollutants are not susceptible to conventional treatment. Advanced oxidation technology, among which heterogeneous photocatalysis (involving the use of a semiconductor) has emerged as one of the more promising techniques to remediate contaminated water. Titanium dioxide (TiO_2) semiconductor photocatalysis is considered to be a good option due to its cost effectiveness, chemical and thermal stability, and inertness in the area of wastewater reclamation and re-use. However the post separation of the titania particles poses a threat to the wastewater remediation. Hence there is a need to develop a supported high surface area photocatalyst that will resolve the post separation challenge. This present study aimed to prepare high surface area TiO_2 anatase nanocrystals supported on a stainless steel mesh. These new composite materials were used to remove methylene blue (MB) from aqueous solutions. The supporting procedure involved the thermal decomposition of a sol gel solution coated upon stainless steel mesh. The nanocrystalline anatase phase was formed by thermal decomposition on a stainless steel mesh coated with 8 % PAN/DMF/TiO_2 sol gel formation calcined at varying temperatures of 300 °C, 400 °C, 500 °C and 600 °C. The heating rate of 50 °C/min and independent holding time of 1 h, 2 h, 3 h and 4 h were applied to find the optimum supporting conditions. The synthesised TiO_2 nanocomposites materials were characterised using the following analytical techniques: XRD, HRSEM, EDS, HRTEM, SAED, FTIR and UV-Vis absorption spectroscopy materials were characterised, and the results indicate that synthesised TiO_2 nanocrystals were in the anatase form, polycrystalline in nature, and contained additional carbon-carbon bonds from the polymer used during preparation with TiO_2 particle sizes range from 13.6 nm to 2285 nm. The

photocatalytic activity of the TiO_2 nanocrystals supported on a stainless steel mesh were tested using 50 ppm methylene blue solution under UV irradiation for 30 minutes, 60 minutes and 90 minutes. The percentage degradation of MB achieved was 96.02% after 30 min under UV radiation in the presence of 0.3 g stainless steel mesh supported TiO_2 nanocrystals prepared by decomposition at 400 °C for 2 h. This study clearly demonstrated that TiO_2 anatase nanocrystals supported on a stainless steel mesh effectively removed methylene blue from aqueous solutions, hence eliminated the post separation problem of powdered forms of TiO_2. This study has successfully produced stably adhered, supported TiO_2 anatase nanocrystals with the high surface area that are highly effective for the degradation of complex organics such as methylene blue.

DECLARATION

I declare that "**Photocatalytic activity of supported TiO_2 nanocrystals**" is my own work and it has not been submitted for any degree or examination in any university, and all the resources l have used or quoted have been indicated and acknowledged by complete references.

Thandiwe Crystal Totito November 2013

Signed……

DEDICATION

To Lindelekile William Totito my late father who left me with the legacy of knowledge, you always said “here is the education that is going to be your bread when I’m not around to give you bread”.

ACKNOWLEDGEMENTS

- My appreciation goes to my father God Almighty for his grace and seeing me through this journey.
- It is a pleasure to show gratitude to my supervisor Prof. L. F. Petrik for the support and guidance in this research.
- I would like to thank Dr O. Babajide, Dr O. Fatoba and Dr G. Madzivire for their suggestions and contributions to my research.
- Special thanks to A. Abbott, V. Kellerman, Ilse Wells and the members of the Environmental Nanoscience Group (ENS) and my friends for their advice, assistance, understanding and encouragement throughout my work.
- I would also like to thank Dr S Botha, Mr A Josephs in the Physics department of UWC and Dr R. Bucher at Ithemba labs for their assistance in HRSEM, EDS, HRTEM, SAED and XRD which was highly appreciated.
- My gratitude also goes to the National Research Fund (NRF) and Water Research Commission (WRC) for their financial assistance.
- Finally I wish to thank Mrs N. Totito my mother, sisters, nieces and nephews and other members of my family for encouragements, understanding, prayers and appreciating my effort.

LIST OF ABBREVIATION

Abs	Absorbance
EDS	Energy Dispersive Spectroscopy
FTIR	Fourier Transform Infrared
HRSEM	High Resolution Scanning Electron Microscopy
HRTEM	High Resolution Transmission Electron Microscopy
MB	Methylene Blue
SAED	Selected Area Electron Diffraction
SEM	Scanning Electron Microscopy
UV	Ultraviolet
UV-vis	Ultraviolet-visible Spectroscopy
VB	Valence band
XRD	X – Ray Diffraction
DQE	Detective Quantum Efficiency
CCD	Charge-Coupled Device
SADP	Selected Area Diffraction Pattern
NIR	Near-infrared
BET	Brunauer–Emmett–Teller
PAN	Polyacrylonitrile
THF	Tetrahydrofuran
ES	Electrospinning
DMF	*N*,*N*-Dimethyl formamide

LIST OF ABBREVIATION

TTiP	Titaniumtetraisopropoxide

TABLE OF CONTENTS

TABLE OF CONTENTS

TABLE OF CONTENTS

TABLE OF CONTENTS

TABLE OF CONTENTS

LIST OF FIGURES

LIST OF FIGURES

LIST OF FIGURES

LIST OF TABLES

CHAPTER ONE: INTRODUCTION

1 Introduction

This chapter introduces the thesis with a brief background relating to titanium dioxide which is mostly used as the semiconductor photocatalyst in photocatalytic processes. The rationale, problem statement, research questions, aim of the research, the research objectives, and research approach are given. Thereafter the scope of the project, and limitations of the thesis are presented, and the outline of the thesis structure is provided.

1.1 Photocatalysis

Titanium dioxide (TiO_2) is generally considered to be one of the best semiconductor photocatalysts available, due to its high photoactivity, photodurability, chemical and biological inertness, mechanical robustness and low cost. The photocatalytic reaction of a metal-oxide semiconductor produces photoexcited electrons (e^-) and positively charged holes (h^+) when interacting with ultraviolet (UV) light. The pairs of mobile charges produced by the semiconductor in UV light reach the surface of the semiconductor particle and initiate a reduction and oxidation process. This later produces the reactive species such as $OH^{\bullet}$ and $O_2^{\bullet}$ that may act as strong oxidants with a high potential to decompose and mineralize a wide range of organic compounds (Martinez et al, 2011). Since photocatalytic reactions mainly take place on the surface of the catalyst, a high surface-to-volume ratio is of significance for increasing the transformation rate. Although a lot of progress has been achieved in this area, the low contact areas for two dimensional films of nanoparticles are still challenges for their commercial applications. Two dimensional nanocrystalline TiO_2 films have already shown very high photocatalytic activity. However, most findings revealed that particulate titania semiconductor crystals offer the best results with

regard to degradation of organic contaminants (Blake et al, 1999) and these organic contaminants are totally completely mineralized and converted into CO_2, H_2O, N_2 and other harmless inorganic anions. Suffice to mention that chlorination, ozonation, and germicidal lamps such as low pressure mercury vapour lamps emitting UV at 254 nm are the most used earlier methods to purify water in developed countries (Blake et al, 1999). The other reported techniques such as disinfection rely on chemical or photochemical induced damage or physical removal by filtration (Blake et al, 1999), which is still being used today. But, available information from literature revealed that TiO_2 nanocrystals offer the best way of detoxifying wastewater contaminated by persistent, recalcitrant, toxic and non-biodegradable pollutants. Anatase titania nanocrystals were obtained from decomposed nanofibres through the interaction of nanopolymer and the titanium precursor in an electrospun process (Hu et al, 2006). The electrospun process was used to spin fibres with the aid of an electric field to sub-micron level diameters. Anatase titania nanocrystals with a high activity, was related to grain size, morphology, specific surface area, surface state, and porosity (Chuangchote et al, 2009).

1.2 Rationale and motivation

It has been reported that TiO_2 materials prepared by the sol gel process are more bioactive than materials of the same compositions prepared by other methods such as hydrothermal or solvothermal methods, or by chemical vapour deposition methods, etc (C˘erna et al, 2011). Wang et al, (2009) observed that enhancing the photocatalytic efficiency of TiO_2 to meet practical requirements is still a challenge because of the bottleneck of poor quantum yield caused by the rapid recombination of photogenerated electrons and holes. Much effort has been made to increase the electron hole pair separation efficiency.

There are various sources of light such as the sun, incandescent lamps, fluorescent lamps, light traps, UV, disinfectant light and so on. These sources emit light with different wavelengths necessary for their specific purposes. TiO_2 mainly absorbs

in the UV region, when the UV illumination is concentrated on the TiO_2 and electron hole pairs are thus produced in TiO_2. The photogenerated valence band hole converts surface hydroxyl groups and adsorbed water molecules to highly reactive OH radicals, which have strong oxidizing power to rapidly degrade a variety of organic contaminants in water (Choi & Hong, 2011). The surface bound OH radical can oxidizes organic compounds adsorbed on the TiO_2 surface. Moreover, OH radicals can diffuse in the reaction medium to cause photocatalytic oxidation away from the surface (Choi & Hong, 2011). Since UV light activated the process without additional chemicals, this route is attractive but suffers various drawbacks such as hole e^- recombination and particulates.

1.3 Problem statement

The earlier reported available methods used for wastewater treatment as contained in the literature are effective against some but not all organic pollutants. Many of these methods such as ozonation, flocculation and or coagulation and activated carbon adsorption are not effective enough to decompose all problem organic pollutions and can at times generate traces of toxic substances during treatment. Advanced oxidation processes are relatively new but expensive and therefore cannot be adopted for bulk water treatment in developing countries where the economic growth is below 2 % per annum. Also, the photocatalytic treatment of wastewater is a promising and sustainable means of detoxifying contaminated water, but it is often difficult to scale-up and the post separation of the particulate photocatalyst is another problematic issue. Therefore, the immobilization of TiO_2 nanocrystals with high surface areas on supporting material will help to overcome these limitations. Hence, it was considered very important to develop an immobilized TiO_2 composite material with a high active surface area.

1.4 Aim of the research

The aim of this research is to prepare a supported, high surface area TiO_2 nanocomposite with high activity for organics degradation. This research is thus designed to achieve the following objectives.

1.5 Research objectives

The objectives of this research are to develop:

- a protocol for the preparation of high surface area TiO_2 anatase in composite form
- to optimise the thermal conditions for three dimensional structure anatase formation on a support
- to test the catalytic activity of the composite under UV irradiation for methylene blue degradation, as model organic pollutant.

1.6 Research questions

- What formulation of sol gel will result in the anatase phase crystal formation on a support?
- Is the sol gel solution best suited for electrospinning the TiO_2 nanofibres on a metal mesh support or for coating the metal mesh directly?
- Which initial method (between electrospinning and coating) can produce supported TiO_2 nanocrystals using fewer processing steps, thus cheaper and produce crystalline supported anatase nanocrystals?

- At what temperature will the TiO_2 deposited in sol gel form upon a stainless steel mesh decompose to form TiO_2 nanocrystals?
- Can sufficient and uniform degree of anatase coating be obtained on the stainless steel mesh?
- Are the synthesised immobilized TiO_2 nanocrystals effective for photocatalysis?

1.7 Research approach

This study is based on studying the effectiveness of photocatalytically active supported TiO_2 nanocrystals prepared using the following approach:

- Preparing the optimum formulation of the Ti precursor containing sol gel solution using suitable chemicals and materials.
- Synthesising TiO_2 nanofibres by electrospinning nanofibres from the sol gel solution and depositing the nanofibres upon a stainless steel mesh.
- Using the sol gel solution directly to coat a stainless steel mesh support without electrospinning.
- Decomposing the sol gel coated stainless steel mesh using a furnace at different temperatures (300 °C, 400 °C, 500 °C and 600 °C) into supported TiO_2 nanocrystal composites by a calcination and carbonization method.
- Characterising the supported TiO_2 nanocrystal using the following analytical techniques: X-Ray Diffraction (XRD), High Resolution Scanning Electron Microscope (HRSEM), Energy-Dispersive Spectroscopy (EDS), Electron Microscopy (HRTEM), Selected Area Electron Diffraction (SAED), Fourier Transform Infrared Spectroscopy (FTIR) and Ultraviolet–visible spectroscopy (UV-vis).

- Studying/evaluating the catalytic activity by photocatalytic degradation of methylene blue.

1.8 Scope of the research

This study focuses mainly on the optimum sol gel formulation to be applied in electrospinning or sol gel coating as well as the best decomposition conditions to form the supported TiO_2 anatase nanocrystals.

1.9 Limitations

Due to the time limit of the research the following studies were not carried out:

- The methods such as hydrothermal method, solvothermal methods were not studied, because sol-gel method was found to be suitable for synthesising the TiO_2 nanofibres.
- Band gap tailoring of TiO_2 was not done.

1.10 Outline of the research

This thesis is divided into five chapters and brief overviews of the following chapters are presented below:

Chapter two: Literature review

Chapter two contains the literature review that covers the fabrication of TiO_2 nanofibres, the methods used to synthesise TiO_2 nanofibres, crystallinity of TiO_2, and the background of the characterisation techniques that were used for the study.

Chapter Three: Methodology, Instrumentation and Characterisation

Chapter three provides the experimental design and materials used as well as all of the methods used for synthesising the TiO_2 nanofibres, and decomposing the electrospun supported TiO_2 nanofibres into supported TiO_2 nanocrystals. The supported TiO_2 nanocrystals were also synthesised through the sol gel stainless steel mesh coating method. The methods applied to characterize the TiO_2 nanofibres and nanocrystals were XRD, HRSEM, EDS, HRTEM, SAED, FTIR, and UV-vis. The photocatalytic activity was tested by methylene blue degradation.

Chapter Four: Results and discussion

Chapter four covers the results and discussion of the preparation and characterisation of TiO_2 nanofibres and supported TiO_2 nanocrystals. This aspect also expands on the findings concerning the effectiveness and the stability of the supported TiO_2 nanocrystals. The results and discussion of the photocatalytic degradation of methylene blue using the supported anatase TiO_2 nanocrystals are also presented in this chapter.

Chapter Five: Conclusion and Recommendations

Chapter five presents the conclusion and the recommendations of the study carried out, summing up the study and answering the research questions. Recommendations for future work are presented.

References

References cover the list of all the journals, books and websites that were used to conduct the literature review.

CHAPTER TWO: LITERATURE REVIEW

2 Literature review

2.1 Introduction

The photocatalysis process is undertaken in the presence of a catalyst. In photogenerated catalysis, the photocatalytic activity depends on the ability of the catalyst to create electron hole pairs, which generate free radicals that can degrade organic materials in wastewater by oxidation through reactions with hydroxyl radicals ($^{\bullet}OH$) which are free radicals. Titanium dioxide has been reported to be the best photocatalyst to create electron hole pairs (Choi & Hong, 2011, Chen & Mao, 2007).

2.2 Photocatalysis

Photocatalysis is the process whereby the photoreaction increases in the presence of a catalyst. A catalyst does not change during the chemical reaction and neither is it consumed, but plays a role by making the chemical reaction happen faster. Photocatalysis, which may also be termed a photoinduced reaction, produces surface oxidation to eliminate harmful substances such as organic compounds when exposed to light such as the sun or a fluorescent lamp (Macwan et al, 2011). This light provides the different wavelengths necessary for the photocatalyst to activate. The photocatalytic process includes chemical steps that produce reactive species that in principal can decompose organic pollutants (Blake et al, 1999). The photodecomposition process involves formation of the reactive species such as the hydroxyl radical, hydrogen peroxide, superoxide, conduction band electron, and valence band hole. Photocatalysis can be used for various steps in purifying a contaminated environment, for example, purifying water, preventing contamination, anti-bacterial action, deodorizing and purifying air (Fujishima et

al, 2000). Riley et al, (2010) reviewed photocatalysts and showed that photocatalysis purifies air and water, and produce fuels such as H_2 and CH_3OH. It also catalyzes polymerization reactions, and enhanced the treatment of tumours. In order to develop efficient catalytic materials, it is necessary to bring the light where it is needed and bring the reactants into contact with the catalyst at the right time and provide sufficient surface area for efficient reaction rates. The most photocatalysts are formed as nanoparticles because it is easy to get the photo hole/electron are usually generated below the surface and then migrated to the surface, recombination depth (Riley et al, 2010).

Chen & Mao, (2007) reported that a large surface area catalyst with a constant surface density of adsorbents leads to faster surface photocatalytic reaction rates. In this sense, the larger the specific surface area, the higher the photocatalytic activity is. On the other hand, the surface is an imperfect site; therefore, the larger the surface area, the faster the recombination. This recombination applies to the TiO_2 nanocrystals as they have a large surface area. High temperature treatment usually improves the crystallinity of TiO_2 nanomaterials, which in turn can induce the aggregation of small nanoparticles and decrease the surface area. Optimal conditions are sought by taking these considerations into account and may vary from case to case. Photocatalytic activity of TiO_2 nanoparticles was determined by Chen & Mao, (2007) for hydrogenation reactions of propyne (CH_3CCH) with H_2O, and it was found that activity increased as the diameter of the TiO_2 particles decreased, especially below 10 nm. These authors suggested that the dependence of the yields on the particle size arose from the differences in the chemical reactivity and not from the nanoscience and properties are exactly physical size related, so the yields are directly related to the physical size. The fact that the chemical activity is also related to the physical size is a secondary property.

Advanced oxidation processes (photocatalysis processes) are seen as promising alternatives to traditional methods of decontamination. Several compounds have been investigated as potential photocatalytic materials for use in water purification, including TiO_2, SiO_2, ZnO, CdS, ZrO_2, V_2O_5, CuO, Fe_2O_3, Al_2O_3, etc. Amongst these photocatalytic materials, TiO_2 is the most suitable

semiconductor for photocatalytic decontamination of water. The deposition of metal elements into the TiO_2 matrix has been used to increase the efficiency of photocatalytic decontamination, resulting in an increase in the electron hole concentration and a decrease in band gap energy (Le et al, 2011). The relevant potential level of the acceptor species is thermodynamically required to be below the conduction band of the semiconductor. The potential level of the donor is required to be above the valence band position of the semiconductor in order to donate an electron to the empty electron hole (Stamate & Lazar, 2007).

2.3 Semiconductor TiO_2

Semiconductor materials are materials whose valence band and conduction band are separated by an energy gap or band gap. Semiconductors are selected as photocatalysts, because semiconductors have a narrow gap between the valence and conduction bands. Photocatalytic reactions are activated by absorption of a photon with sufficient energy from UV light that equals or is higher than the band gap energy of the catalyst. The absorption leads to a charge separation due to promotion of an electron (e^-) from the valence band of the semiconductor catalyst to the conduction band, thus generating a hole in the valence band (Macwan et al, 2011). This movement of electrons forms e^-/h^+ or negatively charged electron/positively charged electron hole pairs. The electron hole pair can oxidize donor molecules. If a photocatalysed reaction must be favoured then recombination of the electron and the hole must be prevented as much as possible.

Titanium dioxide is an attractive semiconductor photocatalyst for organics degradation, dye sensitized solar cells and antibacterial agents, due to its excellent photocatalytic activity, harmlessness and long-term stability (Choi & Hong 2011). TiO_2 photocatalytic treatment reduces toxic organic compounds to non-toxic inorganic compounds, such as carbon dioxide, water, ammonium or nitrates, and chloride ions (Bessergenev et al, 2005).

Among all the semiconductors mentioned in photocatalysis (Section 2.2), the most widely used semiconductor catalyst in photoinduced processes is titanium dioxide (TiO_2). Though TiO_2 has the disadvantage of not being activated by visible light, but by ultraviolet (UV) light, it is advantageous over other semiconductors in that it is chemically and biologically inert, photocatalytically stable, relatively easy to produce and to use, able to efficiently catalyze reactions, and cheap. The performance of TiO_2 for certain technical application is dominantly influenced by its crystallite size, surface area, phase structure, and impurity (dopant) type and concentration (Macwan et al, 2011).

2.4 Principle of Photocatalytic Oxidation

The principle of photocatalytic reaction is used to accelerate nature's cleaning and purifying process using light as energy. On absorption of photons with energy larger than the band gap of TiO_2, electrons are excited from the valence band to the conduction band, creating electron hole pairs. These charge carriers travel to the surface and react with the species adsorbed on the surface to decompose the species. The photodecomposition process involving intermediate species OH, O^{2-}, H_2O_2, or $O^{\bullet}$, plays an important roles in the photocatalytic reaction mechanisms (Chen & Mao 2007). The photogenerated valence band hole converts the surface hydroxyl group and adsorbed water molecules to highly reactive OH radicals, which have strong oxidizing power to rapidly degrade a variety of organic contaminants in water (Choi & Hong 2011). The surface bound OH radicals oxidize organic compounds adsorbed on the TiO_2 surface, and OH radicals can also diffuse into the reaction medium to cause photocatalytic oxidation away from the surface (Choi & Hong 2011).

The photocatalytic activity of a semiconductor is largely controlled by its light absorption properties such as the light absorption spectrum and coefficient, reduction and oxidation rates on the surface by the electron and hole, and the electron hole recombination rate (Chen & Mao 2007). TiO_2 nanoparticles absorb impinging photons with energies equal to or higher than its band gap (>3.0 eV).

Electrons are excited from the valence band into the unoccupied conduction band, leading to excited electrons in the conduction band and positive holes in the valence band see (Figure 2.1). These charge carriers can recombine either dissipating the input energy as heat, or get trapped and react with electron donors or acceptors adsorbed on the surface of the photocatalyst. The competition between these processes determines the overall efficiency for various applications of TiO_2 nanoparticles (Chen & Mao 2007).

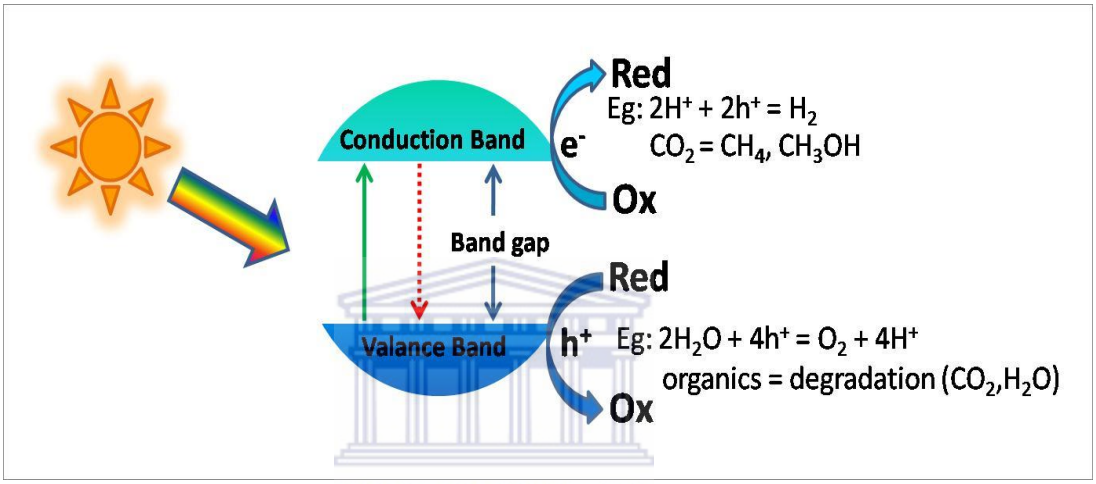

Figure 2.1: Energy band gap of the TiO_2 anatase

There are various sources of light such as the sun, incandescent lamps, fluorescent lamps, UV-visible, light traps, disinfectant light, and so on. Those sources emit light with different wavelengths necessary for their specific purposes, but the light used for the activation of TiO_2 is UV light at 253.7 nm (Radich & Kamat, 2013).

It has been previously stated that TiO_2 is a semiconductor and is active under UV light for photocatalytic activity. When titanium dioxide generates a pair of a conduction band electron and a valence band hole in the solid oxide lattice by absorbing a photon with energy greater than 3.2 eV or $\lambda<388$ nm, the subsequent charge transfers at the interface. This initiates various kinds of redox reactions under ambient condition (Choi, 2006). The energy that excites the electrons is provided by light. Calculating from the energy level where the electrons have to be excited, this light has the wavelength 253.7 nm where ultraviolet light has

enough energy to form free radicals. The resulting free-radicals are very efficient oxidizers of organic matter.

2.5 Properties of TiO_2

Titanium dioxide is a colourless solid at room temperature, melts at 1830 °C, and boils between 2500 °C and 3000 °C (Wang et al, 2011). TiO_2 is naturally obtained as a powder consisting of a mixture of crystalline and amorphous phases. TiO_2 is based upon three crystalline phases (anatase, rutile, and brookite), as well as in multiple forms such as bulk, nanoparticle, thin film, etc. Various methods have been employed to enhance the crystalline quality of TiO_2. However, researchers have focused on understanding the structural and electronic properties of amorphous TiO_2 with the hope that the desirable properties of TiO_2 can be found in this less processed, thus cheaper form of the material (Prasai et al, 2012).

TiO_2 can react under mild operating conditions, although currently ultraviolet light needs to be used for photocatalysis to occur. The excellent photocatalytic characteristics of TiO_2 finds application in various fields including water splitting, environmental purification, self-cleaning and superhydrophilic surfaces, sensors, disinfection, chemical structure, biocompatibility, physical, optical and electrical properties (Wang et al, 2009; Macwan et al, 2011).

TiO_2 has two crystalline forms that have photocatalytic activity; they are known as anatase and rutile. Anatase has been found to be the most active form for photocatalytic reactions. Among the photocatalysts, TiO_2 with anatase phase has been most widely investigated due to its acceptable photocatalytic activity and chemical stability (Doh et al, 2007). The main focus of this study is the homostructure of supported anatase TiO_2 nanocrystals.

2.6 Titanium dioxide and crystalline phases

Titanium dioxide is a naturally occurring oxide of the element titanium with a molecular formula TiO_2 and molecular mass 79.90 g/mol. Titanium dioxide has a monoclinic crystal structure also referred to as titanium (IV) oxide or titania.

Figure 2.2: Titanium dioxide fine white powder

Titanium dioxide is most commonly extracted from titanium tetrachloride by carbon reduction and deoxidation. Alternatively, it may be processed from another oxide called ilmenite, which is subjected to reduction with sulfuric acid to achieve pure titanium dioxide.

Titanium dioxide particles are referred to as primary, aggregates or agglomerates. Primary particles are single crystals that are bound by crystal planes. Aggregates are sintered primary particles that are connected by crystal faces. Agglomerates are multiple primary particles and aggregates that are held together by van der Waal's forces. Scattering of light by titanium dioxide is maximized in particles that are 0.2–0.3 μm in diameter (Lezere 2011).

TiO_2 exists in three polymorphic phases briefly mentioned in the properties of TiO_2 (Section 2.5) and here the geometry and the density of the crystalline phases are given: rutile is a tetragonal crystal structure with a density of 4.25 g/cm^3, anatase is a tetragonal crystal structure with a density of 3.894 g/cm^3 and brookite is a orthorhombic crystal structure with a density of 4.12 g/cm^3 (Ahmad et al,

2008). In these phases, anatase and rutile are the most commonly encountered. Rutile is the thermodynamically stable form of TiO_2 at all temperatures and at normal pressures while anatase is highly photocatalytically active.

In all three polymorphs, titanium is coordinated octahedrally by oxygen, but the position of the octahedra differs between polymorphs. The structure of rutile is the densest and its unit cell is the smallest. Anatase has four formula units which is the empirical formula of any ionic used as an independent entity for stoichiometric calculations per unit cell with a = 0.379 nm and c = 0.951 nm, rutile has two with a = 0.459 nm and c = 0.296 nm and brookite has eight with a = 0.917 nm, b = 0.546 nm and c = 0.514 nm. Rutile TiO_2 has 32 atoms and anatase TiO_2 has 96 atoms in the lattice structure of the unit cell (Prasai et al, 2012).

TiO_2 is stable in aqueous media and is tolerant of both acidic and alkaline solutions. It is recyclable, reusable and relatively simple to produce. It can also be synthesized in nanostructure forms more readily than many other catalysts. Furthermore, its band gap is appropriate to initiate a variety of organic reactions (Ahmad et al, 2008). It is inert and resistant to corrosion, and it requires little post-processing, making it inexpensive as mentioned above.

The semiconductor TiO_2 is most extensively used because it has many advantages. The chemical composition of polymorphic phases of the natural rutile, anatase and brookite contain impurities of up to ≈2% that include iron, chromium, vanadium, aluminium, niobium, tantal, hafnium and zirconium and account for slight variations in density, colour and indices of refraction (Lezere, 2011). Figure 2.3 A, B and C images and structures were all cited from (www.pavemaintenance.wikispaces.com).

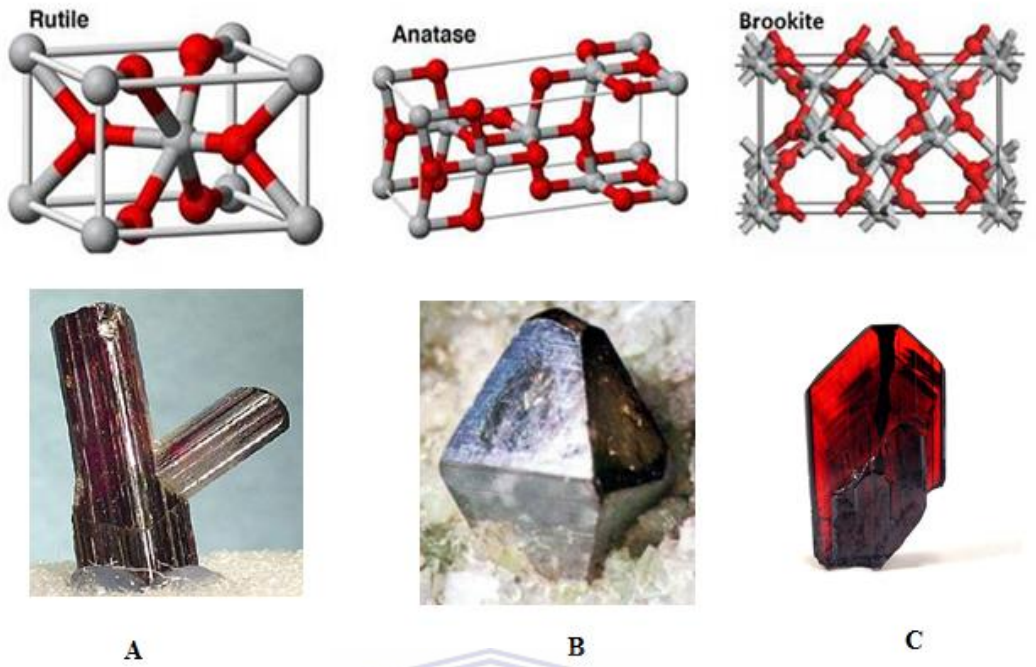

Figure 2.3: A = the crystal form of Rutile, B = the crystal form of Anatase and C = Brookite in crystal form

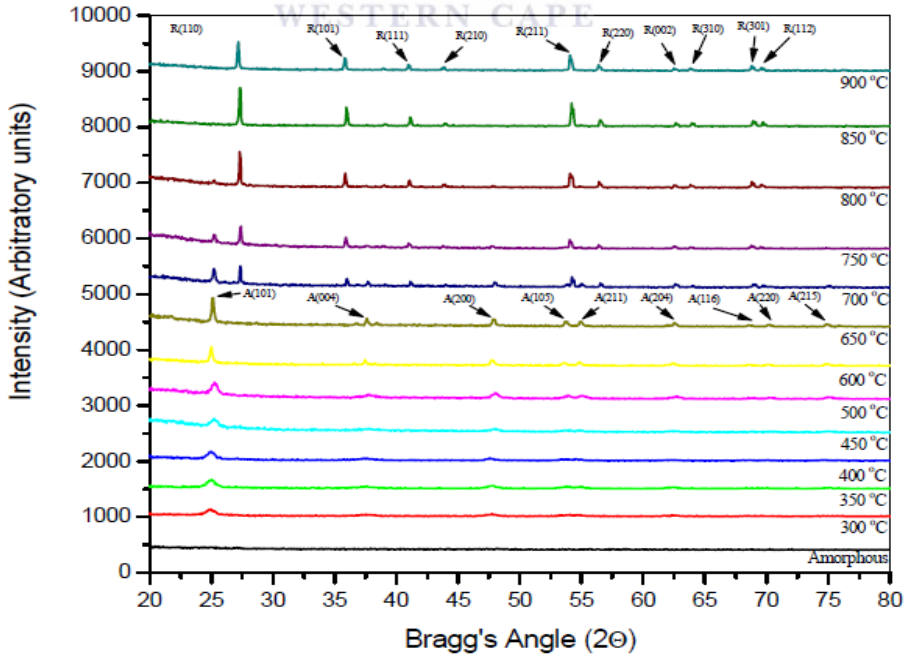

Figure 2.4: X-ray diffraction patterns of TiO_2 annealed at various temperatures (Ahmad et al, 2008)

Among the three above mentioned structures presented in Figure 2.3 A, B and C which show the crystal forms of TiO_2, anatase has the higher photocatalytic activity which is related to its lattice structure. A significant degree of buckling is associated with O-Ti-O bonds in anatase compared to rutile TiO_2 (Ahmad et al, 2008). Crystal symmetry is reduced due to this buckling and in turn it results in a larger unit cell dimension (Ahmad et al, 2008). According to Blake et al, (1999) the most active photocatalysts are formulations based on the anatase crystal phase, and most work has been done using the P25 Degussa form of TiO_2 that is powder material (Figure 2.2). This material is a mixture of phases with an approximate composition of 75% anatase and 25% rutile and has a BET surface area of about 50 m^2/g (Blake et al, 1999). Figure 2.4 shows the x-ray diffraction patterns of TiO_2 annealed at various temperatures (Ahmad et al, 2008) from 300 °C to 650 °C only peaks related to anatase structure are evident. Above 650 °C rutile peaks starts to appear and a mixture of both the anatase and rutile phases of TiO_2 existed up to 800 °C. At 850 °C, peaks show a complete transformation from anatase to rutile.

Rutile and anatase can be described in terms of chains of TiO_6 octahedra, where each Ti^{4+} ion is surrounded by an octahedron of six O^{2-} ions. The two crystal structures differ in the distortion of each octahedron and by the assembly pattern of the octahedral chains. In rutile, the octahedron shows a slight orthorhombic distortion; in anatase, the octahedron is significantly distorted so that its symmetry is lower than the orthorhombic phase. The Ti-Ti distances in anatase are larger, whereas the Ti-O distances are shorter than those in rutile. In the rutile structure, each octahedron is in contact with 10 neighbouring octahedrons (two sharing edge oxygen pairs and eight sharing corner oxygen atoms), while, in the anatase structure, each octahedron is in contact with eight neighbours (four sharing an edge and four sharing a corner). These differences in lattice structures cause different mass densities and electronic band structures between the two forms of TiO_2 (Chen & Mao, 2007).

2.7 Structural properties of TiO_2 nanomaterials

Large crystals of anatase are very characteristic and are not easily confused with any other mineral. They form the eight faced tetragonal dipyramids that come to sharp elongated points. The elongation is pronounced enough to distinguish this crystal form from octahedral crystals, although there are some similarities (Blake et al, 1999).

As the size of the TiO_2 particles decreases, the fraction of atoms located at the surface increases with higher surface area to volume ratios, which can further enhance the catalytic activity. The increase in the band gap energy with decreasing nanoparticle size can potentially enhance the redox potential of the valence band holes and the conduction band electrons, allowing photoredox reactions, which might not otherwise proceed in bulk materials, to occur readily. Practically, there exists an optimal size for a specific photocatalytic reaction (Chen & Mao, 2007). Yu et al, (2010) revealed that the modification of TiO_2 to make it sensitive to visible light is one of the most important objectives in photocatalyst studies. This may be done by increasing the surface area of the TiO_2.

Rutile is the most stable phase at high temperatures, but anatase and brookite are common in fine grained (nanoscale) natural and synthetic samples. On heating concomitant with coarsening, the following transformations were all seen by (Ahmad et al, 2008), (Blake et al, 1999) and (Chen & Mao, 2007): anatase to brookite to rutile, brookite to anatase to rutile, anatase to rutile, and brookite to rutile. These transformation sequences imply very closely balanced energetics as a function of particle size. The surface enthalpies of the polymorphs are sufficiently different that crossover in thermodynamic stability can occur under conditions that preclude coarsening, with anatase and/or brookite stable at small particle size (Chen & Mao, 2007). The crystal structure of TiO_2 nanoparticles depended largely on the preparation method. For small TiO_2 nanoparticles (<50 nm), anatase seemed more stable and transformed to rutile at >700 °C. Chen & Mao

(2007) found that the prepared TiO_2 nanoparticles had anatase and/or brookite structures, which transformed to rutile after reaching a certain particle size. Once rutile was formed, it grew much faster than anatase, then rutile became more stable than anatase for particle size > 14 nm.

Titanium dioxide has also been produced as engineered nanomaterials, which may be equidimensional crystals or sheets and are composed of either titanium dioxide-rutile or titanium dioxide-anatase. A tubular structure has been produced from different layers of titanium dioxide-anatase, which results in tubes with an outer diameter of about 6 nm and an inner tube diameter of about 3 nm (Lezere, 2011). Anatase is 10 times more active than rutile and responds to slightly different wavelengths 253.7 nm and 388 nm (Lezere, 2011).

2.8 Applications of TiO_2

The existing applications of TiO_2 nanomaterials include its use as filler in paint, toothpaste, or for UV protection, photocatalysis, photovoltaics, sensing, and electrochromics as well as photochromics. The optical and biological properties of TiO_2 allows it to be suitable for UV protection applications. TiO_2 nanomaterials can be imparted with clear functions on various glass products, which are mirrors and eyeglasses, having superhydrophilic or superhydrophobic surfaces (Stamate & Lazar, 2007). A surface is superhydrophilic or superhydrophobic when the water-surface contact angle is larger than 130 ° or less than 5 °respectively.

Another application of TiO_2 nanomaterials, when sensitized with dyes or metal nanoparticles, is to build photochromic devices. One of the many applications of TiO_2 nanomaterials is the photocatalytic decomposition of various pollutants (Chen & Mao, 2007). The photocatalytic activity of titania is used in thin coatings of the material exhibiting self-cleaning and disinfecting properties under exposure to UV radiation. These properties make the material a candidate for applications such as medical devices, food preparation surfaces, air conditioning filters, and sanitary ware surfaces (Fujishima et al, 1999).

TiO_2 nanomaterials are being applied for water splitting and hydrogen production due to their suitable electronic band structure, given the redox potential of water. Hoefelmeyer et al, (2011) said that the photocatalyst must be able to use the excited electron to synthesize hydrogen and to use the electron hole to synthesize oxygen. This is somewhere similar to photosynthesis, wherein plants convert sunlight to fuel such as sugars and an oxidizer that is oxygen, but in photosynthesis process several molecular pieces work together. For this reason, photocatalysis within a photoelectrochemical cell is sometimes referred to as artificial photosynthesis. The materials that were investigated by Hoefelmeyer et al, (2011) included nanocrystals of TiO_2, Pt, and RuO_2, dye molecules, and lipids. The materials were organized in chemical reactions and self-assembly steps to produce a reactive free-standing membrane capable of solar photocatalysis in which water was converted to hydrogen and oxygen (Hoefelmeyer et al, 2011). Nanocrystals of TiO_2 were found in their research to be the best free-standing membrane capable of solar photocatalysis. Electrospun PAN was graphitized thermally to yield carbon nanofibers. The electrospun carbon nanofelt out-performed the carbon black as the catalyst support.

An enormous research effort has been dedicated to the study of the properties and applications of TiO_2 under light illumination since the discovery of photocatalytic splitting of water on a TiO_2 electrode (Fujishima et al, 1999). Photocatalytic splitting of water into H_2 and O_2 using TiO_2 nanomaterials continues to be of interest for clean and sustainable energy sources. Water molecules are reduced by the electrons to form H_2 and oxidized by the holes to form O_2, leading to overall water splitting (Chen & Mao, 2007).

2.9 Synthesis of TiO_2

Tang et al, (2005) has reported the synthesis of TiO_2 nanoparticles that uses the low temperature reaction of low valent organometallic precursors. It is said that bis(cyclooctatetraene) titanium reacts with dimethyl sulfoxide in organic solution at temperatures as low as room temperature to produce TiO_2. In the absence of

any supporting ligand, the reaction results in the precipitation of amorphous TiO_2 powder; however, in the presence of basic ligands such as tributylphosphine, tributylphosphine oxide and trioctylphosphine oxide, the precipitation is arrested, and chemically distinct, isolated, internally crystalline TiO_2 nanoparticles are formed.

Nanocrystalline TiO_2 was synthesized by the solution combustion method using titanyl nitrate and various fuels such as glycine, hexamethylenetetramine, and oxalyldihydrazide (Nagaveni et al, 2004). These catalysts were active under visible light, had optical absorption wavelengths below 600 nm, and showed superior photocatalytic activity for the degradation of methylene blue and phenol under UV and solar conditions compared to commercial TiO_2, Degussa P-25. The higher photocatalytic activity was attributed to the structure of the catalyst. Various studies such as X-ray diffraction, Raman spectroscopy, Brunauer-Emmett-Teller surface area, thermogravimetric-differential thermal analysis, FT-IR spectroscopy, NMR, UV-vis spectroscopy, and surface acidity measurements were conducted. It was concluded that the primary factor for the enhanced activity of combustion-synthesized catalyst is a larger amount of surface hydroxyl groups and a lowered band gap. The lower band gap can be attributed to the carbon inclusion into the TiO_2 giving $TiO_{2-2x}C_x$ VO_2 (Nagaveni et al, 2004).

2.10 Electrospinning

Electrospinning is a relatively simple method for fabricating ultrafine fibres which are known as nanofibres. Electrospinning can be used to convert nanoparticles into long nanofibres with the aid of a polymer base (Hu et al, 2006). This process is used to spin fibres having diameter at the sub-micron level using an electric field (Ojha, 2007). The surface of a polymer solution droplet is charged by high voltage to induce the ejection of a liquid jet. The ejected liquid jet is solidified at the collector (Doh et al, 2007). This is a facile technique to produce nanofibres having potential application in a variety of applications (Ojha, 2007).

2.10.1 Electrospinning process when applying high voltage

Li & Xia (2004) explained that when a sufficiently high voltage is applied to a liquid droplet, the body of the liquid becomes charged, and electrostatic repulsion counteracts the surface tension and the droplet is stretched; at a critical point a stream of liquid erupts from the surface. This point of eruption is known as the Taylor cone. If the molecular cohesion of the liquid is sufficiently high, stream breakup does not occur (if it does, droplets are electrosprayed) and a charged liquid jet is formed. As the jet dries in flight, the mode of current flow changes from ohmic to convective as the charge migrates to the surface of the fibre. The jet is then elongated by a whipping process caused by electrostatic repulsion initiated at small bends in the fibre, until it is finally deposited on the grounded collector. The elongation and thinning of the fibre resulting from the bending instability, leads to the formation of uniform fibres with nanometre-scale diameters.

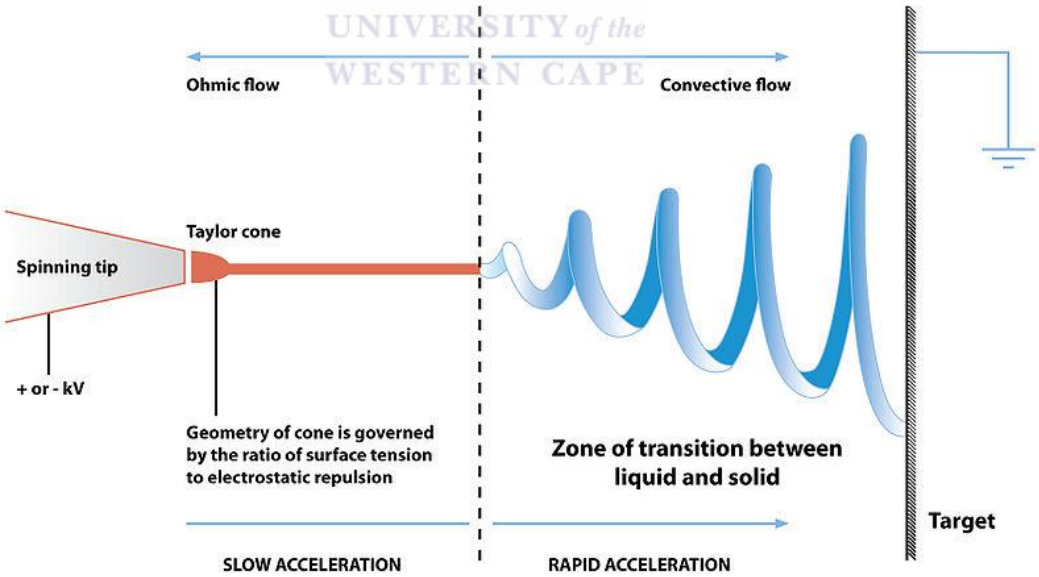

Figure 2.5: Electrospinning process as the high voltage is applied (Li & Xia 2004)

In addition, Chuangchote et al, (2009) reported that the sol gel method is a suitable method, compared to the other liquid processing methods for making TiO_2 nanofibres. Chuangchote et al, (2009) fabricated TiO_2 nanofibres by the combination of electrospinning and sol gel techniques using poly(vinylpyrrolidone) (PVP), titanium(IV) butoxide, and acetylacetone in methanol as a spinning solution. TiO_2 nanofibres (260-355 nm in diameter), with a bundle of nanofibrils (20-25 nm in diameters) aligned in the fibre direction, or particle-linked structures were obtained from the calcination of as-spun TiO_2/PVP composite fibres at temperatures ranging from 300 to 700 °C. These nanofibres were utilized as photocatalysts for hydrogen evolution. The nanofibre photocatalyst calcined at 450 °C showed the highest activity among the TiO_2 nanofibres tested such as those prepared by the hydrothermal method and anatase nanoparticles. Their results indicated that one-dimensional electrospun nanofibres with highly aligned bundled nanofibrils are beneficial for enhancement of the crystallinity, large surface area, and higher photocatalytic activity.

2.10.2 Polymeric nanofibres

The dispersion of metal nanoparticles into polymer nanofibres is of great interest because of not only the novel properties of the nanocomposite materials but also continuously growing demand for further miniaturization of electronic components, optical detectors, chemical and biochemical sensors, and devices (Mishra & Ahrenkiel, 2011). Fibre membranes have been reviewed to be very useful for heterogeneous catalysis and also as supports for catalytic metal nanoparticles and nanowires. Compared to conventional film photocatalysts, nanofibre-based photocatalysts have greater surface-to-volume ratio, and the porous structure allows for higher surface active sites for effective catalysis. The surface area is proportional to the fibre diameter and the volume is proportional to the square of the diameter, the specific surface area is inversely proportional to the fibre diameter, leading to high specific surface areas for small fibres (Dzenis,

2004). The pore fibre depends on the diameter size; therefore, small pore sizes produce non-wovens with a small fibre size (Ojha, 2007).

These nanofibres may provide a connection between the nanoscale and the macroscale, since the diameters are in the nanometer range and the lengths are kilometers. The electrospinning process can be combined with sol technique, sol gel technique and gas-solid reaction, to fabricate nanofibres. Electrospinning is also used for generating TiO_2 fibres when combined with the sol gel process (Park et al, 2011). In a typical electrospinning process for preparation of TiO_2 nanofibres, a Ti-precusor sol gel solution with a polymer matrix is used as the starting material to proceed under a high electrical field (Lin et al, 2011).

According to Zhang et al, (2008), pipe-shaped titania containing multilayer nanofibres were fabricated through the combination of electrospinning with layer-by-layer technique. The morphology of the obtained pipe-shape multilayer nanofibres confirmed that THF is better than methylbenzene as solvent. The obtained pipe-shape with a wall of multilayer of fibre, with an inside diameter of about 700 nm and wall thickness of 140 nm. The obtained multilayer pipe-shape nanofibres has the highest photocatalytic activity to degrade methylene blue solution comparing with the TiO_2 film due to their unique porous structure. Under UV radiation for 60 min the degradation of methylene blue (mg/L) without catalyst was found to be only 3%, that of the TiO_2 film was 50%, while the highest degradation (70%) was obtained with the pipe-shape multilayer PEI/TiO_2 hybrid nanofibers as catalyst. Complete degradation of methylene blue was not obtained with the obtained pipe-shape multilayer PEI/TiO_2 nanofibers in 1 h irradiation.

The electrospinning technique has attracted much attention because it has provided a cost-effective, versatile and simple way to fabricate 1-D TiO_2 nanostructure materials in a short period time. Lim et al, (2008) carried out a study of synthesizing nanofibres that have shown good biological performances such as improved cell adhesion and differentiation; therefore, nanofibrous modification of dental and bone implants might enhance osseo-integration. Their

study investigated the nanofibrous modification of titanium implants. TiO_2 nanofibres were fabricated by the electrospinning method using a mixture of Ti(IV) isopropoxide and poly(vinyl pyrrolidone) (PVP) in an acidic alcohol solution. Then the nanofibres were immobilized on NaOH/HCl-treated titanium plates by inducing alcohol condensation reaction of Ti(IV)isopropoxide with Ti–OH group on the titanium surface and subsequent calcination (500–1000 ^oC). The immobilized TiO_2 nanofibres were characterized by SEM, XRD and a simulated removal test. The diameter of the TiO_2 nanofibres could be controlled within the range of 20–350 nm by changing the amounts of Ti(IV) isopropoxide and PVP. Phase transformation from anatase to rutile was observed after calcination. After the simulated removal test, TiO_2 nanofibres remained on the titanium plate's surface. These TiO_2 nanofibres on titanium plates could be used for the surface modification of titanium implants to improve the osseointegration.

In another study on nucleation and growth kinetic of titania nanoparticles prepared by the sol gel method it was show that the rate constant for coagulation of particles increased with temperature because the velocity of monomer through the particles had a high dependency of temperature. Secondary particles were formed and the growth of particles increased when they passed a critical radius and became stable (Mehranpour et al, 2011). Nakane et al., (2007) has formed TiO_2 nanofibres and TiO_2 nanotubes by calcination of new precursor nanofibres of poly(vinyl alcohol) (PVA)- titanium compound hybrids. The precursor nanofibres were formed by using electrospinning with water as a solvent. It was the most safe method to use water as a solvent on electrospinning. The immobilization of TiO_2 catalysts on various substrates was studied by Nakane et al., (2007) to prepare TiO_2 nanofibre by a modified sol gel method to tune the electronic structure of TiO_2 and improve its photocatalytic activity under visible light.

2.10.3 Decomposition of polymer nanofibres

Kanjwal et al, (2010) had decomposed the formed nanofibre mats by initially drying for 24 h at 80 °C under vacuum and then calcining in an air atmosphere at 5 °C/min up to 600 °C and kept at 600 °C for 1 h. Kanjwal et al, (2010) also fabricated Titania nanofibres by drying electrospun TiO_2/polyvinylpyrrolidone nanofibres for 5 hr in air and subsequent annealing for 3 hr at temperatures from 450 °C to 550 °C in air. To improve the binding strength, a TiO_2 buffer layer with a thickness of 400 nm was spin-coated onto a glass slide prior to electrospinning by using the same precursor solution. Only the anatase TiO_2 phase was observed for the TiO_2/PVP fibres calcined at temperatures between 450 °C and 550 °C, but the fibres calcined at temperatures higher than 600 °C yielded a mixture of anatase and rutile phases. Mehranpour et al, (2011) has decomposed the TiO_2 nanofibres, formed by the sol gel process from a condensed $Ti(OH)_4$ gel preformed by the hydrolysis of a Ti–triethanolamine. The titanium complex was hydrolyzed by gradations in water and completely converted to a rigid gel of $Ti(OH)_4$ after aging at 100 °C for 24 h. Then, the $Ti(OH)_4$ gel was totally transformed into anatase TiO_2 nanoparticles by additional aging at 140°C in an autoclave for three days, secondly aging to get a uniform anatase TiO_2 nanoparticles in powder form. Among the coatings, the highest binding strength of the fibres was achieved for the TiO_2 nanofibre/TiO_2 buffer layer/glass coatings calcined at 500 °C. The TiO_2 buffer layer forms a barrier between TiO_2 nanofibre and glass coatings (Zhang et al, 2010). The extent of adhesion between the fiber and the substrate was analyzed by using a computer image mapping software to measure the fraction of detached area of the fibers after the tape test (Walter et al, 2011). Experimental results revealed that the extent of adherence increased by 10 % when the buffer layer was inserted between the fibres and the glass. Therefore, it can be concluded that the addition of a buffer layer has a modest influence on the binding strength between the nanofibre mat and the glass substrate (Lee et al, 2008).

Nakane & Ogata, (2010) decomposed TiO_2 by calcinating the PVA nanofibres at 400 – 700 °C for 5 hours prepared using two types of precursor nanofibres formed using electrospinning method.

- Precursor-one: PVA (degree of polymerization: 1500) 10 wt% ethanol aqueous solution was prepared. Titanium lactate (TL) $[(OH)_2Ti(C_3H_5O_2)_2]$ (5 g) was added to the PVA solution (10 g) to produce transparent PVA-TL mixed solution (spinning solution).

- Precursor-two: Pure PVA nanofibers formed by ES were immersed in a titanium alkoxide [titanium tetraisopropoxide (TTIP)] (10wt%)-ethanol solution for 10 minutes.

The treated nanofibers were washed in fresh ethanol and then PVA-TTIP hybrid precursor nanofibers were obtained. These precursor nanofibers obtained were calcined up to a given temperature in an electric furnace (in air), and TiO_2 nanofibers were formed. Anatase-type TiO_2 was formed at 400-600 °C, and the peak intensities increased with calcination temperature. Rutile-type (rutile-anatase mixed) TiO_2 was formed at 700 °C. It is well-known that anatase is superior to rutile for photocatalysis. Thus, a calcination temperature of 600-700 °C would be an effective condition when using the TiO_2 nanofibres as a photocatalyst. The relationship of the calcination temperature of the TiO_2 nanofibres, the specific surface area and pore volume were found to decrease with increasing calcination temperature. This is due to the sintering of the TiO_2 by the calcination. They then concluded by saying that the photocatalysis of the TiO_2 nanofibres calcined at 600 °C and 700 °C was lower than that of the TiO_2 nanofibres calcined at 400 °C and 500 °C. In varying the temperatures during calcination Chuangchote et al, (2009) reported that the average diameter of as- calcined nanofibers were smaller than that of as-spun composite nanofibers. The higher the calcination temperature, the greater the shrinkage, up to a calcination temperature of 500 °C, because of the degradation of PVP and other organic contents. However, the calcination did not affect the fibrous nature of the fibers. After the heat treatment mentioned above,

the average diameter of the nanofibers was found to be restrained at ca. 260 nm with a further increase of the calcination temperature from 500 to 700 °C.

2.11 Sol gel coating process

The sol gel coating process involves activation, surface preparation and application. The most common substrates used with sol gel coatings are aluminium and stainless steel. As with any coating, surface preparation is critical, and must be done properly to ensure adhesion. If the surface is too smooth, it can negatively affect both adhesion and mechanical performance. If the surface is too rough, it can cause the coating to be drawn into the surface profile, resulting in a dry, rough finish. With sol gel coatings, there is a specific time by which the activated and filtered coating should be applied to achieve maximum effectiveness. The coatings are applied via conventional spray equipment that is available in one- and two-coat systems or manually (Brinker et al., 1991) & (Huang, 2001). Coatings applications may be done on various materials by simply coating with liquid sol gel hydrolizate, thus changing their characteristics, preventing corrosion, improving biocombatibility or electrical insulating properties. The sol gel coating properties are the subject of many examinations. TiO_2 nanostructures can be prepared through various methods such as

i. liquid processing method sonochemical, microemulsion, sol gel, hydrothermal and solvothermal method;
ii. vapour processing methods such as chemical vapour condensation, arc discharge and laser pyrolysis; and
iii. solid processing methods such as the ball milling method (Tavakoli et al, 2007).

Each method has its own advantages and disadvantages. The liquid processing sol gel method was chosen to be the most suitable route to do this research due to its excellent composition control, ultrafine porous powders, homogeneity of product, and use of matrix support that can modify the properties of nanomaterials.

The sol gel method is one of the most convenient ways to synthesize various metal oxides, with ease of fabrication and low processing temperatures. It is widely used to prepare TiO_2 for films, particles or monoliths. In general, the sol gel process involves the transition of a system from a liquid "sol" (mostly colloidal) into a solid "gel" phase. The homogeneity of the gels depends on the solubility of reagents in the solvent, the sequence of addition of reactants, the temperature and the pH. The precursors normally used for the synthesis and doping of nanoparticles are organic alkoxides (Ahmad et al, 2008).

Sol gel is one of the best techniques that can be applied to prepare nanotitania. Some parameters that on the affect outcome of the sol gel process are metal precursor, temperature, pH of solution and the presence/absence of catalyst (Zhang et al, 2009). The proposed benefits of the sol gel process are considered as easy control of the formation process, high stability of the nanocrystals, better homogeneity, and high purity of the TiO_2 nanocrystals. The sol gel process allows the control of hydrolysis and polycondensation reactions that can be established easily and the appropriate properties obtained. TiO_2 nanomaterial can be synthesized by the sol gel process with different titanium precursors. Typically, synthesizing TiO_2 nanoparticles via the sol gel process includes an acid-catalyzed hydrolysis step of titanium (IV) alkoxide followed by condensation. The development of Ti-O-Ti is carried out in the presence of a small amount of water. The presence of a large excess of water leads to the development of polymeric Ti-O-Ti chains (Zhang et al, 2009).

The sol gel method is based on inorganic polymerization reactions. It includes four steps: hydrolysis, polycondensation, drying, and thermal decomposition (Tavakoli et al, 2007).

In a typical sol gel process, a colloidal suspension, or a sol, is formed from the hydrolysis and polymerization reactions of the precursors, which are usually inorganic metal salts or metal organic compounds such as metal alkoxides. Complete polymerization and loss of solvent leads to the transition from the liquid sol into a solid gel phase (Chen & Mao 2007). According to Tang et al, (2005) the

researchers exploited nonhydrolytic sol gel chemistry that had been developed previously for the manufacture of bulk titania. The sol gel solution can be electrospun to form nanofibres and further decomposed to produce nanomaterial (Ojha, 2007). Lee, (2009) reported that TiO_2 fibres could be prepared via electrospinning directly onto a SnO_2 support, using a mixture containg 3 g poly(vinylacetate), 6 g titanium(IV) isopropoxide (TTiP) and 2.4 g of acetic acid as a catalyst for sol gel reaction in dimethylformamide (DMF) (37.5 mL). Ultrafine titanium dioxide nanoparticles that ranged in size from 1 to 150 nm, with a modal primary particle size of 10–50 nm, were generated from ES by sol gel synthesis with a wide variation in their morphology and size (Lezere, 2011).

2.12 Toxicity of TiO_2 particles to the environment

Blake et al, (1999) has done a study on the effect of the TiO_2 on the people exposed to it. The first epidemiologic survey of respiratory disease among 209 titanium metal production workers showed that 17 % of the subjects had signs of pleural disease which suggests that reductions in ventilation capacity may be associated with the exposure to titanium tetrachloride and titanium dioxide. However, another epidemiologic study of 1576 workers exposed to TiO_2 particles showed no statistically significant association between TiO_2 exposure and risk of lung cancer and chronic respiratory diseases. No cases of pulmonary fibrosis have been found among TiO_2 exposed workers (Blake et al, 1999). Usually, in the absence of UV light neither anatase nor rutile exhibits much biological activity. Titanium dioxide is an ultraviolet (UV)-activated catalyst, and organic polymers that are in contact with it degrade under UV radiation. (Carmine, 2009) reports that TiO_2 can strongly absorb ultraviolet light and channel the absorbed energy into oxidation-reduction reactions. If the TiO_2 particles are made very small, less than about 100 nm, and if the photoactivity is suppressed by coating the TiO_2 particles, transparent films and coatings can be made that offer UV protection. However the latest research (Ahmad et al, 2008) shows TiO_2 bioaccumulates and

is nontoxic thus particulate forms of TiO_2 are problematic since the particles are difficult to completely remove from treated water.

2.13 Methylene blue degradation

Organic contamination occurs when an excess of organic matter, such as manure or sewage, enters the river/dam water. When organic matter increases in a pond, the number of decomposer will increase. These decomposers grow rapidly and use a great deal of oxygen during their growth. This leads to a depletion of oxygen as the decomposition process occurs (López-Chuken, 2012). A lack of oxygen can kill aquatic organisms. As the aquatic organisms die, they are broken down by decomposers which lead to further depletion of the oxygen levels. The destruction of organic contaminants by TiO_2 is catalytic (Prairie, 1993). TiO_2 photocatalytic systems are used for a variety of applications such as decomposition of unwanted and toxic organic compounds, destruction of pollutants from contaminated water and air and killing of harmful bacteria and cancer cells (Macwan, et al, 2011). The feature of the photocatalytic process is that it breaks down the pollutants and harmful organic compounds into simple molecules such as carbon dioxide and water. In this research methylene blue was used as a model organic pollutant to test degradation of organics by the photocatalyst.

Methylene blue (CI 52015) is a heterocyclic aromatic chemical compound with the molecular formula $C_{16}H_{18}N_3SCl$. It has many uses in a range of different fields, such as biology and chemistry. At room temperature it appears as a solid, odourless, dark green powder that yields a blue solution when dissolved in water. The hydrated form has three molecules of water per molecule of methylene blue. Methylene blue should not be confused with methyl blue, another histology stain, methylene blue, nor with the methyl violets often used as pH indicators.

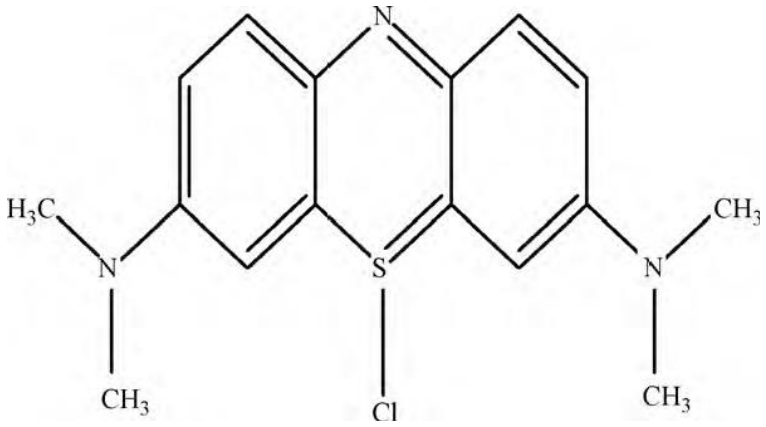

Figure 2.6: Methylene blue chemical structure (Huang et al, 2010)

Shrivastava, (2012) studied the basics of photocatalysis on semiconductors, mainly on TiO_2 and the application of photocatalytic processes for water purification from organic and inorganic matter as well as metal removal. The metal was introduced to improve TiO_2. The research mainly focused on the photocatalytic activity of anatase phases of nanocrystalline TiO_2 for the degradation of different substances under UV light irradiation. Shrivastava, (2012) found that the highest photocatalytic activity was obtained in anatase phase of TiO_2. In their study the removal of methylene blue (MB) dye and metal chromium Cr (VI) was also studied, by varying the influent concentration, loading of photocatalyst, pH and contact time as operating variables. The optimum contact time was fixed at 180 minutes for TiO_2. The results of their study revealed that the dyes could be removed by semiconducting nanomaterial assisted photocatalytic degradation. According to Ochanda et al, (2012) it was anticipated that the adsorption of methylene blue onto the TiO_2 nanostructure surface should be the first step in the reaction mechanism. The reactions of the degradation of the methylene blue were reviewed to be as follows:

- $TiO_2 + dye \leftrightarrow TiO_2 - dye$.....2.1
- $TiO_2 - dye + h\upsilon \leftrightarrow TiO_2 (e^- , h^+) - dye$.....2.2
- $TiO_2 (h^+) H_2O_{(ads)} \rightarrow TiO_2 (OH^{\bullet}_{(ads)})$.....2.3

- $TiO_2\ (h^+) + OH^-_{(ads)} \rightarrow TiO_2\ (OH^{\bullet}_{(ads)})$.....2.4
- $TiO_2\ (e^-) + O_{2(ads)} \rightarrow TiO_2(O^{-2}_{(ads)})$.....2.5
- $OH^{\bullet}_{(ads)}$ + dye → intermediate products → degradation products.....2.6
- $O^{-2}_{(ads)}$ + dye → intermediate products → $CO_2 + H_2O + HCl$.....2.7

Herrmann et al, (2001) reports the TiO_2/UV photocatalytic degradation of methylene blue (MB) investigated in aqueous heterogeneous suspensions to a prompt removal of the colour. This was carried out by oxidizing the dye with TiO_2/UV-based photocatalysis and simultaneously, with an almost complete mineralization of carbon and of nitrogen and sulfur heteroatoms into CO_2, NH_4^+, NO^{3-} and SO_4^{2-}, respectively. It is seen that photocatalysis can decontaminate coloured used waters. Photocatalysis appears as the only sub-discipline of heterogeneous catalysis, which is able to convert organic pollutants to CO_2 in water without heating nor using high pressure of oxygen nor requiring chemical reactants or additives.

2.14 Characterization methods

The characterization techniques used to investigate the properties of materials in this study were as follows: XRD, SEM, EDS, HRTEM, SAED, FTIR, and UV-visible and a brief description of each method is presented in the subsections below.

2.14.1 X-ray diffraction (XRD)

X-ray diffraction (XRD) is a versatile, non-destructive technique that gives comprehensive information about the chemical composition and information about the mineralogical composition and crystallographic structure of natural and manufactured materials. Crystal structure is observed as energy built of layers or

planes (Cullity & Stock, 2001). X-rays with a wavelength comparable to the distances between the planes can be reflected such that the angle of reflection is equal to the angle of incidence. Hence, this behaviour is called diffraction, and it is described by Bragg's Law: $2d\sin\theta = n\lambda$. When Bragg´s Law is satisfied, constructive interference of diffracted X-ray beams occur and a Bragg reflection is picked up by a detector scanning at this angle. The positions of the reflections give information about the inter-layer spacing of atoms in the crystal structure. Peak intensities give information about how much X-ray scattering is subsidizing to that reflection. Analysis of the diffraction pattern allows the identification of mineral phases within a given sample. With that achieved, it may be possible to quantify each phase present, the crystallinity of a sample, the crystal structures and their lattice parameters, crystallite size and strain; all information that can be utilized in material characterization and quality control (Dutrow et al, 2012 & Munekwa & Ferrara , 1998).In this research XRD is used for phase identification of the crystalline material. This characterization is done on the instrument called D8 Advance from Brucker AXS, for the identification of the TiO_2 nanocrystalline phases. The Brucker AXS instrument had the pw3830 X-ray generator coupled with Cu-Kα radiation and is operated at 40 kV and 40 mA. The representative samples for crystal structural forms are step-scanned from 6 to 90 ° 2Ѳ/degree scale at intervals of 0.028° with a step size of 0.02 and a dwell time of 1.2 sec/step.

Sample preparation

The carbonized TiO_2 nanocrystals are ground into small particles and the samples are pressed into rectangular aluminium sample holders using a clean spatula and then clipped into the XRD instrument sample holder.

2.14.2 High Resolution Scanning electron microscope (HRSEM)

A high resolution scanning electron microscope (HRSEM) is a type of electron microscope that images a sample by scanning it with a beam of electrons in a

raster scan pattern. The electrons interact with the atoms that construct the sample producing signals that have information about the sample's surface topography, composition, and other characteristics such as electrical conductivity (Eggertton, 2005). The scanning electron microscope (HRSEM) uses a focused beam of high-energy electrons to produce multiplicity of signals at the surface of solid specimens. The signals that originate from electron to sample interactions give information about the sample including external morphology (texture), chemical composition, crystalline structure and orientation of materials making up the sample. In most applications, data are collected over a selected area of the surface of the sample, and a two dimensional image is generated that displays spatial variations in these properties. Areas ranging from approximately 1 cm to 5 microns in width can be imaged in a scanning mode using conventional HRSEM techniques (magnification ranging from 20X to approximately 30,000X, spatial resolution of 50 to 100 nm). The HRSEM is also capable of performing compositional analyses of selected point locations on the sample; this approach is especially useful in qualitatively or semi-quantitatively determination of chemical compositions using energy-dispersive spectroscopy EDS (Swapp, 2013). In this research the HRSEM is used to observe the external morphology texture, crystalline structure and the orientation of materials making up the sample. The characterization was done using a high resolution field emission gun scanning electron microscope (HRFEGSEM), using an Auriga Gemini FEG SEM.

Sample preparation

A carbon tape was fixed onto an Al stub to fix the specimen, and the supported sample was placed onto the carbon tape. Samples were coated with carbon for the samples to be conductive using the EMITECH K950X carbon evaporator that had a respirator pump pumping all the air out creating a vacuum. A carbon rod was sharpened and was placed onto it to evaporate a thin layer of the carbon onto the samples. The carbon coating was required for the as made nanofibres only as they were not conductive enough causing the HRSEM to charge when taking the images. The carbonized supported TiO_2 nanofibres were just placed onto the carbon tape and imaged directly without carbon coating.

2.14.3 Energy-dispersive spectroscopy (EDS)

Energy-dispersive spectroscopy (EDS) is an analytical technique used for the chemical characterization of a sample. It relies on the interaction of electrons with a sample to excite X-rays. Its characterization capabilities are due in large part to the fundamental principle that each element has a unique atomic structure allowing a unique set of peaks on its X-ray spectrum. EDS is also used to stimulate the emission of characteristic X-rays from a specimen, using a high-energy beam of charged particles such as electrons or protons. At rest, an atom within the sample contains ground state electrons in electron shells bound to the nucleus. The incident beam may excite an electron in an inner shell, ejecting it from the shell while creating an electron hole where the electron was. An electron from an outer, higher-energy shell then fills the hole, and the difference in energy between the higher-energy shell and the lower energy shell may be released in the form of an X-ray. The number and energy of the X-rays emitted from a specimen can be measured by an energy-dispersive spectrometer. As the energy of the X-rays is characteristic of the difference in energy between the two shells, and of the atomic structure of the element from which they were emitted, this allows the elemental composition of the specimen to be measured. EDS is used for qualitative analysis because of the small sample size (Goodge, 2013).

2.14.4 High-resolution transmission electron microscopy (HRTEM)

High-resolution transmission electron microscopy (HRTEM) is an imaging mode of the transmission electron microscope (TEM) that allows the imaging of the crystallographic structure of a sample at an atomic scale. Due to its high resolution, it is a valuable tool to study nanoscale properties of crystalline material such as semiconductors and metals. HRTEM can provide structural information at better than 0.2 nm spatial resolution. In most crystalline inorganic materials, including ceramics, semiconductors, and metals, the positions of individual atomic columns can be resolved, at least in low-index zones. When recorded

under optimum conditions, electron micrographs can be directly interpreted in terms of the projected crystal potential. In other cases, image simulations are necessary to match proposed structures to image features. Digital image recording and quantification of diffraction pattern intensities is possible with the extreme linearity and high detective quantum efficiency DQE of a charge-coupled device CCD camera. Dynamic events induced by the electron beam or indirectly with a heating holder can be followed by video-tape recording from a TV-rate image pick-up system. At lower resolution, amplitude contrast images can be used to observe material features in the 1 µm-0.5 nm range (Barthel & Thust, 2010). In this research the HRTEM is used to observe modulations in chemical identity, crystal orientation, as well as the regular absorption based imaging. The instrument used was a Technai, G2 F20 X-Twin MAT, to analyse the surface morphology of samples and the crystal distribution.

Sample preparation

A small amount of the powdered or supported samples of TiO_2 nanocrystals were diluted in 10 mL of ethanol and sonicated for 15 min. Specimens were transferred onto the sample holder (holey carbon film with double layer 400 mesh copper grids) and allowed to dry for 10 minutes at room temperature. The specimens were then characterized by HRTEM.

2.14.5 Selected area electron diffraction (SAED)

Selected area electron diffraction (SAED), is a crystallographic experimental technique that can be performed inside a transmission electron microscope (TEM). In a TEM, a thin crystalline specimen is subjected to a parallel beam of high-energy electrons. As TEM specimens are typically ~100 nm thick, and the electrons typically have energy of 100 – 400 kev, the electrons pass through the sample easily. In this case, electrons are treated as wave-like, rather than particle-like, because the wavelength of high-energy electrons is a few thousand of a nanometer, and the spacing between atoms in a solid is about a hundred times

larger, the atoms act as a diffraction grating to the electrons, which are diffracted. That is, some fraction of them will be scattered to particular angles, determined by the crystal structure of the sample, while others continue to pass through the sample without deflection. As a result, the image on the screen of the TEM will be a series of spots giving the selected area diffraction pattern (SADP), each spot corresponding to a satisfied diffraction condition of the sample's crystal structure (Asahi et al., 2001).

2.14.6 Fourier transform infrared spectroscopy (FTIR)

Fourier transform infrared spectroscopy (FTIR) is a technique which is used to obtain an infrared spectrum of absorption, emission, photoconductivity or Raman scattering of a solid, liquid or gas. An FTIR spectrometer simultaneously collects spectral data in a wide spectral range. In infrared spectroscopy, IR radiation is passed through a sample. Some of the infrared radiation is absorbed by the sample and some of it is passed through (transmitted). The resulting spectrum represents the molecular absorption and transmission, creating a molecular fingerprint of the sample. Like a fingerprint no two unique molecular structures produce the same infrared spectrum. This makes infrared spectroscopy useful for several types of analysis. It can identify unknown materials; it can determine the quality or consistency of a sample and can also determine the different components in a mixture (Holler et al, 2007). In this research characterization was done with a Perkin Elmer 100 FT-IR spectrometer. The powdered sample was placed on the attenuated total reflectance (ATR) cell which was the sample holder. A baseline was run before the analysis for any interference. The sample was analysed in the range of 4000-380 cm^{-1}, the baseline was corrected on the spectra and spectra were smoothed for clearer peaks that can be identified.

2.14.7 Ultraviolet–visible spectroscopy (UV-Vis)

Ultraviolet–visible spectroscopy (UV-Vis) refers to absorption spectroscopy in the ultraviolet-visible spectral region. This means it uses light in the visible and adjacent (near-UV and near-infrared (NIR)) ranges. The absorption in the visible range directly affects the perceived colour of the chemicals involved. In this region of the electromagnetic spectrum, molecules undergo electronic transitions. This technique is complementary to fluorescence spectroscopy, in that fluorescence deals with transitions from the excited state to the ground state, while absorption measures transitions from the ground state to the excited state. UV-vis spectroscopy is the measurement of the wavelength and intensity of absorption of near-ultraviolet and visible light by a sample. Ultraviolet and visible light are energetic enough to promote outer electrons to higher energy levels. UV-vis spectroscopy is usually applied to molecules and inorganic ions or complexes in solution. The concentration of an analyte in solution can be determined by measuring the absorbance at some wavelength and applying the Beer-Lambert Law (Zalay, 2008). In this research this instrument was used for the characterization of the methylene blue samples to determine the concentration of the methylene blue dye before and after photocatalytic degradation. The reference sample, deionized water, was analysed first and the baseline check was done, to subtract the interferences. The samples were analysed over the range of 400-800 nm wavelength as this was the visible region.

Sample preparation

The 2 mL of the degraded methylene blue sample was placed into a cuvette and was inserted into the cuvette holder of the UV-vis instrument with the clear side facing the light lens.

Summary

Sol gel process have been used to synthesis the immobilized TiO_2 nanocrystals, but the methods used for the synthesis of immobilized anatase TiO_2 are lengthy

and getting a good adhesion of the TiO_2 nanocrystals onto a support is difficult. These available methods and the processes developed and used for the treatment wastewater are unreliable, expensive; some methods cannot treat the wastewater rapidly and some methods leave the traces of toxic substances in water after treatment, for example degussa P25 is in a nano-powder form and also performs degradation to the organic dyes in wastewater, but this method leaves traces of nano-particle of TiO_2 in water after the treatment. Oxidation of these organic pollutants at the surface of TiO_2 catalyst is an important photocatalysis application (Macwan et al, 2011). TiO_2 is toxic and difficult to recover from water. TiO_2 is also difficult for process scale-up, not economically viable but a very good catalyst. The immobilization of TiO_2 nanocrystals on supporting material will overcome the limitation.

In the present research photocatalysis is used for organic decontamination reactions, in the presence of a catalyst which in this study considers supported TiO_2 anatase nanocrystals. The enhancement of the photocatalytic activity is undertaken by immobilization of TiO_2 catalysts on stainless steel mesh substrates. The study aimed to prepare TiO_2 nanocrystals by a modified sol gel method to tune the electronic structure of TiO_2 with high surface area and improve its photocatalytic activity under ultraviolet light. The potential of the band structure of TiO_2 is just the thermodynamical requirement. Other factors such as charge separation, mobility, and lifetime of photogenerated electrons and holes also affect the photocatalytic properties of TiO_2.

Kanjwal et al, (2010) reviewed that the adhesion was increasing by 10 % at 500 °C, therefore the adhesion increases with an increase in temperature, but the drawback is that at the temperatures higher than 550 °C a mixture of anatase and rutile phases is yielded. Most studies show that the anatase phase is the most photocatalytic active crystalline phase. Recently Ahmad et al., (2008) have studied the synthesis and characterization of TiO_2 nanoparticles by sol gel technique. However, the synthesized TiO_2 catalyst in the presence of the UV irradiation was studied previously and able to degrade less than 80 % methylene blue (Zhang et al, 2008). The water-splitting process in turn can affect the local

pH environment and surface structures of the TiO_2 (Chen & Mao, 2007). The literature was reviewed to guide the choice of different methods that were used in Chapter Three and characterization technique that are presented and discussed in Chapter Four.

CHAPTER THREE: METHODOLOGY

3 Methodology

3.1 Introduction

This chapter contains the detailed methodology and the sample preparation and instrumental conditions for the characterization techniques used in this study. The chapter also covers the synthesis of the nanofibres from wet process (sol gel method) and electrospinning the sol gel solution into nanofibres on the supporting material, and there after calcination and or stabilization and carbonization conditions applied to decompose the nanofibres into nanocrystals are provided. This chapter also details the synthesis of the supported TiO_2 nanocrystals through the liquid processing method (sol gel method) by directly coating the stainless steel mesh with sol gel solution and further decomposition through calcination to form supported anatase crystals.

3.2 Materials and Methods

The chemicals used, equipment, characterisation techniques and the procedures of the experiment carried out are discussed in this section in detail, to show how the optimisation of the study was carried out.

Table 3.1: The chemicals used

Chemical	**Specification**	**Supplier**
Polyacrylonitrile (PAN)	Nanopowder	Sigma-Aldrich
N,*N* dimethyl formamide (DMF)	99.5 %	B & M Scientific
Acetyl acetone	99.9 %	B & M Scientific
0.09 M Titanium Tetrachloride in 20% HCl	Solution	Sigma-Aldrich
Titanium tetrachloride	99 %	Sigma-Aldrich
Methylene Blue	95 %	Sigma-Aldrich
Nitrogen gas	99 %	Afrox

Table 3.2: The equipment used

Equipment	**Supplier**
Boro-silica glass pasture pipette	Sigma-Aldrich
Power supply	University of Stellenbosch
Aluminium Foil	-
Magnetic stirrer bar	Kimix Chemicals & Laboratory Suppliers, RSA
Magnetic stirrer plates	Kimix Chemicals & Laboratory Suppliers, RSA
Glass beakers	Sigma-Aldrich
Copper wire	Wire Systems Technology
Labofurn tube furnace	Kiln contracts (Pty) Ltd
Silica glass tube	Glassblower
Silica socket	Glassblower
Stainless steel mesh	Cape Mesh
Titanium mesh	Good Fellow Company
Steel balls	Bearing Man Group

3.3 Schematic and set up of the research procedures

The schematic protocol of the synthesis procedure used to make the TiO_2 nanofibres, the decomposition as well as the transformation of the TiO_2 nanocrystals is presented in Figure 3.1

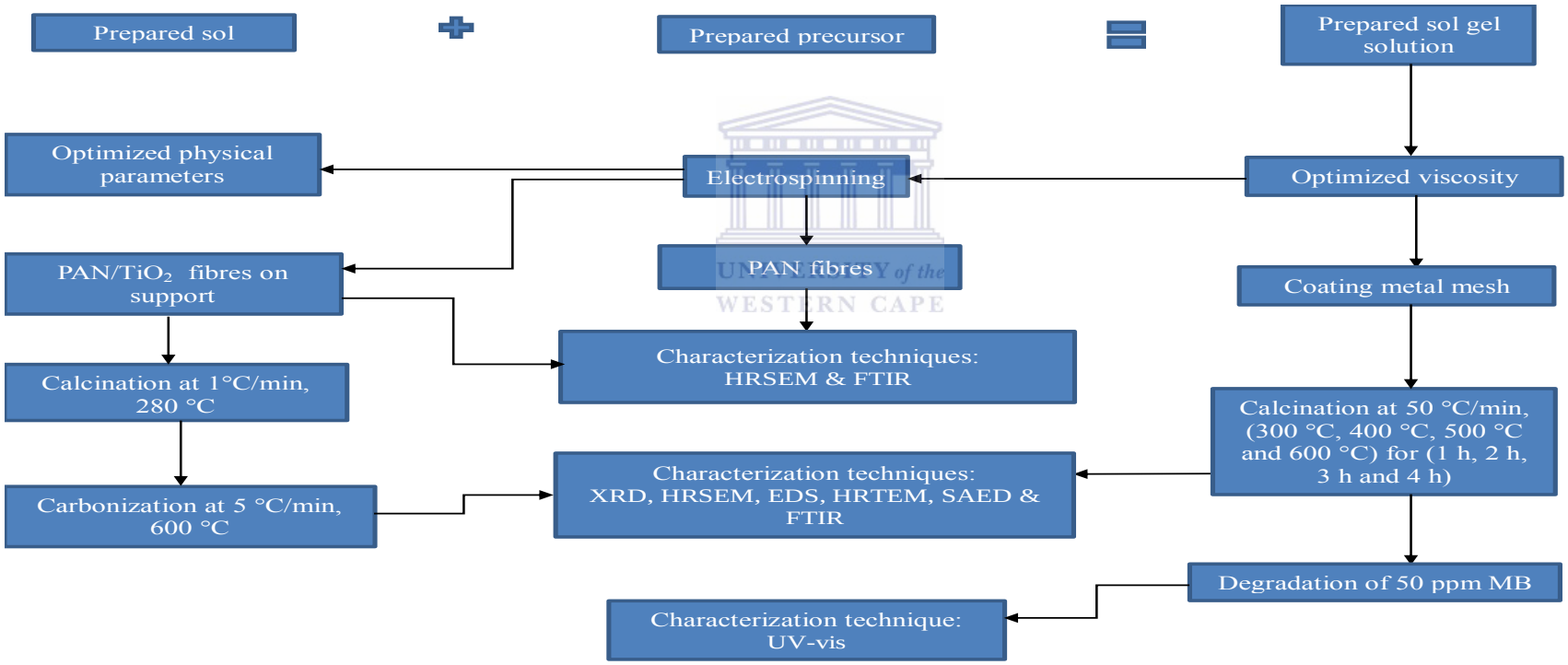

Figure 3.1: Schematic procedure

3.4 Experiment One: Synthesis of the sol gel solution

3.4.1 Sol solution preparation

In experiment one, 8 % (w/w) PAN/DMF sol solution was prepared firstly by weighing 2 g of polyacrylonitrile (PAN) into a 100 mL beaker. 23 g of dimethyl formamide (which acts as the solvent) was then added into the same 100 mL beaker to make the mass of the mixture up to 25 g. The PAN was then dissolved in DMF at room temperature using a stirring bar and a magnetic stirrer at ~ 800 rpm to achieve a homogeneous, viscous PAN/DMF solution.

3.4.2 Titanium precursor preparation

The titanium precursor was prepared by mixing 1.00 mL of 0.0900 M $TiCl_4$ in 20 % HCl (Sigma Aldrich) and adding 1.00 mL of 0.0125 M acetyl acetone (which acts as the surfactant), resulting in a molar ratio of 7:1.

3.4.3 Sol gel solution preparation

The 20 mL of PAN/DMF/TiO_2 sol gel solution was then prepared by dissolving the (7:1) molar ratio of titanium HCl precursor made in the previous step drop by drop into the 8 % PAN/DMF solution made in the first step. This is done at 60 °C with the aim of rapidly dissolving the precursor. As the (7:1) molar ratio of titanium precursor was added into the 8 % PAN/DMF sol solution drop wise, each drop of (7:1) molar ratio formed white balls in the 8 % PAN/DMF sol solution, but these balls dissolved as the solution was continuously stirred.

3.4.4 Effect of the DMF volume on the viscosity of the sol solution

The volume of the dimethyl formamide (DMF) solvent was varied while keeping the mass of polyacrylonitrile (PAN) constant. This was done in order to determine the PAN/DMF solution viscosity relationship that is dictated by the volume of the DMF solvent and mass of the PAN. The studied parameters are presented in Table 3.3.

Table 3.3: Effect of the volume of the DMF

Variable parameters		**Response parameter**
PAN (g)	**DMF (g)**	**Percentage of the sol solution (%)**
2.00	18.00	10
2.00	23.00	8
2.00	28.57	7
2.00	33.33	6
2.00	50.00	4
2.00	100.00	2

The response parameter was calculated according to this example:

% (w/w) PAN/DMF sol solution = (2 ÷ 18) × 100 = 10 %

3.4.5 Sol gel solution prepared from the different sol solution percentages

The different percentages of the PAN/DMF solution are reported in Table 3.3 (Section 3.4). For every 20 mL of these different percentages of the PAN/DMF solution, 15 drops (~ 0.7 mL) of the (7:1) molar ratio of titanium precursor was added dropwise independently and the resulting mixture was stirred vigorously (~ 800 rpm) at 60 °C in order to achieve homogeneity and form the PAN/DMF/TiO_2 sol gel solution.

3.5 Synthesis of TiO_2 nanofibres using electrospinning process

3.5.1 Electrospinning setup

The electrospun TiO_2 nanofibres were synthesized using the setup shown in Figure 3.2. During electrospinning the various prepared PAN/DMF/TiO_2 sol gel solutions were transferred to a borosilicate pasteur pipette, and one end of a copper wire, which is the positive electrode was inserted into the borosilicate pasteur pipette containing the PAN/DMF/TiO_2 sol gel solution. The copper wire was connected to a direct current (DC) power supply for the applied high voltage. The negative side of the DC power supply was connected to the grounded electrode that was the aluminium foil collector plate. The distance between the tip of the borosilicate pasteur pipette and aluminium foil was fixed at 20 cm, while the applied voltage was kept constant at 15 kV over the electrodes.

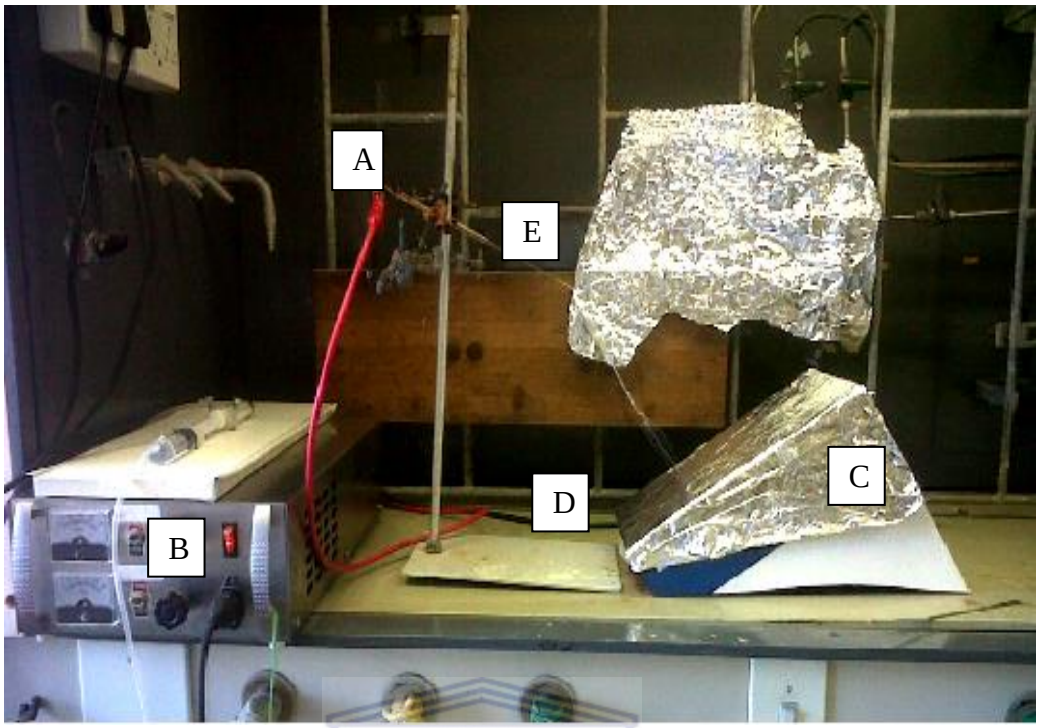

Figure 3.2: Electrospinning setup [A] = copper wire connected to the applied high voltage, [B] = power supply, [C] = aluminium foil collector plate, [D] = the ground electrode wire and [E] = borosilicate pasteur pipette with the sol gel solution and copper wire

3.5.2 Electrospun TiO_2 nanofibres

The electrospun TiO_2 nanofibres were electrospun using the set up reported in Section 3.5.1, and was carried out using exactly the set up shown in Figure 3.2. First the PAN/DMF/TiO_2 sol gel solution was filled into the borosilicate pasteur pipette until there was a drop at the tip of the pasteur pipette. As the drop of the PAN/DMF/TiO_2 sol gel solution dripped off the tip of the pipette because of the force of gravity, the high voltage was applied to the PAN/DMF/TiO_2 sol gel solution through the conductive copper wire inserted into the PAN/DMF/TiO_2 sol gel solution that was in the pasteur pipette, by switching on the power supply and setting the voltage at 15 kV. When the high voltage was applied, the PAN/DMF/TiO_2 sol gel solution coming out of the tip of the pasteur pipette was

spun into PAN/DMF/TiO_2 nanofibres. The electrospinning PAN/DMF/TiO_2 nanofibres are shown in Figure 3.3. Hong et al, (2006) revealed that, electrospinning occurs when the applied voltage is higher than a critical value. By applying a high electrical potential into the PAN/DMF/TiO_2 sol gel solution in the borosilicate pasteur pipette across the collecting plate, fibres were electrospun and deposited as a nanofibre mat on the collecting plate (Watthanaarun et al, 2005).

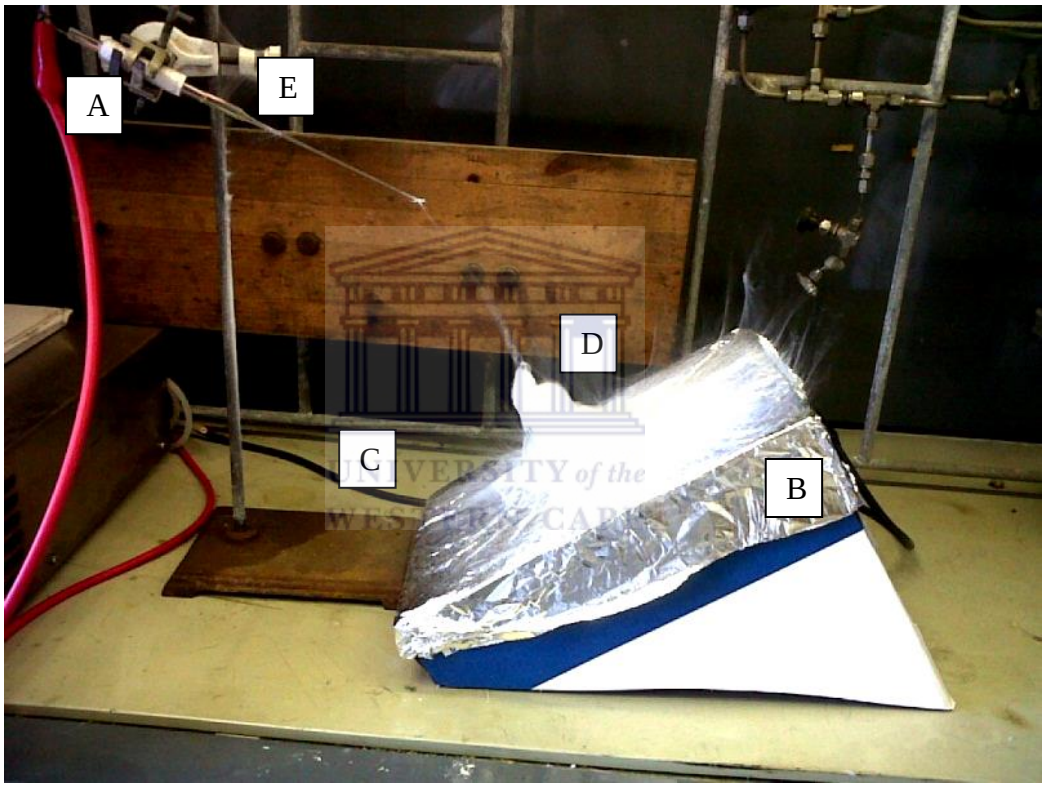

Figure 3.3 A - D: Electrospun nanofibres as they are electrospining [A] = copper wire connected to the applied high voltage, [B] = aluminium foil collector plate, [C] = the ground electrode wire, [D] = TiO_2 nanofibres and [E] = borosilicate pasteur pipette with the sol gel solution and copper wire

3.5.3 Supporting material of TiO_2 nanocrystals

A stainless steel mesh with an aperture of 2 mm and a mesh diameter of 0.23 mm was used as the support for depositing the electrospun PAN/DMF/TiO_2 nanofibres as well as support for the immobilized PAN/DMF/TiO_2 nanocrystals during decomposition.

3.6 Decomposition of the PAN/DMF/TiO_2 nanofibres

A Labofurn tube furnace was used to decompose the supported PAN/DMF/TiO_2 nanofibres and transform them into supported TiO_2 nanocrystals. The tube furnace used is shown in Figure 3.4 and can heat up to 1000 °C. The furnace has a microprocessor program controller to set the temperature, heating rate and holding time for the independent decomposition experiments that were carried out.

Figure 3.4: Furnace

Calcination is the process of subjecting a substance to the action of heat in air, but without fusion, for the purpose of causing some change in its physical or chemical constitution. Oxidation and hydrolysis reactions of the $TiCl_4$ to TiO_2 took place during calcination in air. The temperature of the furnace was set up to 280 °C for calcination at a heating rate 1 °C/min in air to decompose the organic materials and give the oxidation and hydrolysis reactions enough time to occur. Calcination is the stabilization process for the carrier of the $TiO_{2,}$ which was the PAN. The cyclization and the dehydration of PAN was allowed to occur gradually while the temperature was increased incrementally by 1 °C/min to 280 °C in air and held at 280 °C for 2 h, maintaining the fragment stability in sequence and allowing the exothermic reactions of the PAN during cyclization to take place at a slow heating rate (Chen, et al 2009). The holding period at temperature was varied as set out below in the carbonization section. The heating period was calculated depending on the heating rate for both examples. the total heating period should in fact also include the additional holding time at the highest temperature.

Carbonization is the term for the conversion of an organic substance into carbon or a carbon-containing residue through pyrolysis. The carbonization was the second step of decomposing the organic out of supported PAN/DMF/TiO_2 nanofibres and transforming them further into TiO_2 nanocrystals. This step was carried out in an inert environment to avoid any unwanted reactions such as hydrolysis and oxidation that may occur in air, therefore nitrogen gas was introduced at the beginning of this step to give an inert atmosphere by flowing the N_2 gas at 2.83 L/h. Carbonization was carried out at 600 °C at a heating rate of 5 °C/min. The holding time at temperature was 600 °C for 2 h. The heating period was calculated depending on the heating rate for both examples. the total heating period should in fact also include the additional holding time at the highest temperature.

3.7 Experiment Two: Preparation of the 8 % (PAN/DMF/TiO_2) sol gel solution using 99 % pure $TiCl_4$ as the titanium precursor (TT2)

In experiment two, 8 g of Polyacrylonitrile (PAN) was weighed out and 92 g of N, N-dimethylformamide (DMF) was also weighed, making up 100 g of PAN and DMF mixture in solution. The PAN was dissolved in DMF at room temperature (25 $^{\circ}$C) over night (12 hour) in a sealed vessel ensuring that the mixture was homogeneous, making up the 8 % PAN/DMF clear sol solution. This solution was slightly viscous. Then 50 mL of the PAN/DMF solution was measured into a beaker. 4 mL of 99 % pure concentrated $TiCl_4$ was measured and added to the 50 mL of the PAN/DMF solution drop by drop while stirring with a magnetic stirrer at room temperature making up the PAN/DMF/TiO_2 sol gel solution. This experiment was undertaken in the fumehood as the $TiCl_4$ released white fumes of HCl. During the addition of the concentrated $TiCl_4$ the PAN/DMF/TiO_2 sol gel solution turned yellow and released heat, so the reaction that occurred was exothermic.

Clean stainless steel mesh was used as the supporting material. Two stainless steel meshes were used as supports to electrospun PAN/DMF/TiO_2 fibres onto using the electrospinning technique presented in Section 3.5 and thereafter the spun PAN/DMF/TiO_2 fibres were hydrolysed by wetting the supported TiO_2 nanofibres using deionised water in one case and acetone in the other case to adhere the nanofibres onto the supporting material. Separate stainless steel meshes were also manually coated with the PAN/DMF/TiO_2 sol gel solution following the method presented in Section 3.10. After the TiO_2 containing 8 % (PAN/DMF/TiO_2) sol gel was coated onto the meshes, these meshes were then calcined in air at 280 $^{\circ}$C by heating rate of 1°C/min over 4 hr 25 min and held at 280 $^{\circ}$C for 2 h to hydrolyse and oxidize the $TiCl_4$ while stabilizing the PAN. Then nitrogen gas was introduced into the furnace and carbonization of the PAN/DMF/TiO_2 sol gel or nanofibres on the meshes was done by heating up to 600 $^{\circ}$C with a heating rate of

5 °C/min over 1 hr 4 min and held at 600 °C for 2 h following the procedure presented in Section 3.6.

3.8 Experiment Three: Preparation of the 8 % (PAN/DMF/TiO_2) sol gel solution using 99 % pure $TiCl_4$ and acetic acid as the titanium precursor

In experiment three, 3 g of the Polyacrylonitrile (PAN) was weighed out and 34.5 g of N, N-dimethylformamide (DMF) was also weighed and added together, making up 37.5 g of PAN and the DMF. The PAN was dissolved in DMF at room temperature (25 °C) over night (12 hour) in a sealed vessel ensuring that the entire polymer was dissolved making up the 8 % PAN/DMF clear solution. This solution was slightly viscous. Then 6 g of 99% concentrated $TiCl_4$ was weighed out and added to the 8 % PAN/DMF solution drop by drop while stirring with a magnetic stirrer at room temperature making up the 8 % (PAN/DMF/TiO_2) sol gel solution. This experiment was undertaken in fumehood as the $TiCl_4$ released white fumes of HCl. During the addition of the concentrated $TiCl_4$ the solution turned yellow and released heat, so the reaction occurring was exothermic. Then 2.4 g of acetic acid was weighed and also added to the stirring 8 % (PAN/DMF/TiO_2) solution drop by drop ensuring that the 8 % (PAN/DMF/TiO_2) sol gel solution was homogeneous. This method was adopted from Lee, (2009). Clean stainless steel mesh was coated with the 8 % (PAN/DMF/TiO_2) sol gel solution, and was left to dry for a few 10 – 15 minutes using the technique explained in Section 3.10. The coated meshes were then calcined in air at a heating rate of 50 °C/min up to 280 °C and held at 280 °C for 2 h and then carbonized in air at a heating rate of 5 °C/min up to 600 °C and carbonized for 2 h at 600 °C.

The time taken to heat up the samples for the two temperatures is calculated as follows:

Temperature 1: 280 °C – 25 °C = 255 °C

255 °C ÷ 50 °C/min = 5.1 min

Temperature 2: 600 °C – 280 °C = 320 °C

320 °C ÷ 5 °C/min = 64 min

64 min ~ 1 h 04 min

3.9 Experiment Four: Preparation of the 8 % (PAN/DMF/TiO_2) sol gel solution using 99 % pure $TiCl_4$ as titanium precursor (TT4)

Experiment four has the same preparation as experiment three till after the addition of $TiCl_4$. The decomposition procedure of the coated stainless steel meshes was as follows: the support samples were coated manually with 2 mL of 8 % (PAN/DMF/TiO_2) sol gel solution and then calcined in air by heating within the temperature range 300 °C to 600 °C at the heating rate 50 °C/min and holding at 600 °C for 2 h. The heating period was calculated depending on the heating rate. The total heating period should in fact also include the additional holding time at the highest temperature.

3.10 Coating the 250 mm^2 stainless steel mesh with the 8 % PAN/DMF/TiO_2 sol gel solution

The 250 mm^2 stainless steel mesh was coated manually with 0.5 mL 8 % (PAN/DMF/TiO_2) sol gel solution drawn from a glass vessel containing 50 mL of the 8 % (PAN/DMF/TiO_2) sol gel solution (Section 3.8 and 3.9) placed on a magnetic stirrer to ensure that the (PAN/DMF/TiO_2) sol gel solution was homogeneous. The 0.5 mL (~0.1965 g) of the sol gel solution was deposited as a zig zag pattern on the 250 mm^2 stainless steel mesh and the (PAN/DMF/TiO_2) sol gel solution was spread evenly throughout the stainless steel mesh manually. As soon as the stainless steel mesh was coated with (PAN/DMF/TiO_2) sol gel solution, the solution colour on the stainless steel mesh changed from yellow to a violet colour. The coated mesh was then placed on a ceramic boat and left for 10 –

15 minutes in the fumehood to dry at room temperature after which it was calcined according to the procedure set out in Section 3.11.

3.11 Decomposition parameters

The prepared sol gel solutions on the stainless steel mesh are calcined by heated up at the same heating rate of 50 °C/min to different temperatures of 300 °C, 400 °C, 500 °C and 600 °C, then held at these temperatures for 1, 2, 3, 4 hours.

3.12 Quantity of the deposited TiO_2 nanocrystals onto the 250 mm^2 stainless steel mesh

Optimisation of the calcined supported TiO_2 nanocrystals was carried out by weighing the 250 mm^2 stainless steel meshes before coating them with the 8 % (PAN/DMF/TiO_2) sol gel solution prepared in Experiment four (Section 3.9) and there after the 250 mm^2 stainless steel meshes were coated with 2 mL of the 8 % (PAN/DMF/TiO_2) sol gel solution prepared and the solution was left to dry for a few minutes on the surface of the stainless steel meshes. The coated stainless steel meshes were triplicated and calcined at different temperatures and after calcination the stainless steel meshes were again weighed. The analytical balance situated in a stable environment was used to determine the masses of the deposited supported TiO_2 nanocrystals.

Table 3.4: Experimental conditions of each run which was hydrolyzed with deionised water

Unique number	Formulation	Procedure	Calcined at	Carbonized at	Remarks	Results
TT1.1 (Exp 1)	7 % and 8 % PAN/DMF	Electrospinning	-	-	Free fibres	Section 4.2.3 (Figure 4.4)
TT1.2 (Exp 1)	7 % PAN/DMF/TiO_2	Electrospinning	-	-	Free fibres	Section 4.2.3 (Figure 4.5)
TT1.3 (Exp 1)	8 % PAN/DMF/TiO_2	Electrospinning	-	-	Free fibres	Section 4.2.3 (Figure 4.6)
TT1.1 (Exp 1)	7 % PAN/DMF/TiO_2	Electrospinning	Heated at 1 °C/min to 280 °C and held for 2 h in air	Heated at 5 °C/min to 600 °C in N_2 and held for 2 h	Supported TiO_2 crystals	Section 4.2.5 (Figure 4.10 A)
TT1.2 (Exp 1)	7 % PAN/DMF/TiO_2	Electrospinning	Heated at 1 °C/min to 280 °C and held for 2 h in air	Heated at 5 °C/min to 600 °C in N_2 and held for 2 h	Supported TiO_2 crystals	Section 4.2.5 (Figure 4.10 B)

Unique number	Formulation	Procedure	Calcined at	Carbonized at	Remarks	Results
TT1.3 (Exp 1)	8 % PAN/DMF/TiO_2	Electrospinning	Heated at 1 °C/min to 280 °C and held for 2 h in air	Heated at 5 °C/min to 600 °C in N_2 and held for 2 h	Supported TiO_2 crystals	Section 4.2.5 (Figure 4.10 C)
TT (Blank) (Exp 1)	Titanium precursor (7:1)	Manual Coating	Heated at 1 °C/min to 280 °C and held for 2 h in air	Heated at 5 °C/min to 600 °C in N_2 and held for 2 h	Supported TiO_2 particles	Section 4.2.6 (Figure 4.11)
TT1.4 (Exp 1)	Ti-precursor (7:1) base and 8 % PAN/DMF/TiO_2 topping	Manual Coating	Heated at 1 °C/min to 280 °C and held for 2 h in air	Heated at 5 °C/min to 600 °C in N_2 and held for 2 h	Supported PAN/DMF/TiO_2	Section 4.2.7 (Figure 4.12)
TT1.5 (Exp 1)	7 % PAN/DMF/TiO_2	Manual Coating	Heated at 1 °C/min to 280 °C and held for 2 h in air	Heated at 5 °C/min to 600 °C in N_2 and held for 2 h	Supported PAN/DMF/TiO_2	Section 4.2.7 (Figure 4.13)

Unique number	Formulation	Procedure	Calcined at	Carbonized at	Remarks	Results
TT1.6 (Exp 1)	8 % PAN/DMF/TiO_2	Manual Coating	Heated at 1 °C/min to 280 °C and held for 2 h in air	Heated at 5 °C/min to 600 °C in N_2 and held for 2 h	Supported TiO_2 crystals	Section 4.2.7 (Figure 4.14)
TT2.1 (Exp 2)	8 % PAN/DMF/TiO_2	Electrospinning	Heated at 1 °C/min to 280 °C and held for 2 h in air	Heated at 5 °C/min to 600 °C in N_2 and held for 2 h	Supported TiO_2 fibres acetone hydrolysed	Section 4.3 (Figure 4.15 A)
TT2.2 (Exp 2)	8 % PAN/DMF/TiO_2	Electrospinning	Heated at 1 °C/min to 280 °C and held for 2 h in air	Heated at 5 °C/min to 600 °C in N_2 and held for 2 h	Supported TiO_2 fibres distilled H2O hydrolysed	Section 4.3 (Figure 4.15 B)
TT2.3 (Exp 2)	8 % PAN/DMF/TiO_2	Manual Coating	Heated at 1 °C/min to 280 °C and held for 2 h in air	Heated at 5 °C/min to 600 °C in N_2 and held for 2 h	Supported TiO_2 crystals	Section 4.3.1 (Figure 4.16)

Unique number	Formulation	Procedure	Calcined at	Carbonized at	Remarks	Results
TT3.1 (Exp 3)	8 % PAN/DMF/TiO_2	Manual Coating	Heated at 50 °C/min to 280 °C in air and held for 2 h	Heated at 5 °C/min to 600 °C in air and held for 2 h	Supported TiO_2 crystals	Section 4.4 (Figure 4.17)
TT4.1 (Exp 4)	8 % PAN/DMF/TiO_2	Manual Coating	Heated at 50 °C/min to 300 °C in air and held for (1 h, 2 h, 3 h, 4 h, 5 h and or 6 h)	-	Supported TiO_2 crystals	Section 4.5.3 (Figure 4.19)
TT4.2 (Exp 4)	8 % PAN/DMF/TiO_2	Manual Coating	Heated at 50 °C/min to 400 °C in air and held for (1 h, 2 h, 3 h, 4 h)	-	Supported TiO_2 crystals	Section 4.5.3 (Figure 4.20)
TT4.3 (Exp 4)	8 % PAN/DMF/TiO_2	Manual Coating	Heated at 50 °C/min to 500 °C in air and held for (1 h, 2 h, 3 h, 4 h)	-	Supported TiO_2 crystals	Section 4.4 (Figure 4.21)

Unique number	Formulation	Procedure	Calcined at	Carbonized at	Remarks	Results
TT4.4 (Exp 4)	8 % PAN/DMF/TiO_2	Coating	Heated at 50 °C/min to 600 °C in air and held for (1 h, 2 h, 3 h, 4 h)	-	Supported TiO_2 crystals	Section 4.5.3 (Figure 4.22)

3.13 Evaluation of the photocatalytic activity of the supported TiO_2 nanocrystals using methylene blue

3.13.1 Preparation of methylene blue solution

50 ppm of methylene blue solution was prepared by weighing out 0.1 g of methylene blue (Sigma-Aldrich, 95 %) powder and transferring it into a 2 L volumetric flask and dissolving it with deionised water. The solution in the volumetric flask was made up to the mark with deionised water.

3.13.2 Photocatalytic activity of the supported TiO_2 nanocrystals

50 mL of the prepared 50 ppm methylene blue solution was measured into a 100 mL glass beaker. The preweighed samples of TiO_2 nanocrystals supported on 250 mm^2 stainless steel meshes were immersed into 50 mL of 50 ppm methylene blue and placed onto a magnetic stirrer. Then a 36 Watt 1.2 m UV lamp that releases UV light at 253.7 nm wavelength was fixed 6 cm above each container of the methylene blue solution and the catalyst sample was agitated by magneticly stirring the solution. The UV radiation was irradiated onto the solution to degrade the methylene blue in time intervals (30 min, 60 min and 90 min). The setup of the experiment carried out is presented in Figure 3.5.

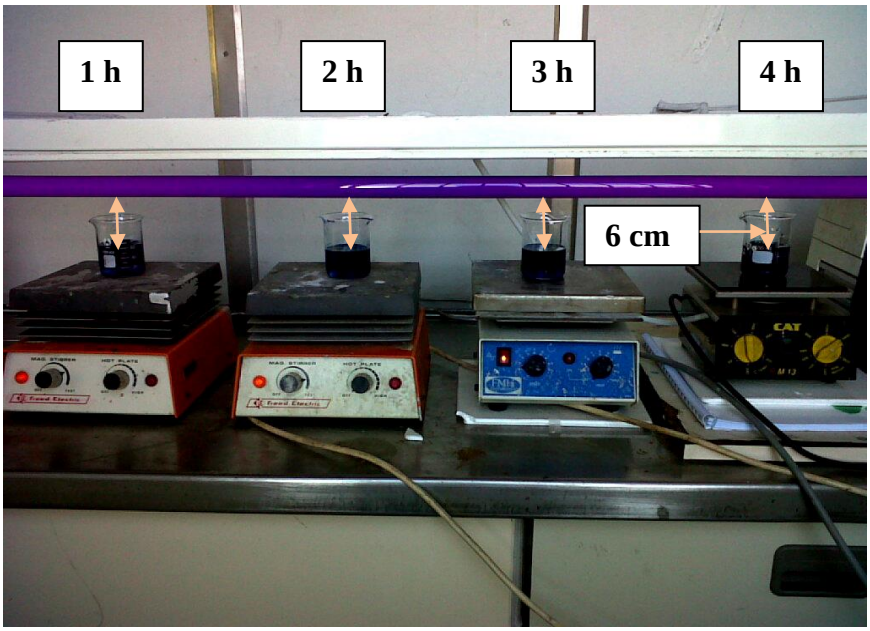

Figure 3.5: Methylene blue degradation step up under the UV light

The catalyst samples were immersed inside the solutions. At given time intervals, 2 mL of the degrading methylene blue mixture was sampled and analysed by recording variations of the maximum absorption at 664 nm with a UV-vis spectrometer. The reaction of the degradation can be illustrated as follows (Hoffmann et al, 1995):

$$25.5O_2 + C_{16}H_{18}N_3SCl \longrightarrow 16CO_2 + 6H_2O + 3HNO_3 + H_2SO_4 + HCl \quad \text{.....3.1}$$

As the aqueous solution was irradiated in the presence of TiO_2 catalyst, the adsorbed H_2O molecules reacted with holes in the valence band to form hydroxyl radicals and release hydrogen ions. The methylene blue molecules may also be decomposed to form organic acids as the intermediate products. Decolourization as measured by UV-vis spectroscopy was taken as a measure of degradation. Intermediate species may have formed but this study did not measure or identify such.

3.14 Characterization methods

The synthesized PAN/DMF/TiO_2 nanofibres and the sample where the nanofibres were further decomposed into TiO_2 nanocrystals, as well as the supported TiO_2 nanocrystals were characterized using these characterization techniques: XRD, SEM, EDS, HRTEM, SAED, FTIR and UV-visible to study the physical and chemical properties of the synthesized PAN/DMF/TiO_2 nanofibres and the decomposed and transferred, supported TiO_2 nanocrystals.

CHAPTER FOUR: RESULTS AND DISCUSSION

4 Results and Discussion

4.1 Characterization of synthesised supported TiO_2 nanocrystals

The results of the characterization techniques used for the study of the samples prepared from different PAN/DMF/TiO_2 sol gel solutions used to synthesize PAN/DMF/TiO_2 nanofibres or immobilized TiO_2 nanocrystals on stainless steel mesh are presented and discussed in this chapter.

4.2 Experiment One: Different sol gel solutions

Different (w/w) percentages were obtained using the PAN/DMF sol solution prepared from the PAN and the DMF whereby the mass of the PAN was fixed at 2 g and the mass of the DMF was varied for the different viscosities of the PAN/DMF sol solution as set out in Section 3.4. The different PAN/DMF sol solutions prepared had different independent reactions during addition of the titanium precursor when preparing the PAN/DMF/TiO_2 sol gel solution. The different PAN/DMF/TiO_2 sol gel solutions prepared are shown in Figure 4.1, Figure 4.2 and Figure 4.3 presented below.

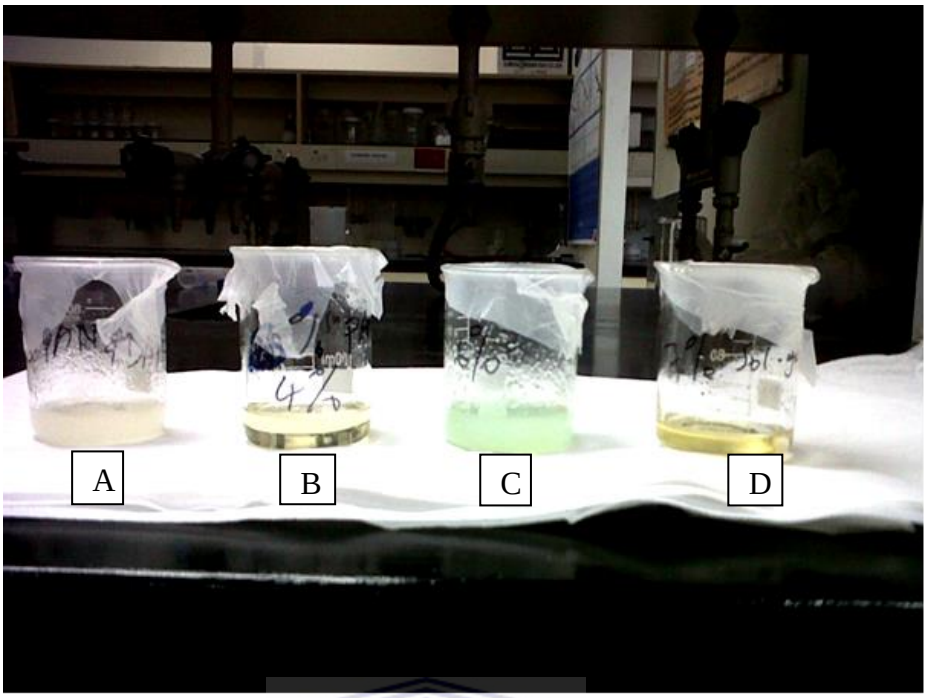

Figure 4.1: PAN/DMF/TiO_2 sol gel solution prepared from [A] = 2 % PAN/DMF sol solution, [B] = 4 % PAN/DMF sol solution, [C] = 6 % PAN/DMF sol solution and [D] = 7 % PAN/DMF sol solution

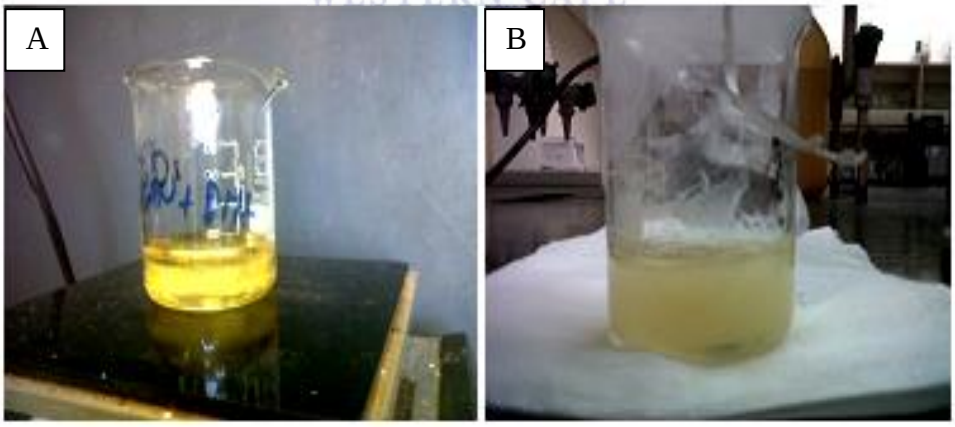

Figure 4.2: [A] = 8 % PAN/DMF/TiO_2 sol gel solution and [B] = 10 % PAN/DMF/TiO_2 sol gel solution

The different PAN/DMF/TiO_2 sol gel solutions shown in Figure 4.1 were prepared from 2 %, 4 %, 6 % or 7 % PAN/DMF solutions. In A the PAN/DMF/TiO_2 sol gel mixture had white solid particles that formed during addition of the 15 drops (~ 0.7 mL) of the (7:1) molar ratio titanium precursor, and due to these solid particles that formed the PAN/DMF/TiO_2 sol gel mixture could not be electrospun into PAN/DMF/TiO_2 nanofibres. In B the observed PAN/DMF/TiO_2 sol gel solution (4 %) was light yellow in colour and transparent. The observed colour changed from colourless to light yellow during addition of the 15 drops (~ 0.7 mL) of the (7:1) molar ratio titanium precursor to the PAN/DMF sol solution. This 4 % PAN/DMF/TiO_2 sol gel solution could not be electrospun into PAN/DMF/TiO_2 nanofibres because the solution had a very low viscosity and as a result it ran through the borosilicate pasteur pipette when the solution was tested for electrospining using the set up shown in Section 3.5.1 (Figure 3.2). In C the 6 % PAN/DMF/TiO_2 sol gel mixture had a light green colour from solid particles that formed during addition of the 15 drops (~ 0.7 mL) of the (7:1) molar ratio titanium precursor, and due to these solid particles that formed the PAN/DMF/TiO_2 sol gel mixture could not be electrospun into PAN/DMF/TiO_2 nanofibres. In D the observed 7 % PAN/DMF/TiO_2 sol gel solution was bright yellow in colour and the solution was transparent in appearance. The observed colour of the 7 % PAN/DMF solution was colourless and during addition of the 15 drops (~ 0.7 mL) of the (7:1) molar ratio titanium precursor to the PAN/DMF sol solution, the colour of the solution changed from colourless to yellow. This 7 % PAN/DMF/TiO_2 sol gel solution was more viscous than the 6 % PAN/DMF/TiO_2 sol gel solution and when transferred to the borosilicate pasteur pipette for electropinning the PAN/DMF/TiO_2 sol gel solution ran down the pipette nicely and made a drop at the tip of the pipette, therefore this PAN/DMF/TiO_2 sol gel formulation was able to produce PAN/DMF/TiO_2 nanofibres using the set up shown in Section 3.5.1 (Figure 3.2). The results of the electrospun PAN/DMF/TiO_2 nanofibres are presented in Table 4.1 and 4.2 shown below.

In Figure 4.2 A the observed PAN/DMF/TiO_2 sol gel solution (8 %) was yellow in colour and also transparent in appearance. The observed colour of the PAN/DMF solution was colourless and during addition of the 15 drops (~ 0.7 mL) of the (7:1) titanium precursor to the PAN/DMF solution, the solution changed in colour from colourless to yellow. This PAN/DMF/TiO_2 sol gel solution was more viscous than the 6 % or 7 % PAN/DMF/TiO_2 sol gel solution, and when transferred to the borosilicate pasteur pipette for electropinning the PAN/DMF/TiO_2 sol gel solution ran down the pipette nicely and made a drop at the tip of the pipette, therefore this PAN/DMF/TiO_2 sol gel formulation was also able to be used to produce PAN/DMF/TiO_2 nanofibres using the set up shown in Section 3.5.1 (Figure 3.2).

In Figure 4.2 B the observed 10 % PAN/DMF/TiO_2 sol gel solution was yellow in colour and transparent. The observed colour of the PAN/DMF solution was colourless and during addition of the 15 drops (~ 0.7 mL) of the (7:1) molar ratio titanium precursor to the PAN/DMF solution the colour of the solution changed from colourless to yellow. This 10 % PAN/DMF/TiO_2 sol gel solution was more viscous than all the other PAN/DMF/TiO_2 sol gel solutions, and when transferred to the borosilicate pasteur pipette for electropinning the PAN/DMF/TiO_2 sol gel solution ran down the pipette too slowly because of the high viscosity and by the time the PAN/DMF/TiO_2 sol gel solution reached the tip of the pipette it had solidified, therefore this PAN/DMF/TiO_2 sol gel formulation was not able to produce PAN/DMF/TiO_2 nanofibres.

4.2.1 Characteristics of the prepared PAN/DMF/TiO_2 sol gel solution

The PAN/DMF/TiO_2 sol gel solutions had different viscosities as the concentration of the $TiCl_4$ changed by altering the solvent volume. The 7 % and 8 % PAN/DMF/TiO_2 sol gel solutions were electrospun and the fibres electrospun were collected on the collecting plate. The fibres produced differed, depending on the viscosity of the PAN/DMF/TiO_2 sol gel solution.

The derived formulation [see equation 1 below] was used to calculate the viscosity of the PAN/DMF/TiO_2 sol gel solutions.

$$\mu = \frac{r^2 \times g \times [\int_{sphere} - \int_{df}]}{9 \times V} \quad \text{(www.pipeflow.co.uk)....}\ldots\ldots\ldots\ldots\ldots\ldots\ldots\ldots\ldots\ldots 4.1$$

The viscosity was established from the Stokes' Law equation where μ is the viscosity of the fluid, r is the radius of the sphere g is the gravitational acceleration and $\int_{sphere}$ is the density of the sphere, $\int_{df}$ is the density of the fluid and V is the velocity of the fluids relative to the sphere. The viscosity for the 8 % PAN/DMF sol solution at 60 °C set out in Section 3.4 was measured at a flow rate of 1.42 mL/s and the viscosity was determined to be 180.08 kg/(m.s). The 8 % PAN/DMF/TiO_2 sol gel solution containing 15 drops (~ 0.7 mL) of the (7:1) molar ratio titanium precursor at 60 °C was measured at a flow rate of 1.93 mL/s was also measured and the viscosity was determined to be 230.77 kg/(m.s).

4.2.2 Synthesised TiO_2 nanofibres

The 0.7 mL and or 1.4 mL of the (7:1) molar ratio titanium precursor of 0.09 M $TiCl_4$ in 20 % HCl were independently dissolved into the 20 mL PAN/DMF sol solutions to make up the PAN/DMF/TiO_2 sol gel solution as described in Section 3.4. The PAN/DMF/TiO_2 sol gel solutions prepared were independently electrospun following the set up shown in Section 3.5.1 (Figure 3.2). Table 4.1 and 4.2 below show the mass yielded of the electrospun PAN/DMF/TiO_2 nanofibres synthesized from the PAN/DMF/TiO_2 sol gel solution prepared from 7 % or 8 % PAN/DMF sol solutions.

Table 4.1: Electrospun TiO_2 nanofibres conditions using the 7 % (PAN/DMF/TiO_2) sol gel solution

Variable parameters			**Response parameter**	
7% PAN/DMF sol gel solution	**Titanium precursor volume**	**Electrospun sol gel solution volume**	**Electrospinning time**	**Mass of the fibres**
20 mL	15 drops (~ 0.7 mL)	5 mL	1 h 51 min	0.14 g
20 mL	30 drops (~ 1.4 mL)	5 mL	56 min	0.19 g

Table 4.2: Electrospun TiO_2 nanofibres conditions using the 8 % (PAN/DMF/TiO_2) sol gel solution

Variable parameters			**Response parameter**	
8 % PAN/DMF sol gel solution	**Titanium precursor volume**	**Electrospun sol gel solution volume**	**Electrospinning time**	**Mass of the fibres**
20 mL	15 drops (~ 0.7 mL)	5 mL	5 h 15 min	0.15 g

In Table 4.1 shows the thinner solutions have a higher conductivity thus electrospinning occurs faster. While in Table 4.2 the 5 mL PAN/DMF/TiO_2 sol gel solution prepared from the 8 % PAN/DMF solution containing the 0.7 mL (7:1) molar ratio titanium precursor took 5 h 15 min to electrospin and yielded 0.15 g of PAN/DMF/TiO_2 nanofibres. The formed nanofibres with 0.7 mL precursor were electrospun on the stainless steel mesh to form a web-like fibre structure. The formed 1.4 precursor do not attached to the stainless steel mesh as they stay as single strands and do form a web structure. Therefore the 7 %/1.4 mL solution delivers a faster electrospinning rate than the 7 %/0.7 solution.

4.2.3 The morphology of the synthesised supported TiO_2 nanofibres

The morphologies of the electrospun PAN/DMF and PAN/DMF/TiO_2 nanofibres were studied using high resolution scanning electron microscope (HRSEM), and are presented and discussed in the images below (Figure 4.4 – 4.6).

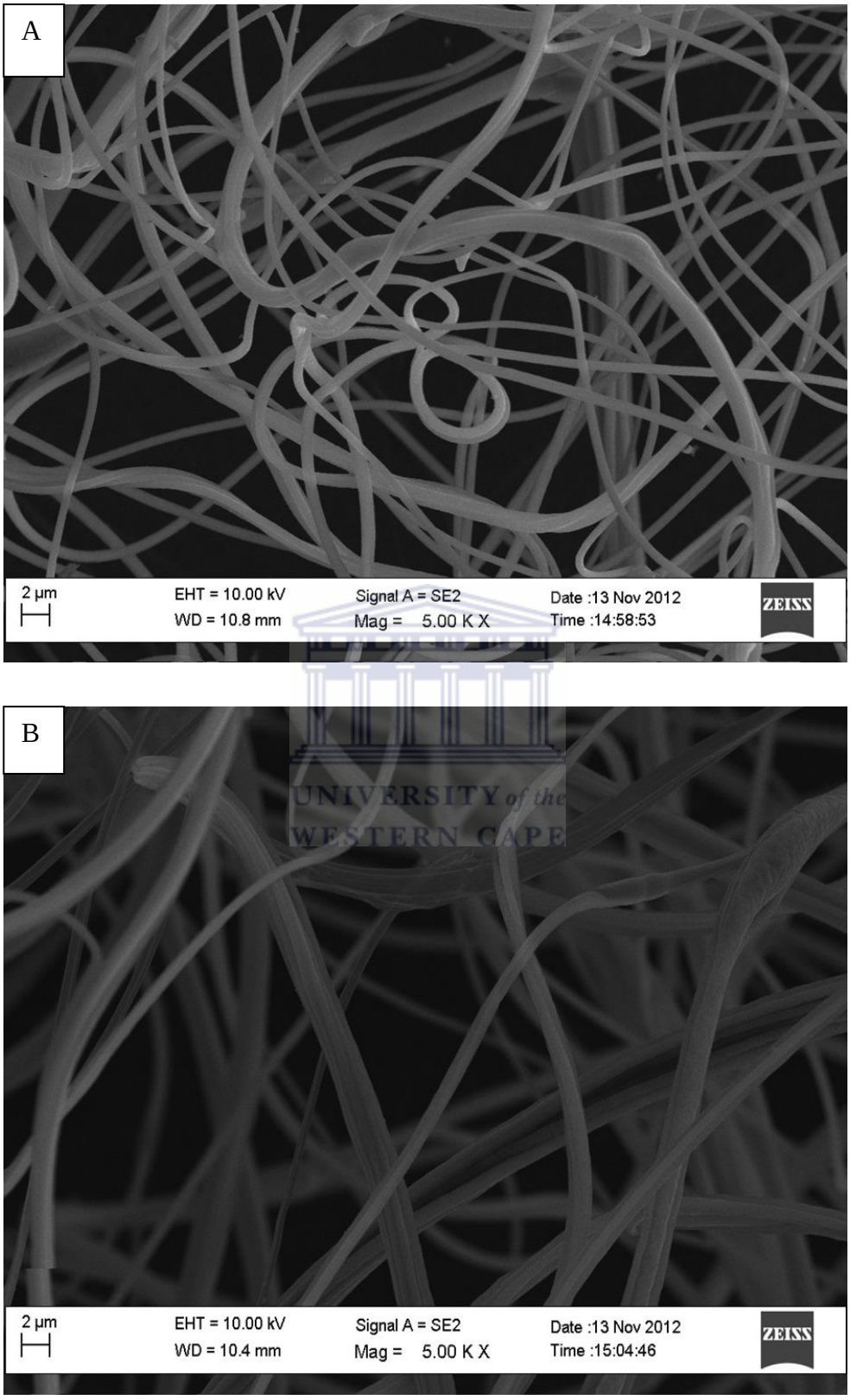

Figure 4.3: HRSEM images of TT1.1 - 7 % and TT1.1 - 8 % nanofibres

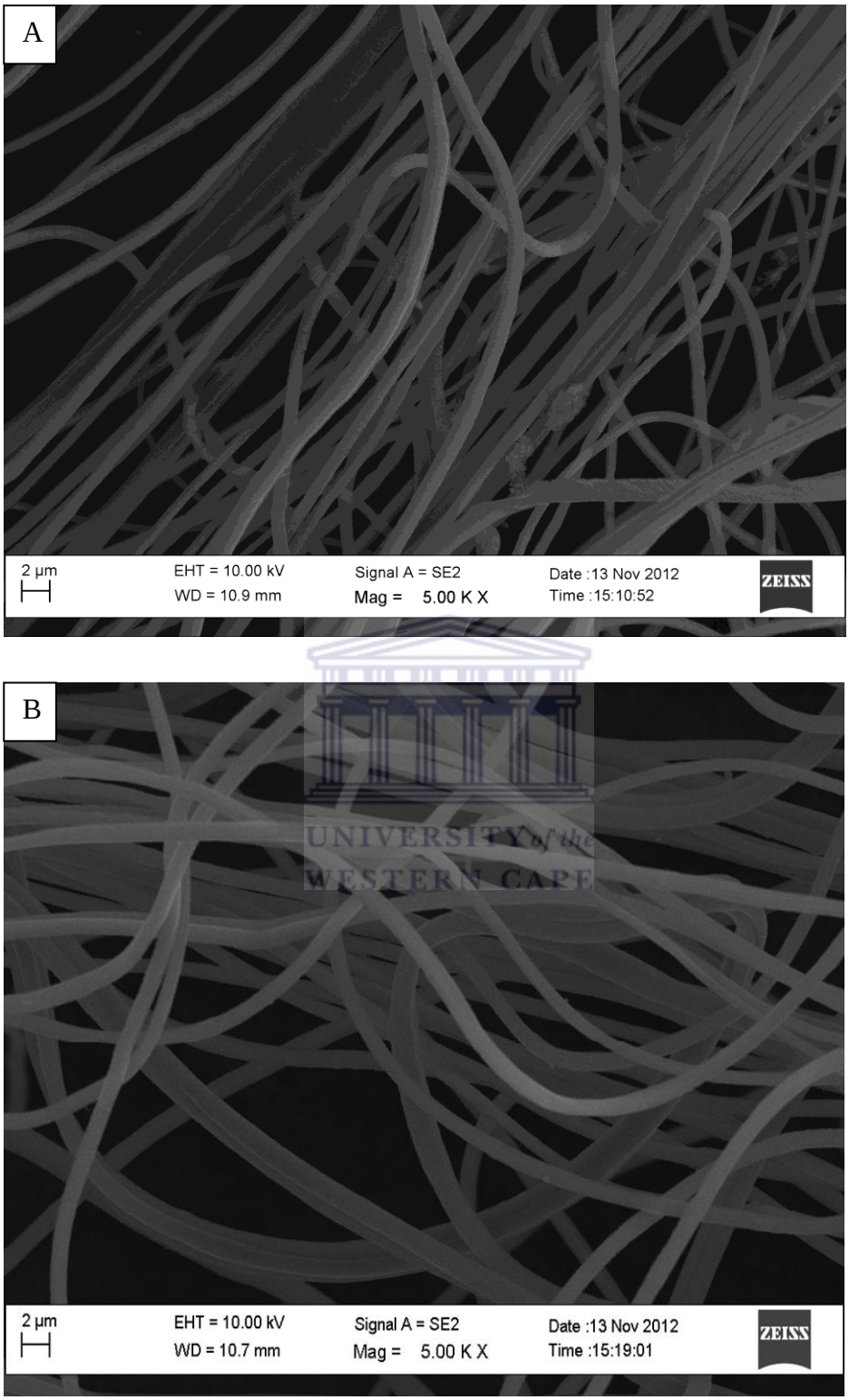

Figure 4.4: HRSEM images of TT1.2 (0.7 mL and 1.4 mL) of 7:1 titanium precursor

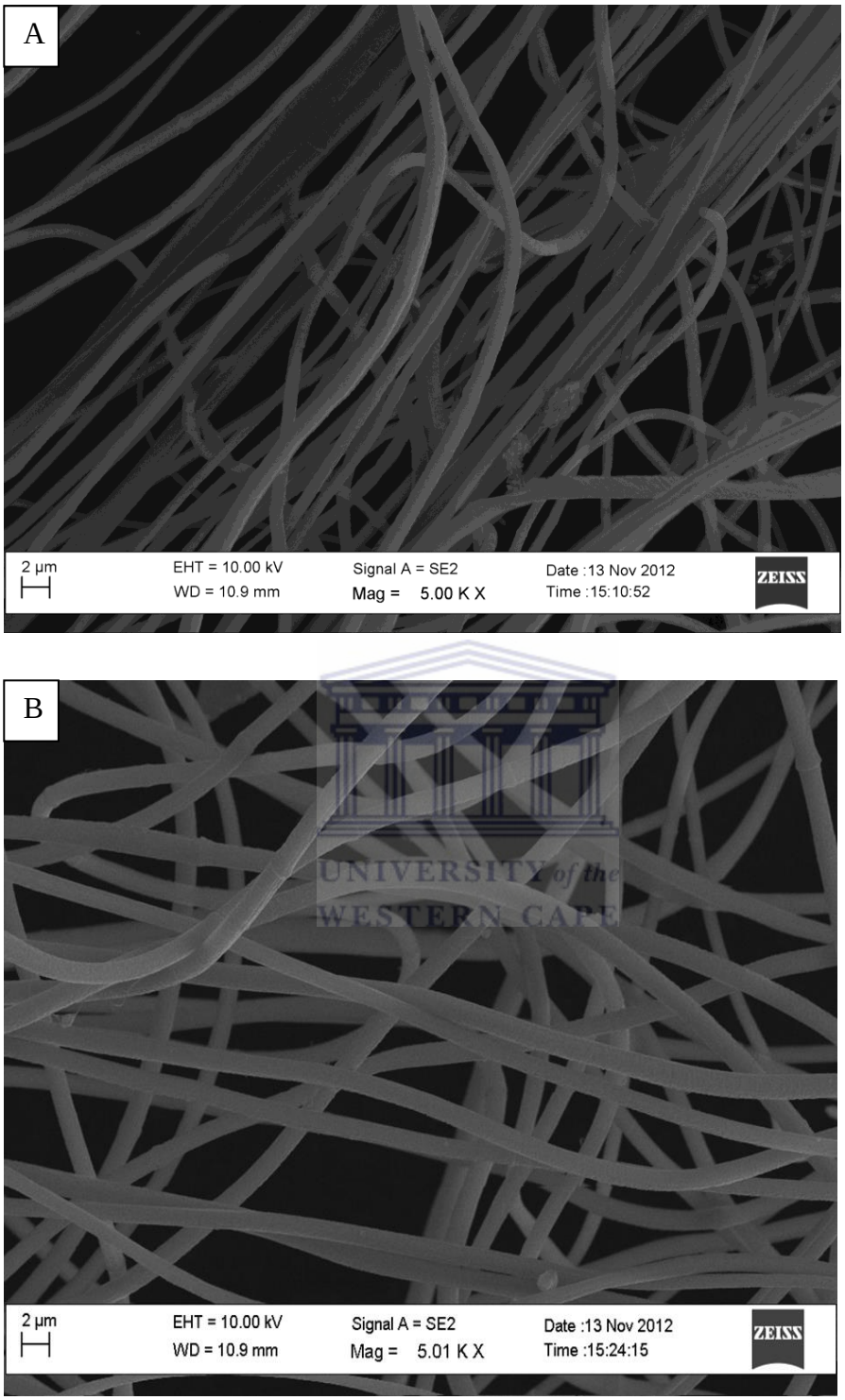

Figure 4.5: HRSEM images of TT1.2 and TT1.3 with 0.7 mL 7:1 titanium precursor

Figure 4.3 presents the HRSEM images and show the 7 % and 8 % PAN/DMF fibres electrospun without any Ti precursor added. The nanofibres showed a

smooth surface. Figures 4.4 and 4.5 demonstrates the morphology of the electrospun PAN/DMF/TiO_2 nanofibres and the images show smooth and singular fibres, hence the Exp 1 PAN/DMF/TiO_2 sol gel solution had the required viscosity for electrospinning. The 8 % composite PAN/DMF/TiO_2 nanofibres formed a fibrous structure with varying fibre diameters varying from 980 nm to 1.36 µm. The 7 % PAN/DMF/TiO_2 resulted in electrospun composite fibres with diameters in the range of 820 nm and 1.32 µm. It can be seen that the more viscous the PAN/DMF sol solution, the thicker the fibre diameter, but all the fibres were quite thick due to the electrospinning setup and not really nanometer in diameter.

4.2.3.1 The chemical bonding of the PAN/DMF/TiO_2 nanofibres

The chemical bonding of the synthesized PAN/DMF/TiO_2 nanofibres was studied using the FTIR and results are presented in Figure 4.6, 4.7 and 4.8.

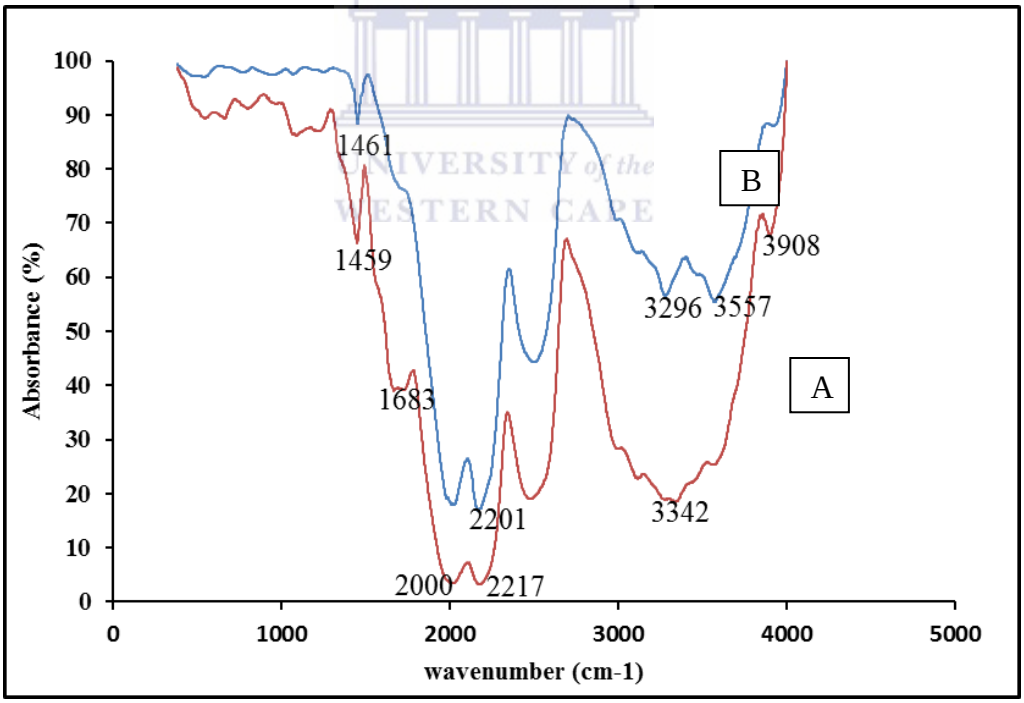

Figure 4.6: FTIR spectra for the nanofibres synthesized from [A] = TT1.1 8% and the [B] = commercial PAN (polyacrilonitrile nanopowder)

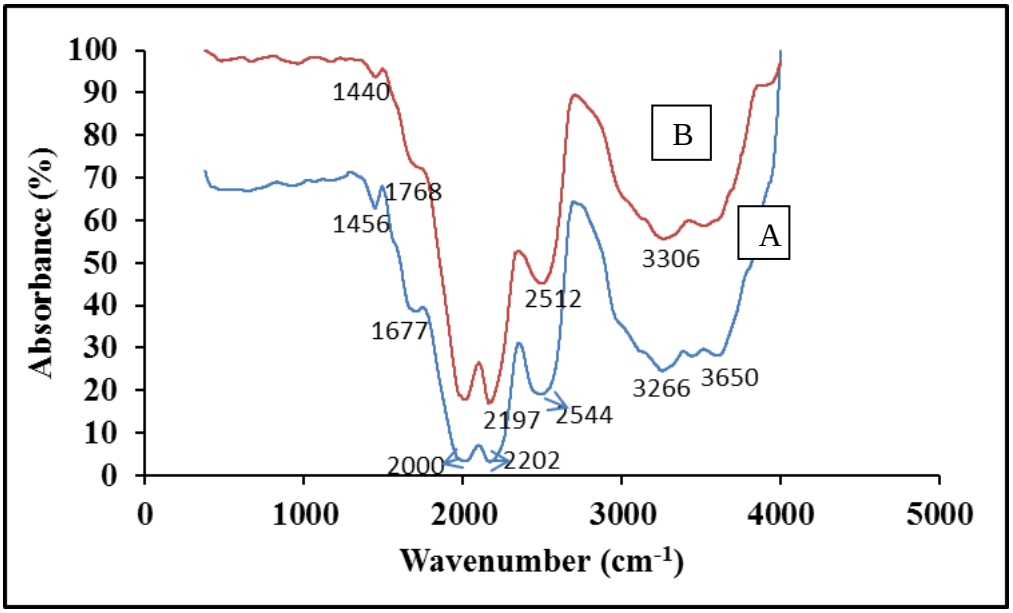

Figure 4.7: FTIR peaks for the TT1.2 (0.7 mL and 1.4 mL) 7:1 Ti-precursor

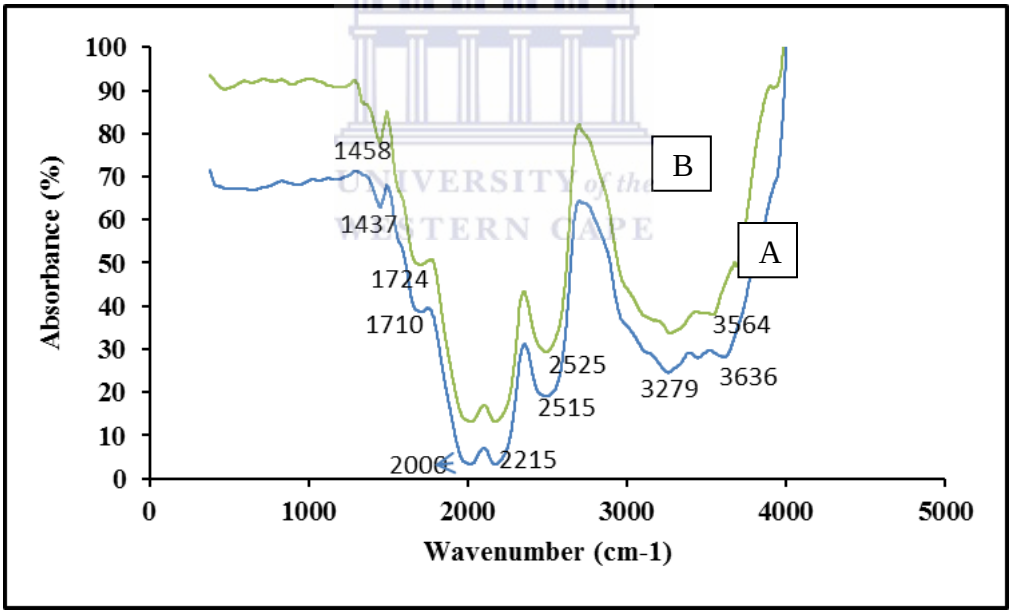

Figure 4.8: FTIR peaks for the TT1.2 and TT1.3 with 0.7 mL7:1 Ti-precursor

In Figure 4.6 B the FTIR spectrum of the commercial PAN which is the pure PAN powder bought from Sigma-Aldrich, contained the following absorption bands: 1070 cm^{-1} (skeletal vibrations of C-C bonds), 1455 (bending vibrations of CH_2 groups), 2247 cm^{-1} (stretching vibrations of C-N bonds), and 2865 and 2390 cm^{-1} (stretching vibrations of C-H bonds). In Figure 4.6 A of the spectra of the

nanofibre samples made from the PAN/DMF solutions without Ti-precursor, the most intense and easily identified bands were those of stretching vibrations of C=O bonds of DMF with a frequency of 1680 cm $^{-1}$. A spectroscopic method for determination of DMF content in PAN samples was based on measurement of the absorption of C=O bonds at 1680 cm^{-1} (Litovchenko & Girshgorn, 2004). The bands at 3296 and 3557 cm^{-1} have transformed on the PAN/DMF nanofibres to the band at 3306 cm^{-1} that corresponds to the OH broad peak, this proves the polymerization that took place during PAN/DMF solution preparation. In Figure 4.7 it is seen that as the volume of the titanium precursor increases the OH broad peak shortens, indicating the presence of TiO_2 in the nanofibres due to the Ti-OH bond. In Figure 4.8 the spectrums have similar peaks corresponding to the same functional groups.

4.2.3.2 The morphology of the decomposed supported PAN/DMF/TiO_2 nanofibres

The HRSEM technique was used for the study of the morphology of the supported TiO_2 nanocrystals, decomposed from the supported PAN/DMF/TiO_2 nanofibres synthesized through the liquid processing procedure explained and demonstrated in Section 3.4 (Exp one) and the PAN/DMF/TiO_2 nanofibres were synthesized according to the electrospinning details given in Section 3.5 and decomposed using the calcinations/stabilization and carbonization procedure explained in Section 3.6. The experimental conditions used for each experiment performed are presented in Table 4.3.

Table 4.3: Decomposed supported electrospun PAN/DMF/TiO_2 fibres

Unique name	Sample name	Solution	Method	Decomposition	Results (SEM images)
TT1.2 (Exp 1)	7 % PAN/DMF	7 % (0.7 mL 1: 2.5 Ti – precursor)	Electrospinning (Section 3.5)	Calcination and carbonization (Section 3.6)	Figure 4.10 A
TT1.2 (Exp 1)	7 % PAN/DMF	7 % (1.4 mL 1: 2.5 Ti – precursor)	Electrospinning (Section 3.5)	Calcination and carbonization (Section 3.6)	Figure 4.10 B
TT1.3 (Exp 1)	8 % PAN/DMF	7 % (1.4 mL 1: 2.5 Ti – precursor)	Electrospinning (Section 3.5)	Calcination and carbonization (Section 3.6)	Figure 4.10 C

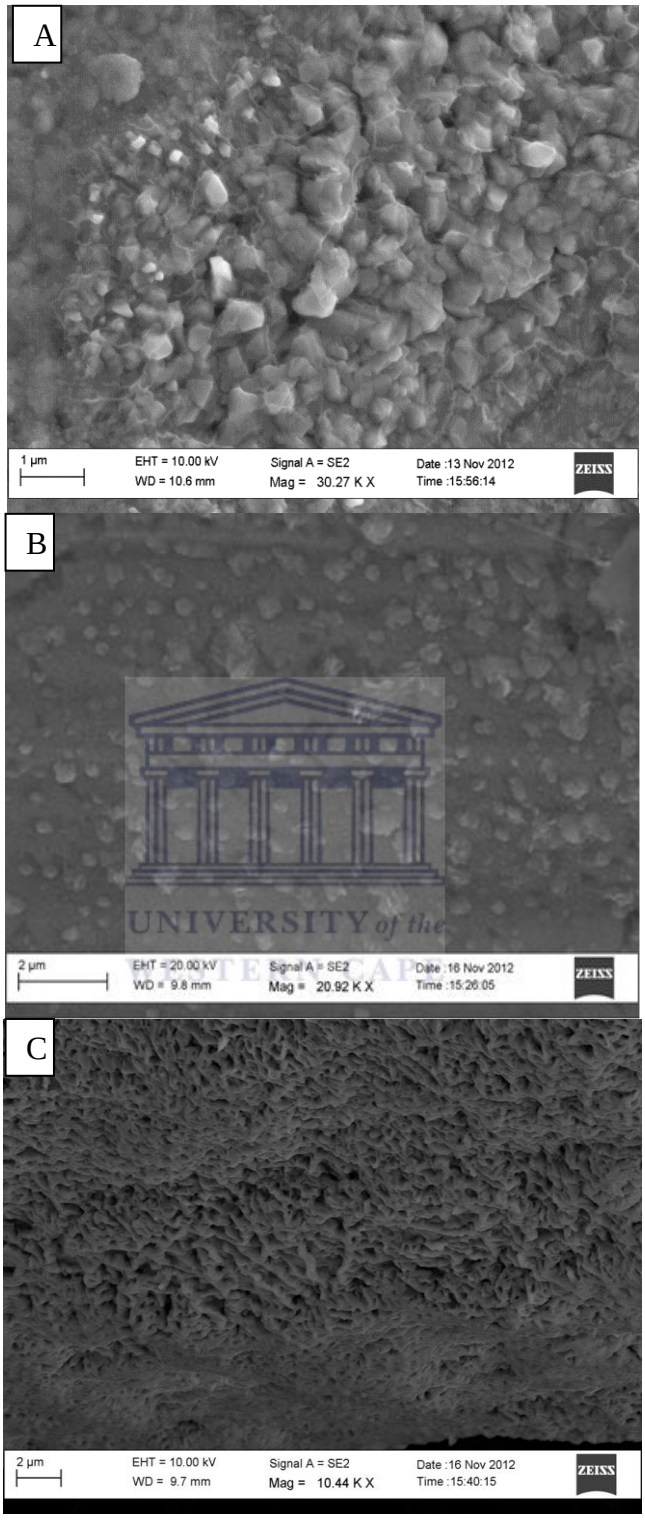

Figure 4.9: HRSEM images of TT1.2 (0.7 mL and 1.4 mL)7:1 titanium precursor and TT1.3 with 0.7 mL 7:1 titanium precursor

In Figure 4.9 HRSEM images presents the morphology of the supported composite TiO_2 nanocrystals as they were prepared from the different PAN/DMF/TiO_2 sol gel solutions decomposed through the process explained in Section 3.6. Image A (TT1.1) demonstrated the agglomeration of three dimensional embedded polycrystalline structures of the TiO_2 nanocrystals with diverse diameters prepared from 7 % PAN/DMF sol solution containing 0.7 mL of (7:1) molar ratio titanium precursor. Image B (TT1.2) presented the supported TiO_2 nanocrystals formed using 7 % PAN/DMF sol solution containing 1.4 mL of (7:1) molar ratio titanium precursor and shows that TiO_2 crystals were scattered consistently on the stainless steel mesh with diverse diameters. Image C (TT1.3) demonstrated the agglomerated TiO_2 nanocrystals structures made from 8 % PAN/DMF sol solution containing the 0.7 mL of (7:1) molar ratio titanium precursor with the crystal structure that are not completely developed.

4.2.3.3 Morphology of the decomposed supported precursor on the stainless steel mesh

The HRSEM images were taken to show the morphology and distribution of the TiO_2 nanocrystals that may have grown on the stainless steel mesh coated with the titanium precursor only as described in Section 3.4.2 and calcined/stabilized and thereafter carbonized using the technique described in Section 3.6. This baseline experiment was done as the blank to check if the supported TiO_2 nanocrystals were to grow and immobilise on the stainless steel mesh, and also proved the necessity of using the PAN/DMF/TiO_2 sol gel solution. The experiments conditions used for each experiment are presented in Table 4.4, with EDS results, showing atomic % TiO_2 in the composite.

Table 4.4: Experimental conditions for each synthesis and EDS data showing Ti%

Unique number	EDS (Ti %)	Results (SEM images)
TT (Exp 1)	0.5	Figure 4.11
TT1.4 (Exp 1)	0.4	Figure 4.12
TT1.5 (Exp 1)	0.2	Figure 4.13
TT1.6 (Exp 1)	0	Figure 4.14

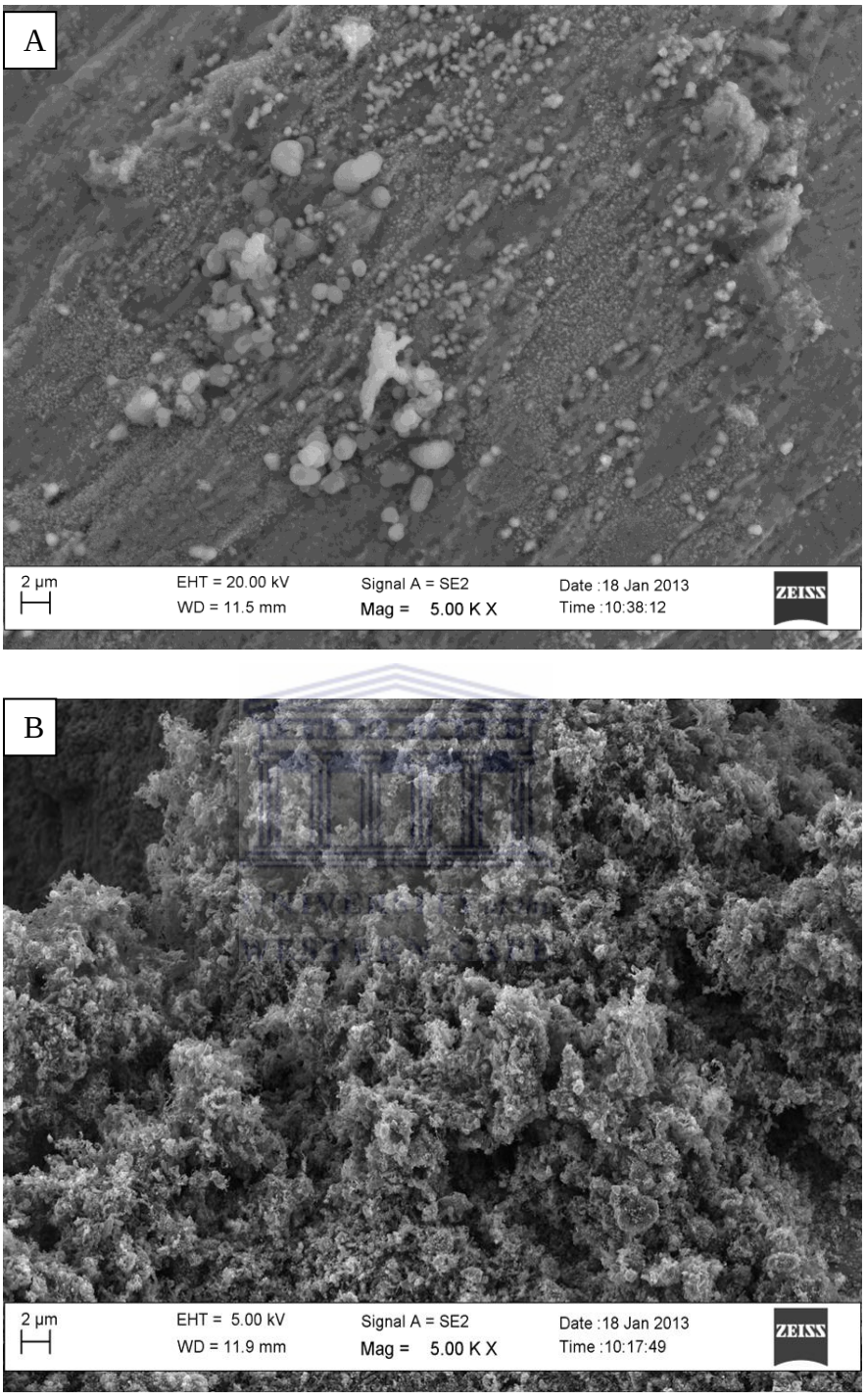

Figure 4.10: HRSEM images of TT (Blank)

Figure 4.10 (images A and B) show the stainless steel mesh that was coated with the (7:1) molar ratio titanium precursor (TT) without any PAN/DMF after morphology of the powder that grew on the stainless steel mesh. Characteristically the EDS showed a carbonization and the visual observation was

that the stainless steel mesh was coated with black powder. Image B shows the random analysis of the Ti element present after carbonization of the sample to be 0.5 atomic % (Table 4.5).

Table 4.5 presents the EDS random elemental content composed of Al, Cr, Mn, Si, Ca, Fe and Ni that represents the stainless steel mesh composition. There is also a trace of solvents and Cl which is the residue of the $TiCl_4$ used as the (7:1) molar ratio titanium precursor.

Table 4.5: EDS random element contents

Element	Atomic %
Al	1.4
Si	2.5
Cl	1.4
Ca	1.0
Ti	0.5
Cr	16.1
Mn	1.0
Fe	69.6
Ni	6.6
Total:	**100**

4.2.3.4 Morphology of the decomposed stainless steel mesh coated with sol gel solution

The HRSEM images of the decomposed coated stainless steel mesh are presented in Figure 4.11. The stainless steel mesh was first coated with the 7:1 molar ratio titanium precursor (Section 3.4.2) and left to dry, thereafter the stainless steel

mesh was again manually coated with the 8 % PAN/DMF/TiO_2 sol gel solution prepared in Section 3.4.3.

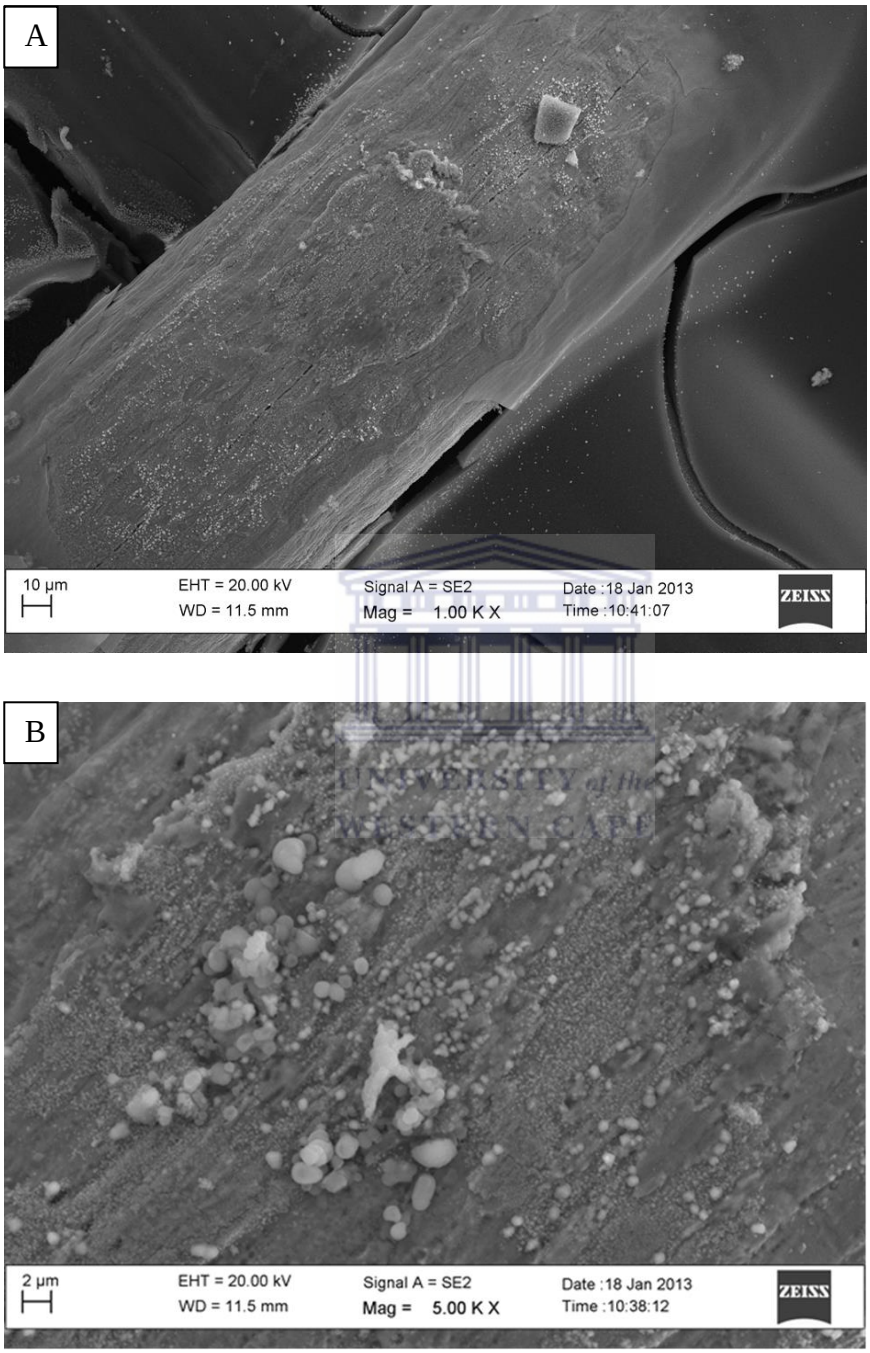

Figure 4.11: HRSEM images of (TT1.4)

Figure 4.11 HRSEM images of (TT1.4) show that there were small randomly orientated particles that were not distributed evenly upon the stainless steel mesh

after carbonization and decomposition. Characteristically the EDS showed a random analysis of the amount of Ti element present on the sample to be 0.4 atomic %, thus the small particles supported on the stainless steel mesh are assumed to be TiO_2. The HRSEM images of the decomposed coated stainless steel mesh are presented in Figure 4.12. The stainless steel mesh was coated with the 7 % sol gel solution and 7:1 titanium precursor.

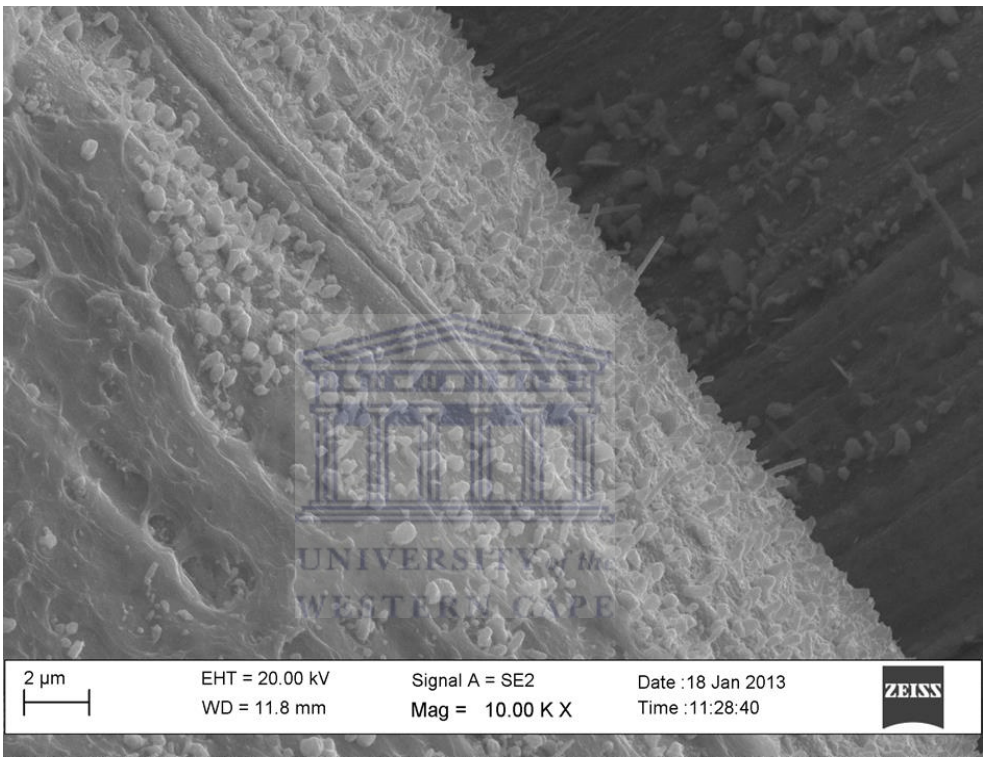

Figure 4.12: HRSEM image (TT1.5)

The HRSEM image (TT1.5) in Figure 4.12 shows small particles that are assumed to be TiO_2 nanocrystals with crystal morphology materializing on the surface of the support. Characteristically the EDS showed a random analysis of the amount of Ti present on the sample to be 0.2 %.

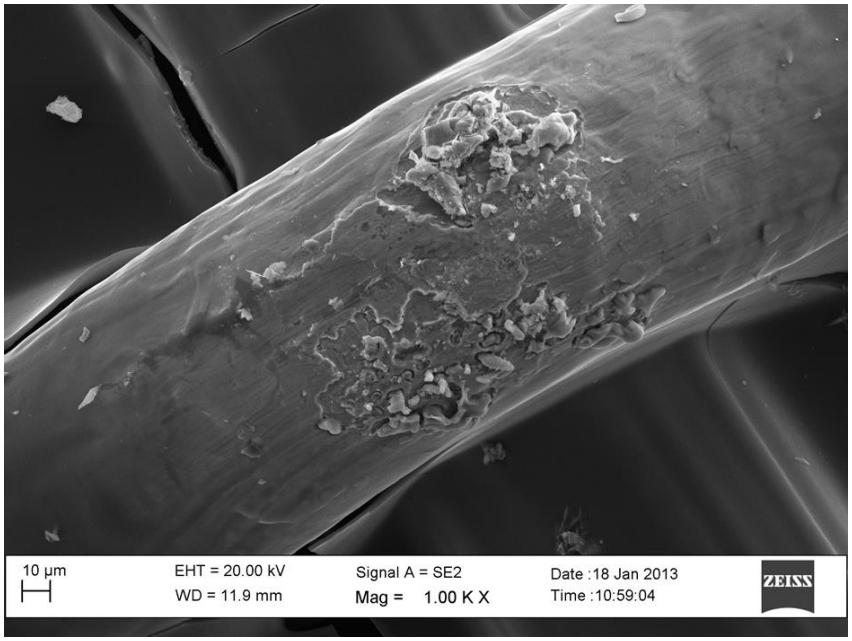

Figure 4.13: HRSEM image of TT1.6

Figure 4.13 of (TT1.6) shows no TiO_2 nanoparticles deposited on the surface of the supporting material. Characteristically the EDS showed a random analysis of the Ti element present on the sample of only 0.04 atomic %. Therefore the titanium precursor prepared using 0.09 M $TiCl_4$ in 20 % HCl contained a diminutive amount of Ti, resulting in a restricted amount of TiO_2 nanocrystals formation which are too few for the best photocatalysis. Hence these formulations and coating methods were not useful. However the results showed that the concentration of the $TiCl_4$ used to prepare the titanium precursor necessitates to be increased.

4.3 Experiment Two: Morphology of the decomposed electrospun supported TiO_2 nanofibres prepared from the 99 % pure $TiCl_4$ precursor

The HRSEM images were taken to show the morphology of the TiO_2 nanofibres that may have grown on the stainless steel mesh after the meshes coated with the 8 % sol gel solution by electrospinning. The experimental conditions used for

each experiment are presented in Table 4.6, with the EDS results showing the atomic % of Ti deposited on the supports.

Table 4.6: Experimental conditions for each synthesis

Unique name	Solution	Method	Decomposition	EDS (Ti %)	Results (SEM images)
TT2.1 (Exp 2)	8 % sol gel solution and acetone hydrolisation (Section 3.6)	Electrospining (Section 3.5)	Calcination and carbonization (Section 3.7)	7.77	Figure 4.15 A
TT2.2 (Exp 2)	8 % sol gel solution and distilled water hydrolisation (Section 3.6)	Electrospining (Section 3.5)	Calcination and carbonization (Section 3.7)	1.19	Figure 4.15 B
TT2.3 (Exp 2)	8 % sol gel solution (Section 3.6)	Manual Coating (Section 3.10)	Calcination and carbonization (Section 3.7)	0.71	Figure 4.16 A
TT2.3 (Exp 2)	8 % sol gel solution (Section 3.6)	Manual Coating (Section 3.10)	Calcination (Section 3.10)	2.29	Figure 4.16 B

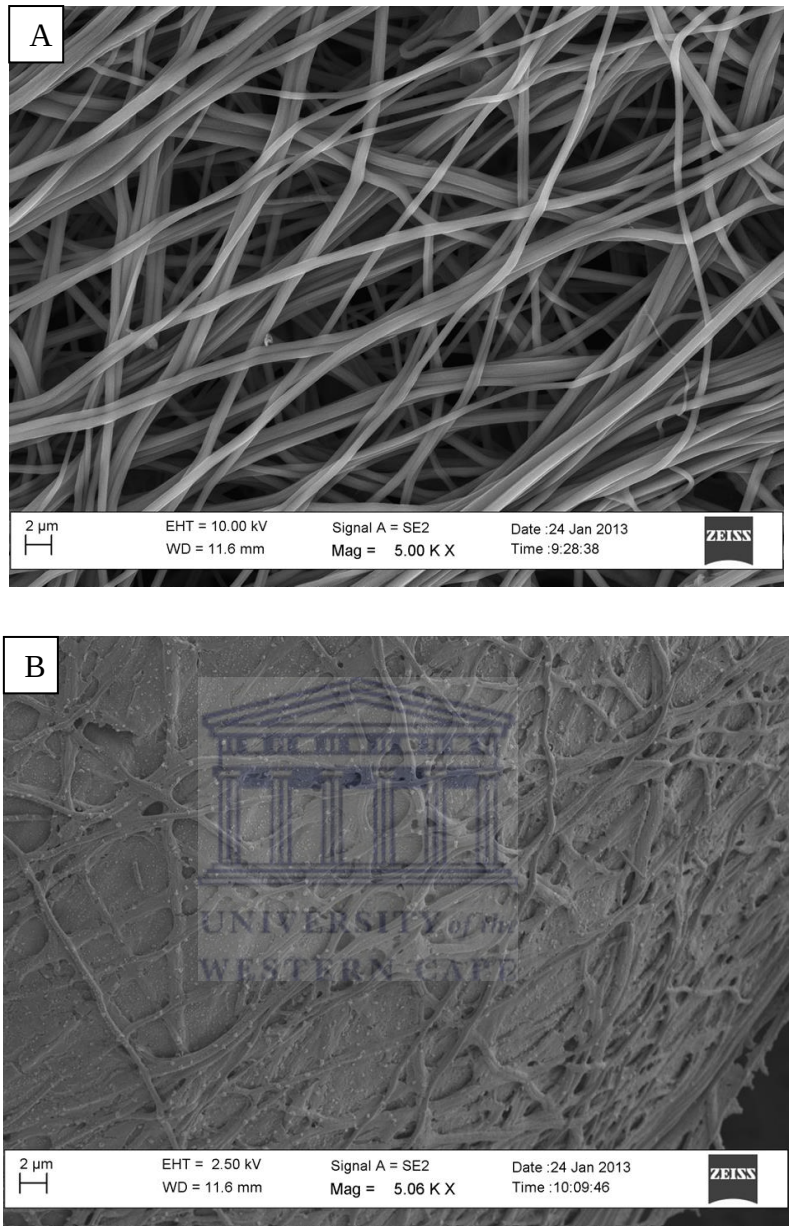

Figure 4.14: HRSEM images of (TT2.1) and (TT2.2)

Figure 4.14 TT2.1 sample from Table 4.6 and shows that the carbonized PAN/DMF/TiO_2 nanofibres remained intact when hydrolysed with acetone and carbonization but no particles materialised on the surface of the stainless steel mesh and unpredictably the EDS confirmed the random significant presence of the Ti at 7.8 atomic % for the decomposed supported PAN/DMF/TiO_2 nanofibres, but not well adhered. TT2.2 demonstrated the supported PAN/DMF/TiO_2 nanofibres after deionised water was used to hydrolize them before carbonization,

and the TiO_2 nanofibres were well adhered to on the surface of the stainless steel mesh after carboniation. The EDS confirmed the random presence of the Ti at 1.2 atomic %. Even though the EDS for the TT2.1 (Figure 4.15 A) gave the highest titanium qualitative element composition there were no TiO_2 nanocrystals materialised on the surface of the stainless steel mesh after carbonization, hence the acetone hydrolyzation promotes the Ti concentration in the supported TiO_2 decomposed fibres. However does not enhance the growth of the TiO_2 nanocrystal structure having large surface area for photocatalysis. Therefore the TiO_2 containing nanofibre prepared by this route did not produce crystalline structures.

The present research synthesized the TiO_2 nanofibres by the combination of electrospinning and sol gel techniques using PAN/DMF sol solution and the titanium precursor ($TiCl_4$ in 20 % HCl and acetyl acetone). Chuangchote et al, (2009) fabricated TiO_2 nanofibres by the combination of electrospinning and sol gel techniques using poly(vinylpyrrolidone) (PVP), titanium(IV) butoxide, and acetylacetone in methanol as a spinning solution.The electrospinning method was used for generating TiO_2 fibres combined with the sol gel process (Park et al, 2011). For preparation of TiO_2 nanofibres, a Ti-precusor sol gel solution with a polymer matrix was used as the starting material to proceed under a high electrical field (Lin et al, 2011). The good quality composite PAN/DMF/TiO_2 nanofibres were synthesized from the 8 % PAN/DMF/TiO_2 sol gel solution with a 7.8 atomic % Ti content but they were unsupported and thus not suitable for ease of separation. TiO_2 nanocomposites were fabricated by coating the support with the Ti-precursor/polymer mixture solution, followed by decomposition at high temperatures for enhancing the adhesion of PAN/DMF/TiO_2 nanocrystals to the substrates.

4.4 Morphology of the supported nanocrystals formed from a 8 % (PAN/DMF/TiO_2) sol gel solution coated stainless steel mesh

The HRSEM technique was used to investigate the morphology of the (TT2.3) TiO_2 nanocrystals developed on the 8 % The manual coating method is straight

forward, unlike the electrospinning process that requires the power supply to electrospun the fibre and hydrolysis technique to adhere the fibres onto the stainless steel mesh.

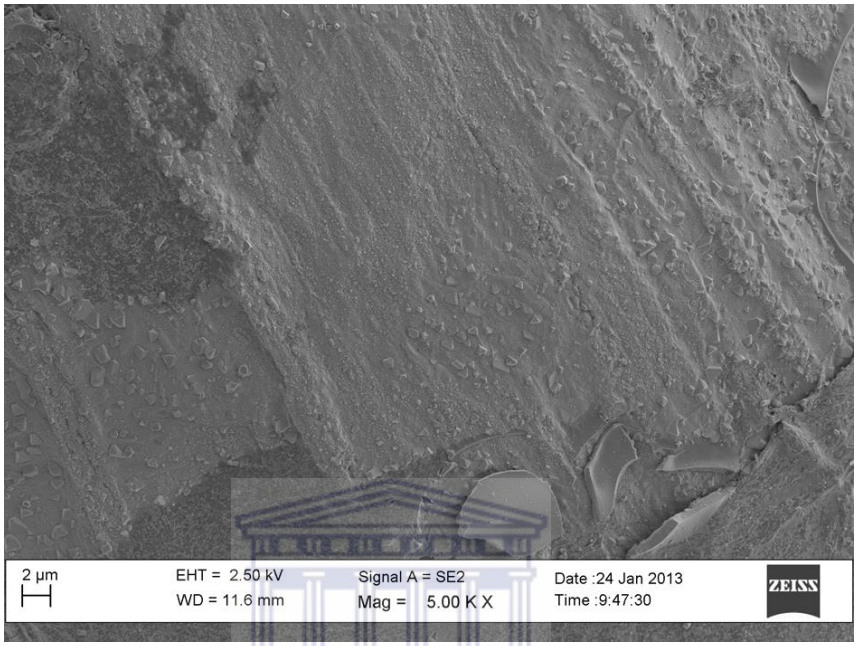

Figure 4.15: HRSEM image of TT2.3

Figure 4.15 of (TT2.3) nanocrystals were materializing on the mesh after calcining and carbonizing but still did not have three dimensional structural morphology. These supported TiO_2 nanocrystals were embedded within the stabilised PAN, as some of the TiO_2 nanocrystals were fully deposited on the surface of the supporting material. The EDS confirmed the random presence of the Ti at 0.7 atomic %. Therefore, the full decomposition of the PAN was required to obtain the TiO_2 nanocrystals on the surface of the stainless steel mesh. The stainless steel mesh coated with the 8 % sol gel solution was heated at a very high heating rate of 50 °C/min to 600 °C and deformed the polymer PAN.

4.5 Experiment Three: Calcined stainless steel mesh coated with the 8 % (PAN/DMF/TiO_2) sol gel solution prepared from the 99 % pure $TiCl_4$

The purpose of this experiment was to develop the porous supported TiO_2 nanocrystals with an easy deposition method and at a shorter period in the furnace for decomposition. The experimental conditions used for this experiment are presented in Table 4.7 with the EDS results showing the Ti content.

Table 4.7: Conditions applied to prepare TiO_2 nanocrystals supported on the stainless steel mesh and EDS results

Unique name	Solution	Method	Decomposition	EDS (Ti atomic %)	Results (SEM images)
TT3.1 (Part 3)	8 % PAN/DMF/TiO_2 (Section 3.11)	Coating (Section 3.10)	50 °C/min at 280 °C in air and 5 °C/min at 600 °C in air	2.29	Figure 4.17

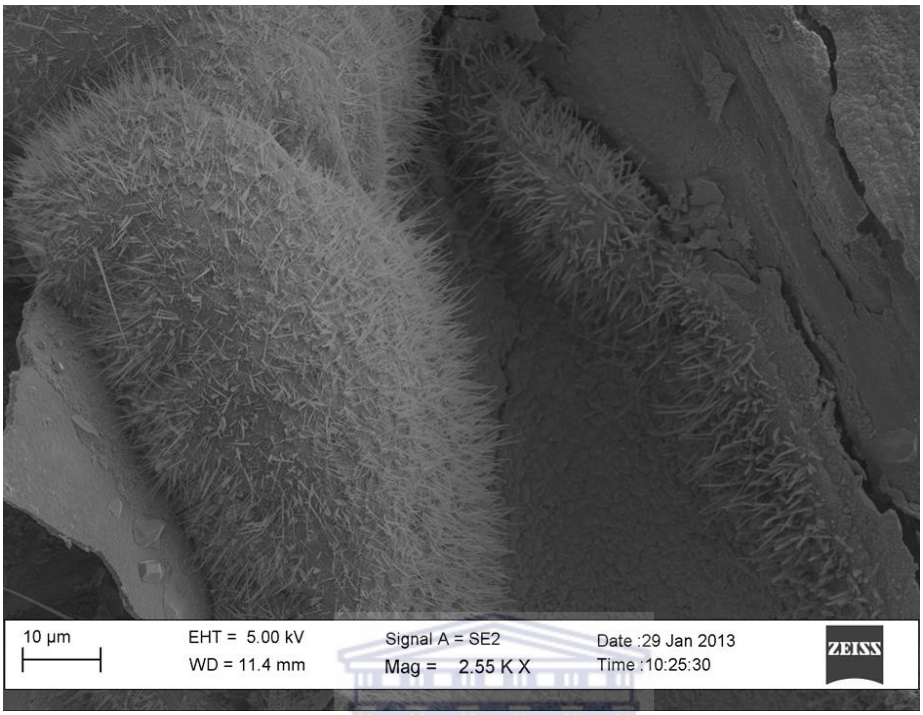

Figure 4.16: HRSEM image of TT3.1

Figure 4.16 (TT3.1) shows the presence of TiO_2 nanocrystals with a needle-like structure. TiO_2 nanocrystals were well developed across the surface of the stainless steel mesh proving that the polymer PAN had decomposed though fragmentation and deformation under the applied conditions. The EDS confirmed the random presence of Ti at 2.3 atomic %. Therefore, the carbonization condition applied in air, which were the calicination/stabilization was adequate to form TiO_2 supported upon the stainless steel support. Hence the fragmentation of the polymer PAN was necessary to create TiO_2 nanocrystals. However the temperature and the holding time needed further optimization to master the deposition of the composite TiO_2 nanocrystals, which is presented in the following sections.

4.6 Experiment Four: Optimization of the conditions to form supported TiO_2 nanocrystals on the stainless steel mesh support

The mass deposited on the stainless steel mesh after optimized calcination conditions using the method described in Section 3.11 is presented in Table (4.4, 4.5, 4.6 and 4.7) according to the decomposition temperatures applied. The standard deviation of the deposited TiO_2 nanocrystals on the 250 mm^2 stainless steel mesh was calculated to check the variation of the masses deposited and to see the precision of the masses deposited (see Appendix one). The experimental conditions are given in Table 4.8. Each sample was replicated three times and the average mass of TiO_2 are presented in Table 4.9, 4.10, 4.11 and 4.12.

Table 4.8: Experimental conditions for each synthesis

Unique name	Decomposition	Results (SEM images)
TT4.1 (Exp 4)	50 °C/min to 300 °C in air holding time = (1 h, 2 h, 3 h, 4 h, 5 h or 6 h)	Figure 4.19
TT4.2 (Exp 4)	50 °C/min to 400 °C in air holding time = (1 h, 2 h, 3 h or 4 h)	Figure 4.20
TT4.3 (Exp 4)	50 °C/min to 500 °C in air holding time = (1 h, 2 h, 3 h or 4 h)	Figure 4.21
TT4.3 (Exp 4)	50 °C/min to 600 °C in air holding time = (1 h, 2 h, 3 h or 4 h)	Figure 4.22

4.6.1 Mass percentage TiO_2 deposited after degradation

The mass percentage of the deposited TiO_2 nanocrystals on the stainless steel mesh that was achieved through the stainless steel mesh coating method (Section 3.10) using 8 % PAN/DMF/TiO_2 sol gel solution (Section 3.11) and decomposed by calcination (Section 3.11) is presented in Figure 4.17. Various temperatures and holding times were applied as set out in Table 4.8 - 4.11.

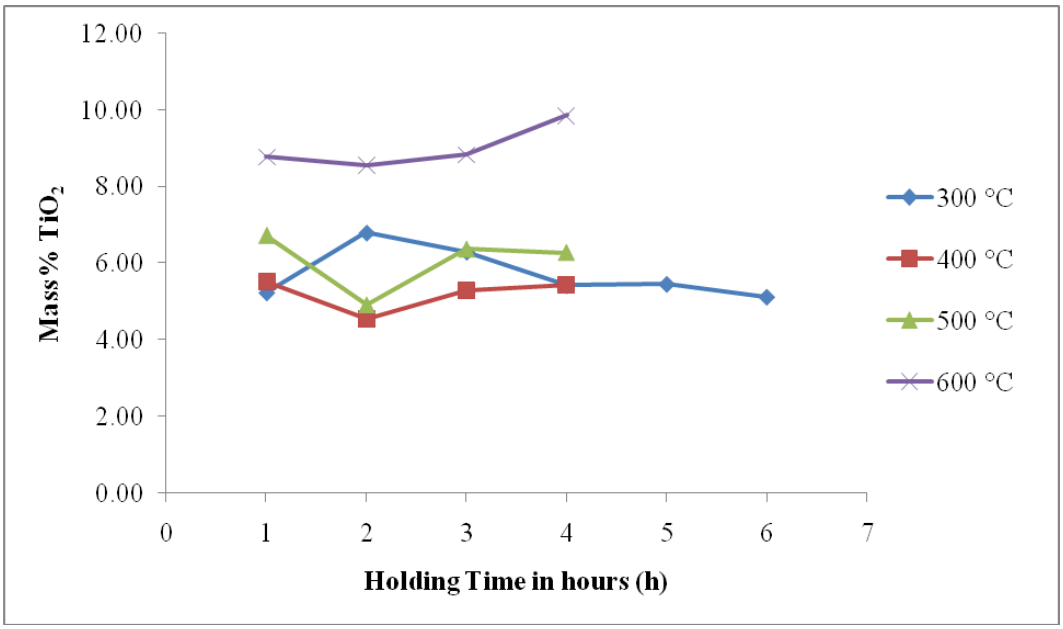

Figure 4.17: Mass percentage of immobilised TiO_2 obtained by various decomposition temperatures and holding times using the 8 % PAN/DMF/TiO_2 sol gel solution coating method

Figure 4.17 shows that the mass of TiO_2 decomposed onto the stainless steel support at 300 °C for 1 h up to 6 h holding time fluctuated slightly between 10 – 12 mass percent loading. The mass percent loading of the TiO_2 composite decomposed at 300 °C is higher than the mass loading decomposed at 400 °C as the polymer is not fully decomposed. The mass percentage loading decomposed at 400 °C is fairly even and probably polymer is mainly decomposed. The samples with the mass loading decomposed at 500 °C vary between 10 - 14 mass percent loading. The mass percentage loading decomposed at 600 °C is gradually increasing with the increase in holding time and this increase may be due to the excess formation of the oxides, furthermore the anatase may be starting to transform to rutile phase, as the rutile is denser than the anatase (4.25 g/cm^3 versus 3.894 g/cm^3) (Ahmad et al, 2008). The increase in temperature causes the TiO_2 anatase to expand its crystal structure and forming more oxides, hence increasing the mass of the sample loaded on the support. The qualitative identification of the mineral phase formed after coating and decomposing 8 %

(PAN/DMF/TiO_2) sol gel solution on the stainless steel, forming the crystalline compounds was then measured using the XRD.

4.6.2 Characterization of calcined TiO_2 nanocrystals using the XRD technique

XRD characterisation was carried out to identify the crystalline phase from the XRD patterns and determine the particle size of the TiO_2 nanocrystals. The XRD results of samples coated using the 8 % PAN/DMF/TiO_2 sol gel solution (Section 3.11) and a heating profile of (300 °C, 400 °C, 500 °C and 600 °C) for 2 h are presented in Figure 4.18.

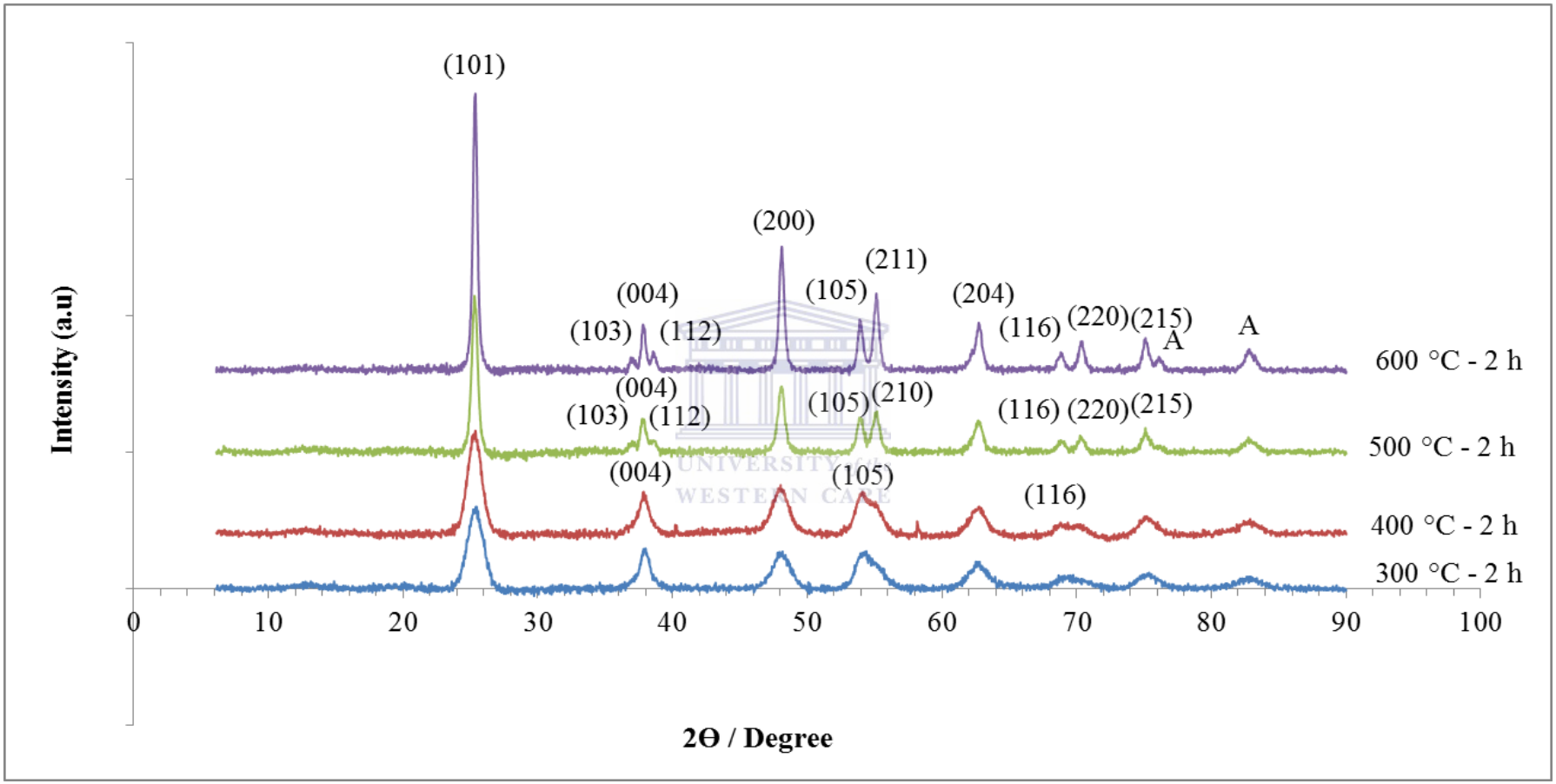

Figure 4.18: XRD pattern of 8 % (PAN/DMF/TiO_2) decomposed TiO_2 at 50 °C /min and different holding temperatures for 2 h for samples (TT4.1B), (TT4.2B), (TT4.3B) and (TT4.4B)

Figure 4.18 shows representative patterns of the X-ray diffraction (XRD) obtained for TiO_2 nanocrystals with the anatase crystal phase.. All samples prepared by various methods produced the anatase phase with varying degree of crystallinity. The peaks illustrated in the XRD patterns correspond to the (101), (103), (004), (112), (200), (105), (211), (204), (116), (220) and (215) planes of TiO_2 tetragonal anatase phase. These patterns can be well indexed to tetragonal anatase. The recorded XRD matches with the JCPDS pattern of TiO_2 anatase, body centered tetragonal, a = 3.8101 Å, b = 3.8101, c = 9.3632, α = 90°, β = 90°, γ = 90° (Hackeyley and Ferraris, 2001).

Crystallinity of the calcined supported 8 % (PAN/DMF/TiO_2) TiO_2 nanocrystals at various temperatures were studied. The crystallite size was estimated from the Debye–Scherrer equation (Mahshid et al, 2006) using the XRD line broadening as follows:

$$B = (k \lambda) / (s \cos \theta) \quad \text{.....4.2}$$

The s is the crystallite size, λ is the wavelength of the X-ray radiation (Cu$K\alpha$ = 0.15406 nm), k is a constant taken as 0.94, θ is the diffraction angle and B is the line width at half maximum height. The (101) plane diffraction peak is used for anatase as it is the most intense peak. The effect of calcination temperatures on the crystallinity of TiO_2 is reported in Table 4.13. As seen in Table 4.13, the smallest crystallites are obtained at lower calcination temperatures. At higher calcination temperatures, the formed crystallites are larger in size, which can be attributed to the thermally promoted crystallite growth. The size of the anatase crystallites increased from 13.6 to 19.3 nm when the calcination temperature was raised to 400 °C for 3 h holding time. Furthermore, the crystallite size is increased from 455 to 2285 nm at 600 °C. In Table 4.13 the particle size determined by Debye Scherrer equation applied to the XRD data of each decomposed 8 % (PAN/DMF/TiO_2) samples are presented. There are peak splitting at the XRD pattern for TT4.2 B at (105) and (116) this was assumed to be the crystallinity that is still forming, as at TT4.3 B at (105) the peaks were completely separated to

(105) and (210), while at (116) the peaks were completely separated to (116) and (220).

Table 4.9: Size of decomposed 8 % (PAN/DMF/TiO_2) TiO_2 nanocrystals from XRD

Sample name	Condition	Crystal size (nm)
TT4.1 A (Exp 4)	300 °C – 1 h	13.6
TT4.1 B (Exp 4)	300 °C – 2 h	15.3
TT4.1 C (Exp 4)	300 °C – 3 h	15.3
TT4.1 D (Exp 4)	300 °C – 4 h	15.1
TT4.1 E (Exp 4)	300 °C – 5 h	15.8
TT4.1 F (Exp 4)	300 °C – 6 h	15.9
TT4.2 A (Exp 4)	400 °C – 1 h	15.1
TT4.2 B (Exp 4)	400 °C – 2 h	17.3
TT4.2 C (Exp 4)	400 °C – 3 h	19.3
TT4.2 D (Exp 4)	400 °C – 4 h	455
TT4.3 A (Exp 4)	500 °C – 1 h	455
TT4.3 B (Exp 4)	500 °C – 2 h	760
TT4.3 C (Exp 4)	500 °C – 3 h	759
TT4.3 D (Exp 4)	500 °C – 4 h	760
TT4.4 A (Exp 4)	600 °C – 1 h	1141
TT4.4 B (Exp 4)	600 °C – 2 h	761
TT4.4 C (Exp 4)	600 °C – 3 h	2285
TT4.4 D (Exp 4)	600 °C – 4 h	2285

4.6.3 Supported TiO_2 nanocrystals formed from 8 % PAN/DMF/TiO_2 sol gel solution prepared with the 99 % pure $TiCl_4$ precursor

HRSEM characterisation was used to image the morphology of the TiO_2 nanocrystals developed using the 8 % (PAN/DMF/TiO_2) sol gel solution coated stainless steel mesh using the method illustrated in Section 3.10 and decomposed by calcination 50 °C/min at 300 °C for (1 h, 2 h, 3 h, 4 h, 5 h or 6 h) described in Section 3.11. In this section samples prepared as set out in Table 4.8 and in Figure 4.19 TT4.1 (A - F) are presented.

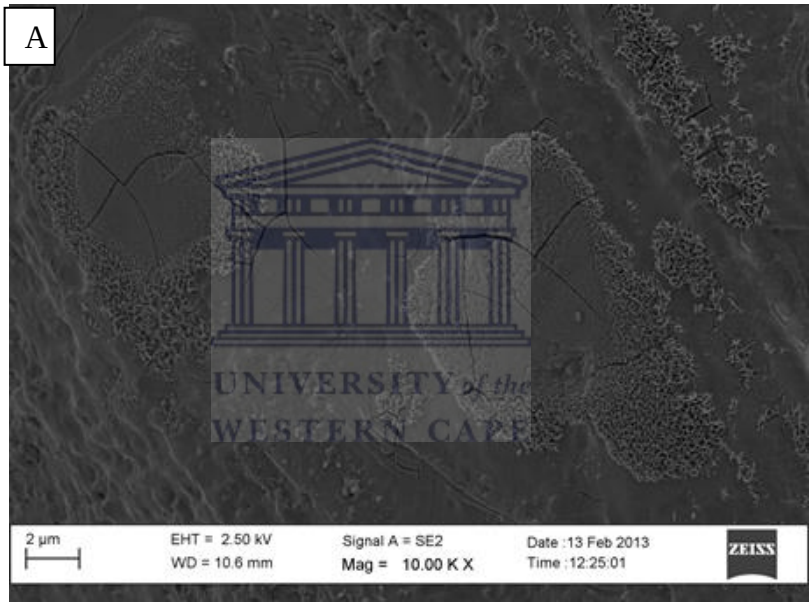

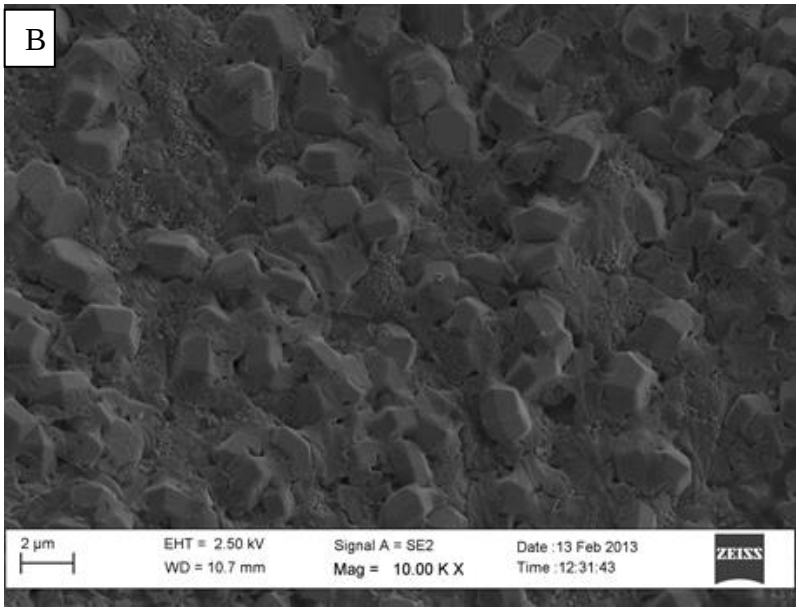

C

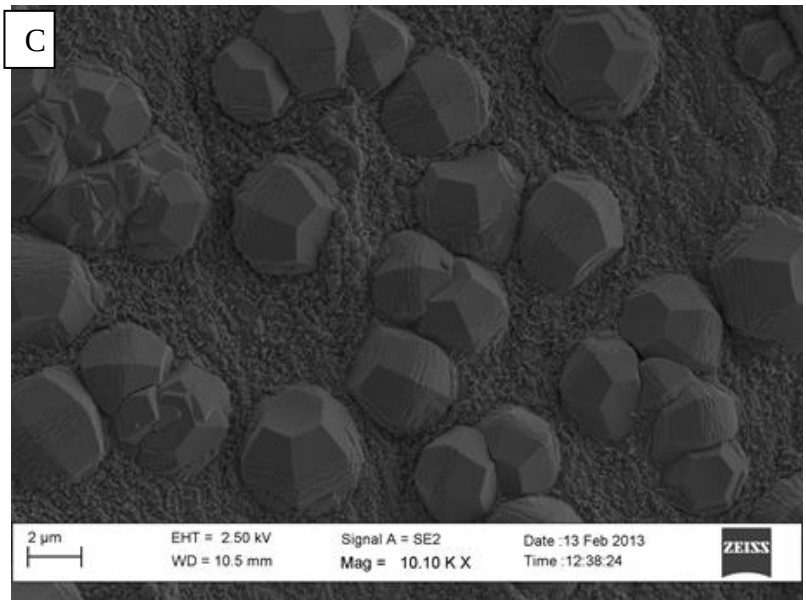

D

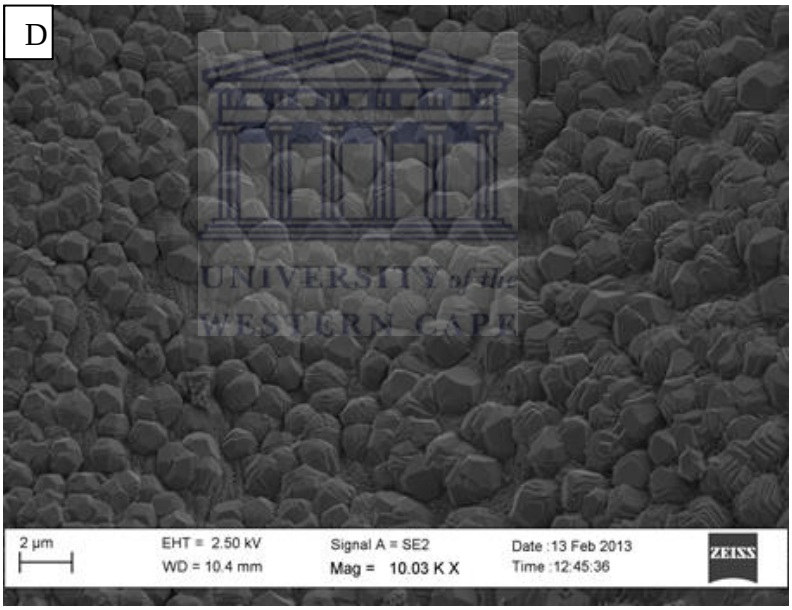

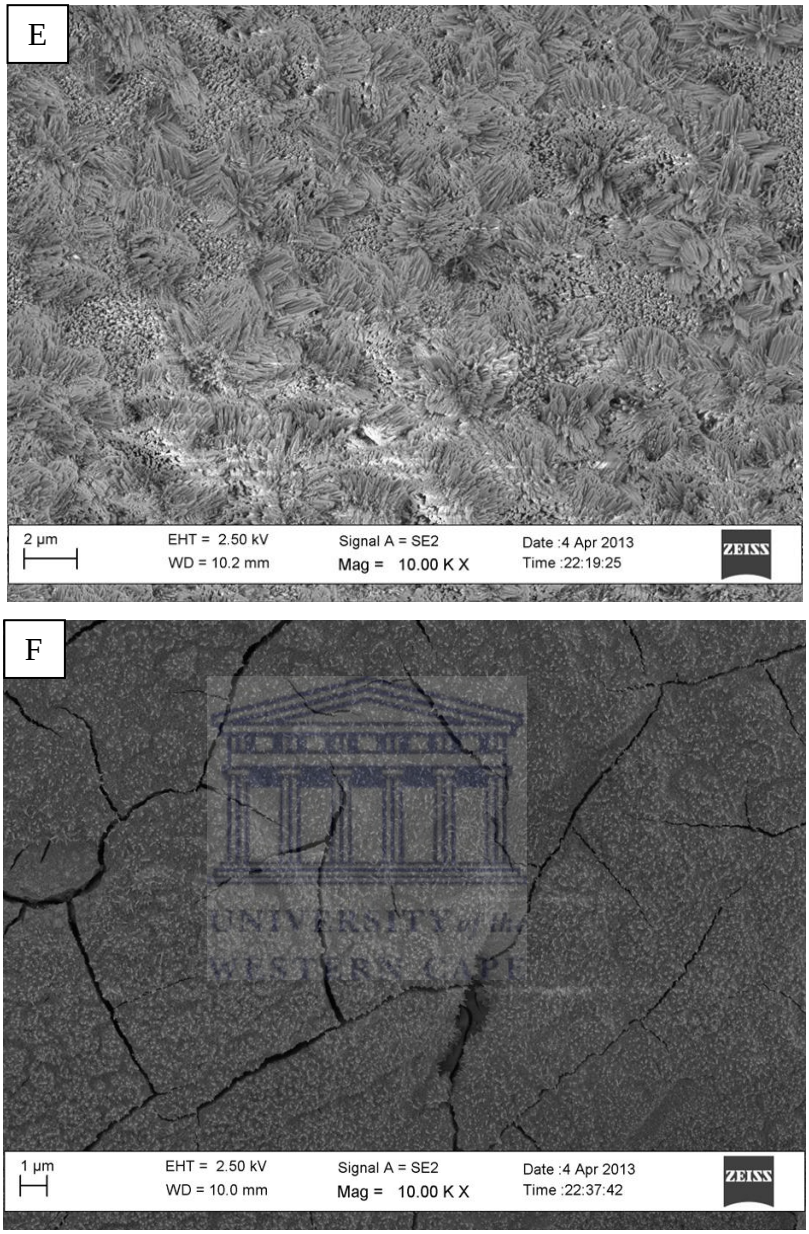

Figure 4.19: HRSEM images of TT4.1

In Figure 4.19 A (TT4.1) there are no TiO_2 crystals to be seen after carbonization in air for 1 h at 300 °C while in B (TT4.1) TiO_2 crystals appear after 2 h carbonization at 300 °C but are not fully developed and are still embedded inside the polymer (PAN). In C (TT4.1) after 3 h carbonization at 300 °C the crystals are visible with clear morphology; they are large with spaces in between them and have a 3 dimensional hexagonal structure. In D (TT4.1) after 4 h at 300 °C the TiO_2 crystals are smaller and more densely packed with hexagonal structure

morphology compared to the crystals obtained at a shorter time. Image E (TT4.1) shows the TiO_2 crystals obtained after 5 h at 300 °C, which had a rod-like agglomerated morphology. In sample F (TT4.1) there are agglomerated TiO_2 nanocrystals to be seen after carbonization for 6 h at 300 °C, with cracks appearing in the film on the stainless steel support. HRSEM images (Figure 4.19) of samples obtained between 4 h and 6 h show that the morphology of the supported TiO_2 nanocrystals is agglomerated and as time increased to 6 h at 300 °C the TiO_2 nanocrystals are not fully developed on the surface of the stainless steel mesh.

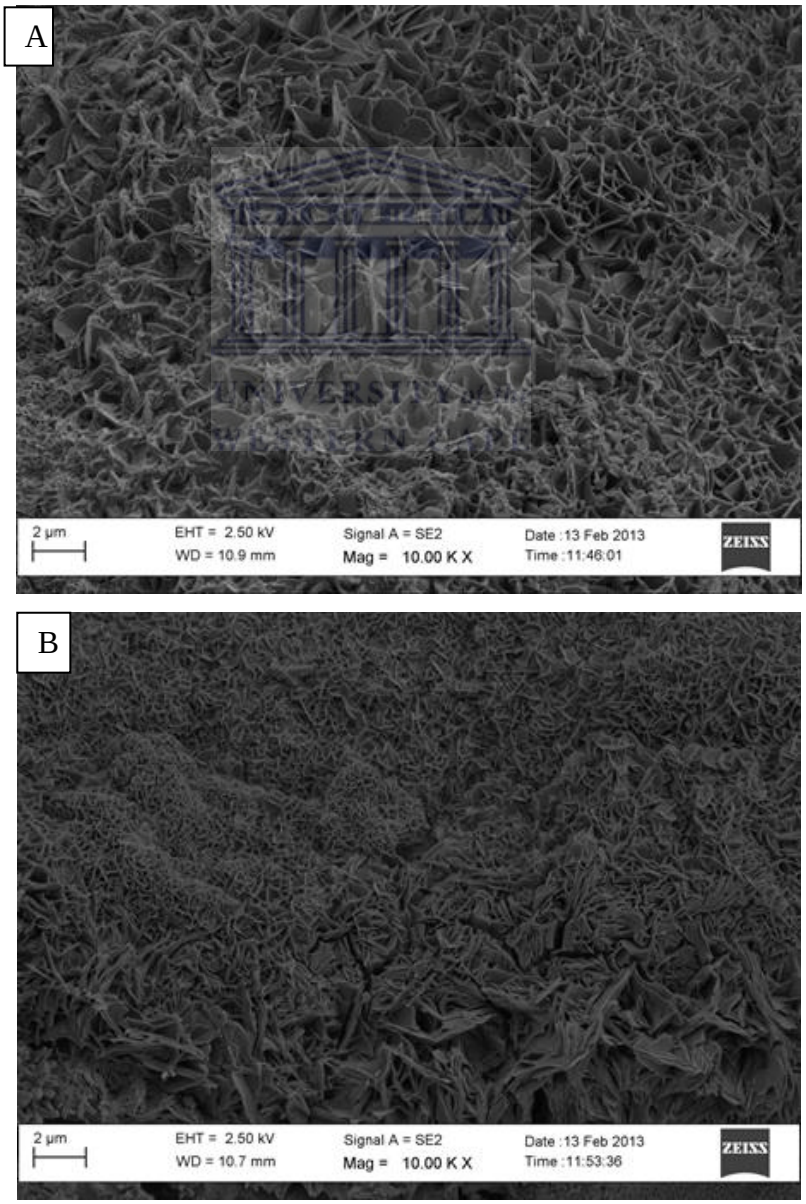

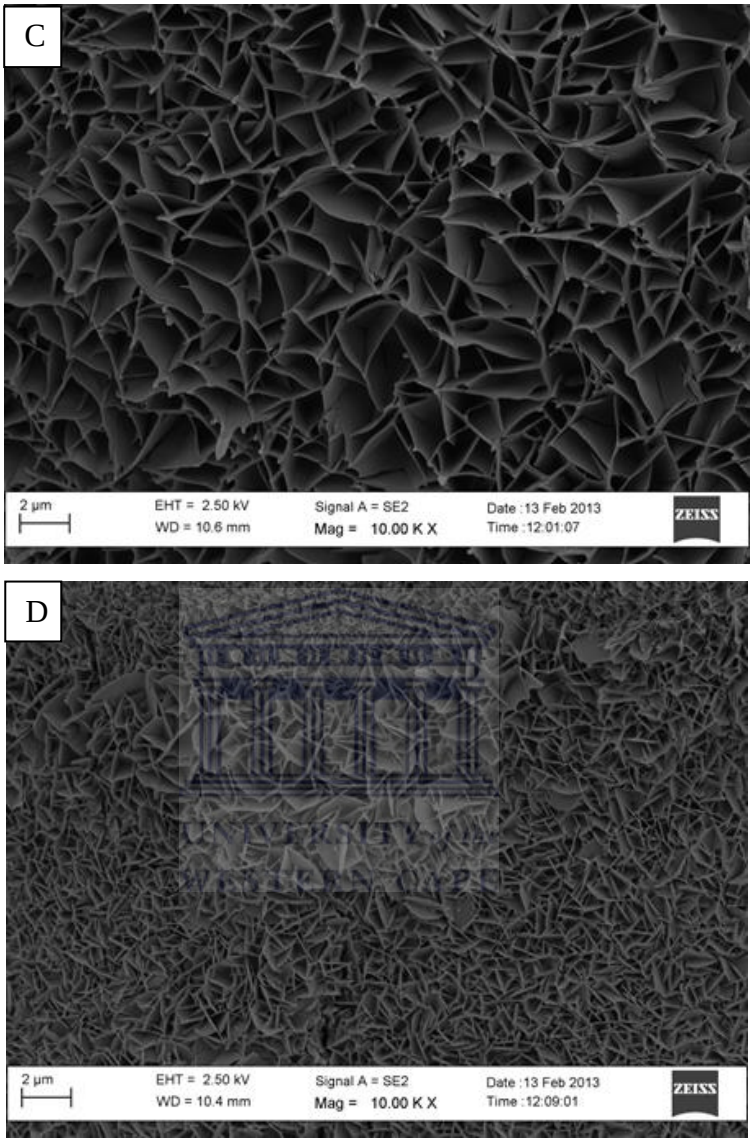

Figure 4.20 A - D: HRSEM images of TT4.2

In Figure 4.20 all the images of samples prepared at 400 °C at the specified holding time have a crystalline TiO_2 structure. The image of sample (TT4.2) a shows that after 1 h the crystal structure was not fully formed, while in B of the (TT4.2) sample prepared at 400 °C for 2 h, crystal structures are small. In C of the sample (TT4.2) prepared at 400 °C for 3 h the leaf-like TiO_2 crystal structures are large and aligned in a structured manner with clear morphology, have high surface area and are aggregated. In (TT4.2 D) of the sample prepared at 400 °C for 4 h the

leaf-like crystal structures are again small and have different sizes and are aggregated. Therefore these series of experiments showed that the most well developed TiO_2 structure could be obtained when using 8 % PAN/DMF/TiO_2 sol gel solution made of 8 % PAN/DMF sol solution and 99 % pure $TiCl_4$ titanium precursor followed by carbonization using a heating rate of 50 °C/min in air, up to 400 °C and held at 400 °C for 3 h. TT4.3 samples decomposed at 400 °C for 1 h up to 3 h the mass is gradually decreasing and when it reaches 4 h then increases.

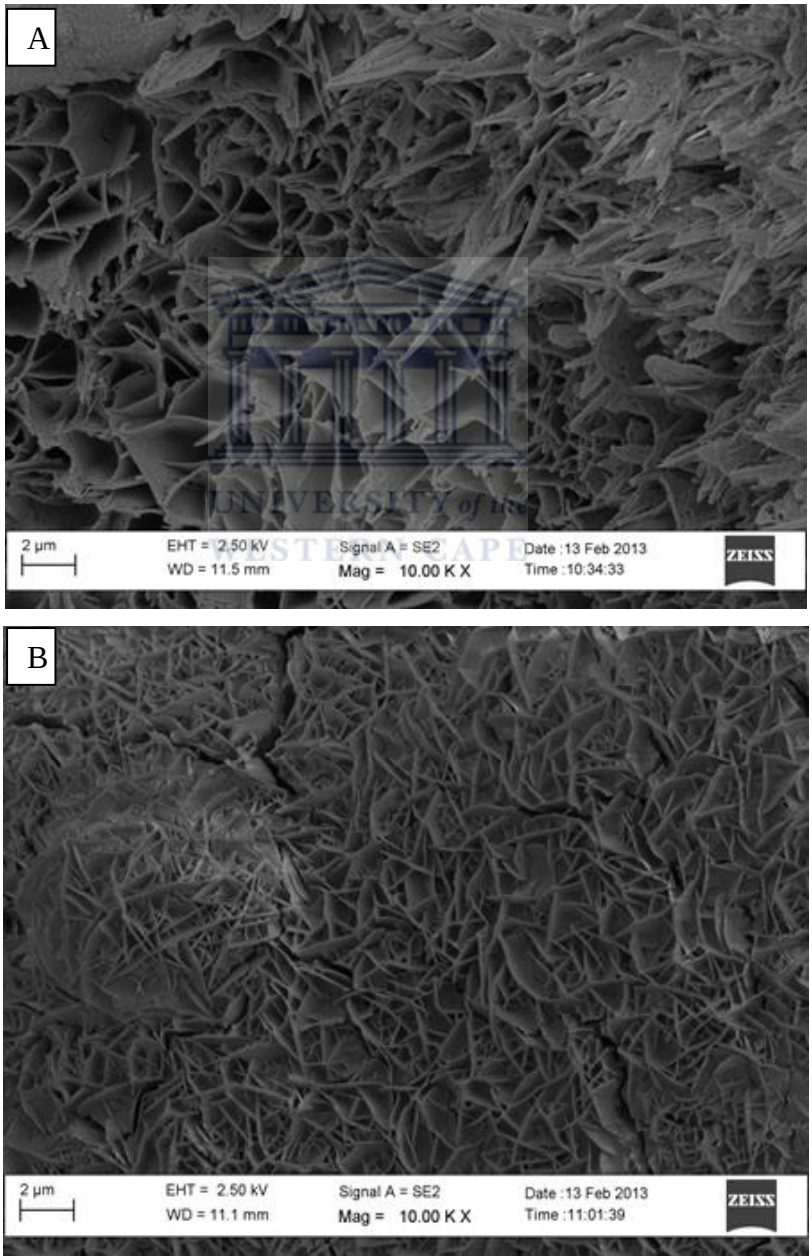

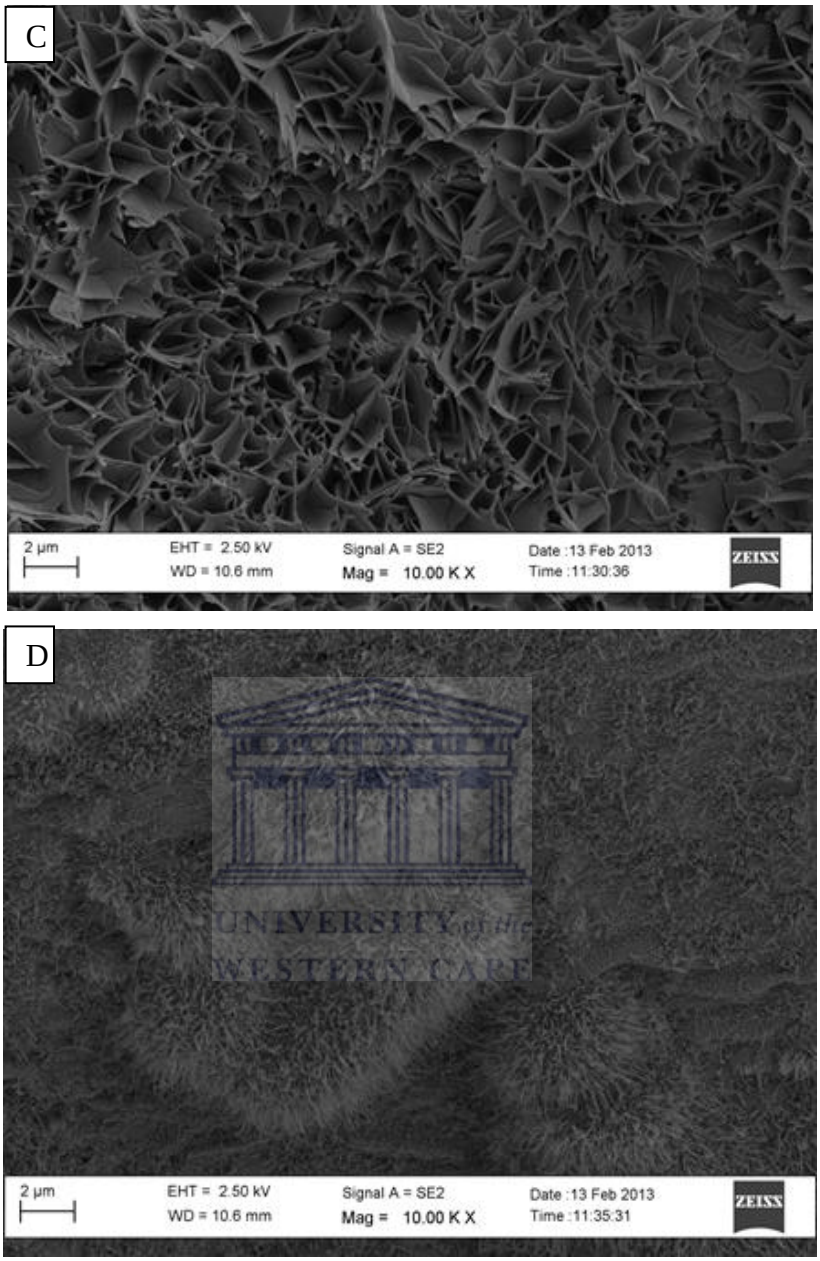

Figure 4.21A - D: HRSEM images of TT4.3

In Figure 4.21 A – D of sample (TT4.3) all the images show that at 500 °C a leaf like crystallite structure of the TiO_2 crystals was obtained between 1 – 3 h but not for the sample carbonized at 4 h (image D) which had a sharp needle-like structure. The higher temperature of 500 °C caused the TiO_2 structures to be less uniform than those obtained at 400 °C and cracks were apparent in image TT4.3 B. The decomposed structures for 1 h (TT4.3) A up to 4 h (TT4.3) D holding time does not correlate throughout.

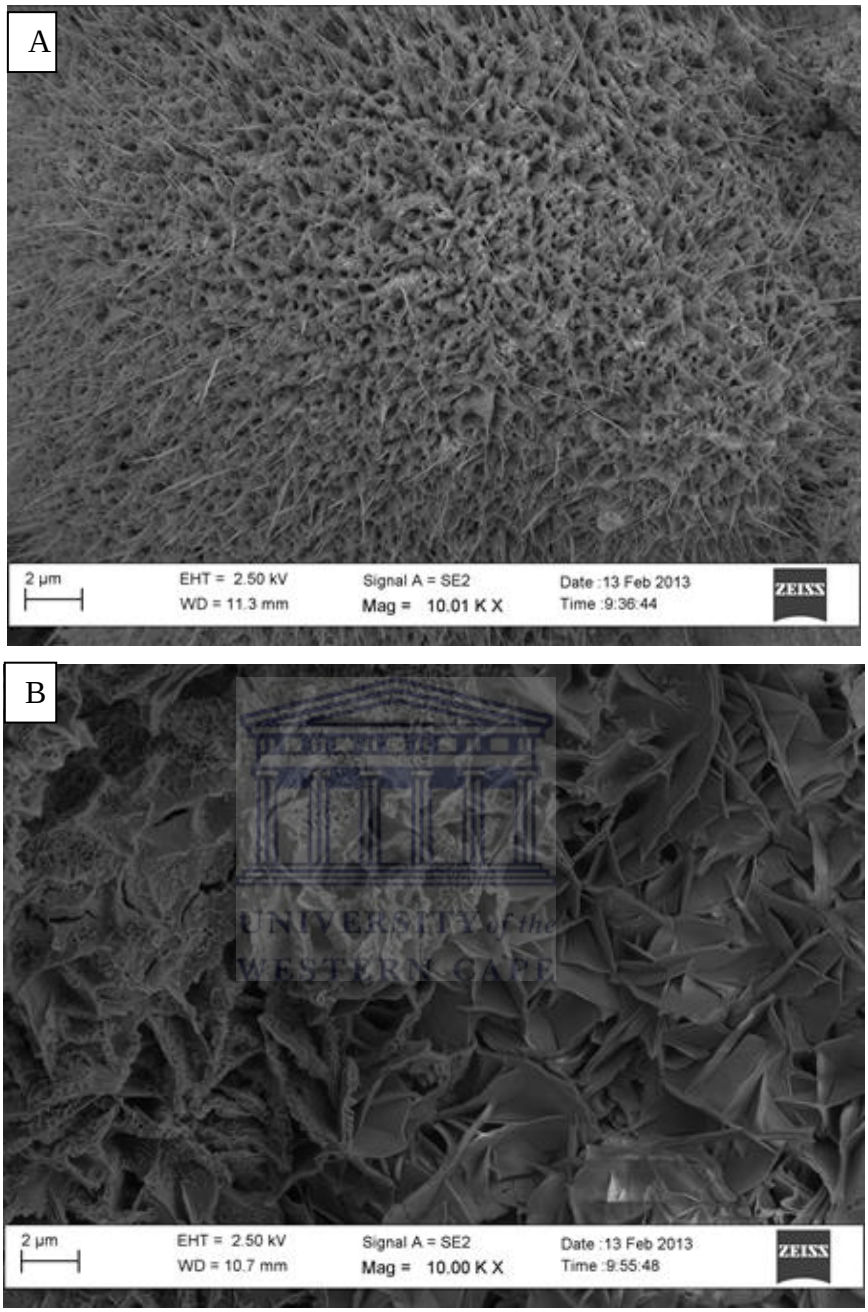

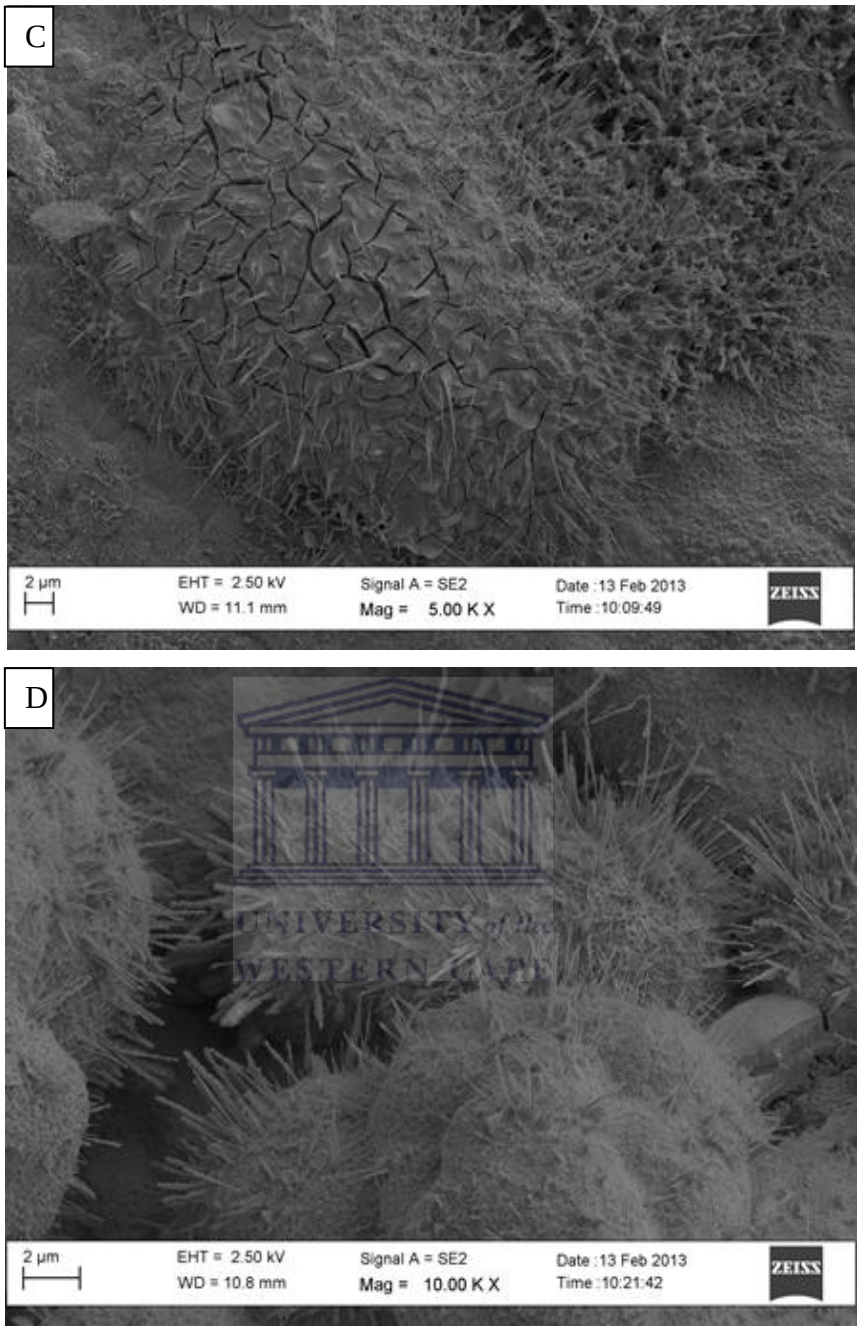

Figure 4.22 A - D: HRSEM images of TT4.4

In Figure 4.22 (A – D) (TT4.4) the applied temperature of 600 °C resulted in various needle-like structures that were inhomogeneous and not well adhering to the stainless steel substrate.

The HRSEM illustrated that the heating time and temperature had a substantial impact on the morphology of the supported TiO_2 nanocrystals and resulted in

equidimensional structures at 400 °C. The supported TiO_2 nanocrystals decomposed at 300 °C resulted in different hexagonal morphology with the change in holding time, whereas the higher temperature (500 °C – 600 °C) results in inhomogeneous structures. The trend for 1 h (TT4.4) A up to TT4.4 - 4 h D holding time showed an increasing mass of oxide. In another study on nucleation and growth kinetic of titania nanoparticles prepared by sol gel method it was showed that the rate constant for coagulation of particles increased with temperature because the velocity of monomer through the particles had a high dependency of temperature (Mehranpour et al, 2011). This present study is novel due to the process to improve the adhesion of TiO_2 nanocrystals on a stainless steel support; and the method used for the adhesion of such nanocrystals was very simple with fewer chemicals used than usual or processing steps, therefore the findings of this research are unique.

4.6.4 Comparing the HRSEM images

The HRSEM images with the best high surface area morphology and agglomeration of the TiO_2 nanocrystals at each temperature are compared with each other.

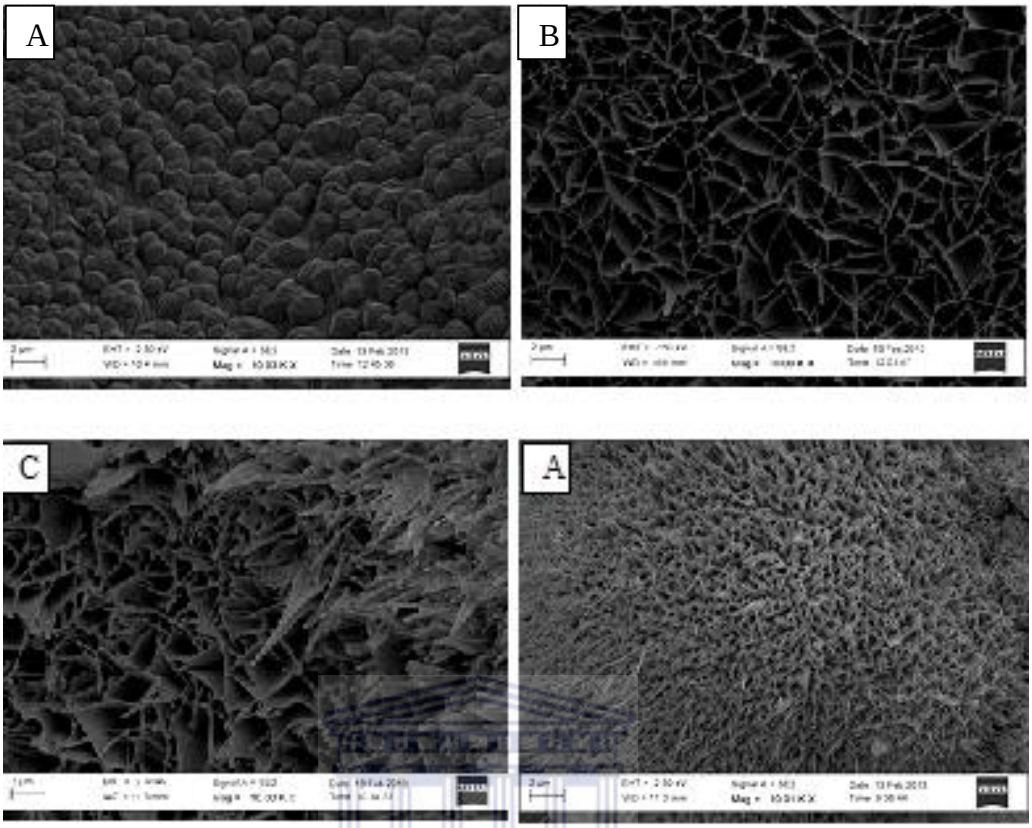

Figure 4.23: HRSEM comparison images: TT4.1 D, TT4.2 C, TT4.3 A and TT4.4 A

For Figure 4.23 it can be seen that as the temperature increased, the shorter holding times at higher temperatures gave more consistent high surface area TiO_2 nanocrystals, therefore this does seem to indicate that the higher the temperature the shorter the holding time should be. Use of the 8 % (PAN/DMF/TiO_2) sol gel solution to coat the TiO_2 containing sol gel onto supporting material gave better results than the 7 % (PAN/DMF/TiO_2) sol gel solution thus the higher concentration of Ti precursors was assumed to have yielded denser TiO_2 nanocrystals on the supporting material.

4.6.5 HRTEM images of the catalyst that degraded the methylene blue at its best for each decomposition temperature

High resolution transmission electron microscopy (HRTEM) was used for further investigation of structure and crystalline quality of the synthesised 8 % (PAN/DMF/TiO_2) sol gel solution TiO_2 nanocrystals. This characterization technique was used to observe modulations in chemical identity, crystal orientation and structure of various samples that were selected on the basis of their photocatalytic activity.

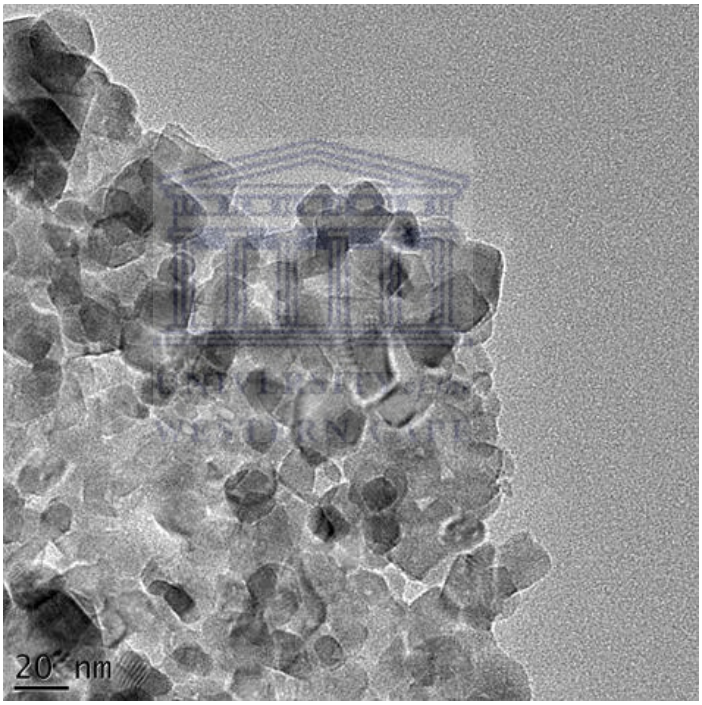

Figure 4.24: HRTEM image of TT4.2 B

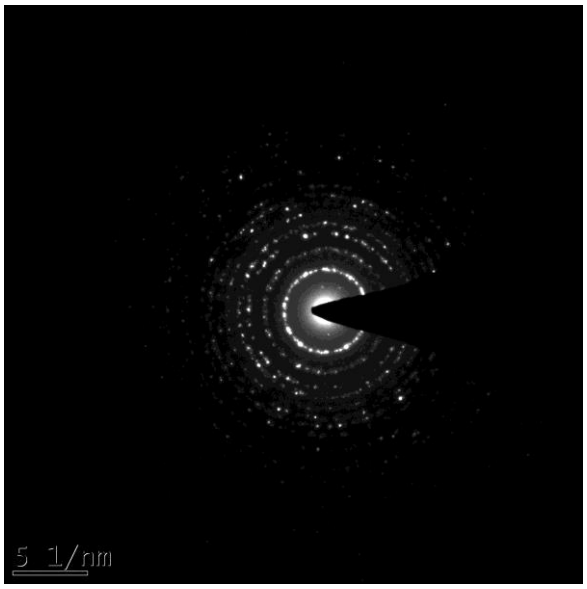

Figure 4.25: SAED pattern of TT4.2 B

The characteristic HRTEM image is shown in Figure 4.24. Figure 4.25 shows the SAED pattern of the sample presented in Figure 4.24. The sample (TT4.2 B) was composed of aggregated TiO_2 nanocrystals when decomposing PAN at a high heating rate when calcinating. The images shown in Figure 4.24 possess equidimensional nanocrystals with polycrystalline particles. The SAED of the nanocrystals confirms their polycrystallinity. The polycrystalline diffraction ring indexed confirmed that the TiO_2 nanocrystals were composed of highly nanocrystalline anatase phase. The SAED pattern and XRD as well as EDS confirmed the presence of the TiO_2.

4.6.6 Chemical bonding of the calcined TiO_2 nanocrystals characterized using fourier transform infrared spectroscopy (FTIR)

The calcined TiO_2 nanocrystals were characterized by FTIR for the chemical bonding and the functional groups present after the 8 % PAN/DMF/TiO_2 sol gel solution was decomposed in the furnace at different temperatures leaving the TiO_2 nanocrystals in the anatase crystal phase. Figure 4.26 shows a typical FTIR spectrum obtained for the sample prepared using a carbonization temperature of

TT4.2. The FTIR spectra are all similar and only the one in Figure 4.26 are a representative example.

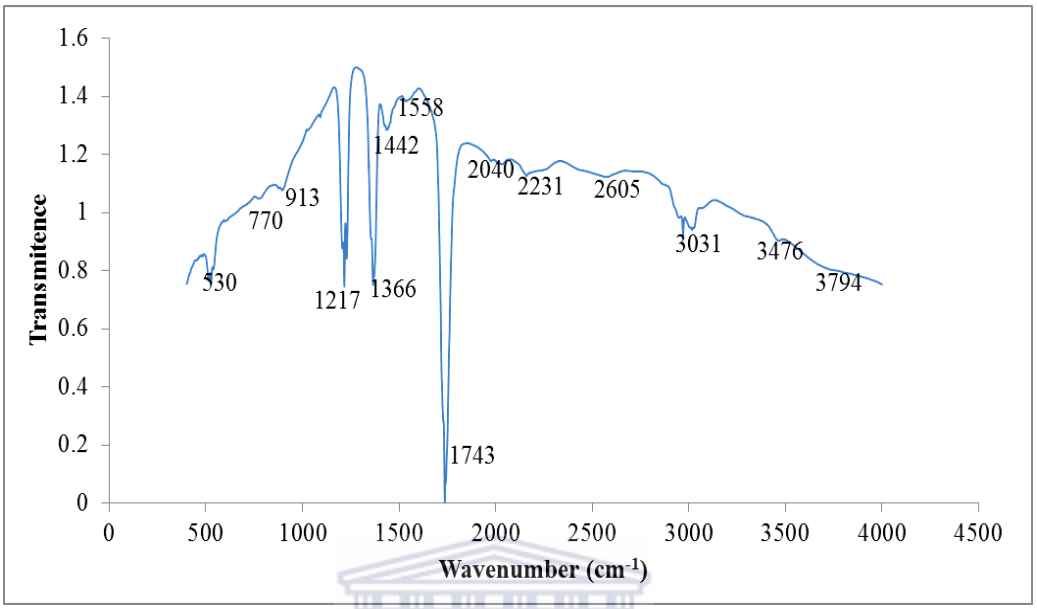

Figure 4.26: FTIR of sample (TT4.2) B

Figure 4.26 presents the FTIR spectral data with some similar vibrational bands of the anatase TiO_2 functional groups. Vibrational bands that appeared at 528 - 544 cm^{-1} were ascribed to the vibration peak of the skeletal O–Ti–O bonds of anatase phase (Cristallo et al, 2001). The characteristic peaks of C=O, C=C and C-N stretching vibrations were seen at 1737 -1751, 1440 -1457, and 1217 -1218 cm^{-1}, and the good adhesion of TiO_2 nanocrystals onto the support was ascribed to these carbon bonds. The band at 3000 - 3500 cm^{-1} was attributed to the hydroxyl group of Ti-O-H. Hence the conspicuous bands at 528 - 544 cm^{-1} represented the Ti-O and Ti-O-Ti stretching vibration modes and according to Saravanan et al, (2010) the same stretching vibration modes were distinguished at 542 cm^{-1}. The peaks observed between 1440 and 1457 cm^{-1} can also be attributed to the Ti-O-Ti vibration.

4.7 Photocatalytic degradation of methylene blue by prepared photocatalysts

The evaluation of photocatalytic activity of the (TT4.1, TT4.2, TT4.3 and TT4.4) samples was carried out using 50 ppm methylene blue. The electrospun supported TiO_2 nanofibres and decomposed electrospun supported TiO_2 nanofibres were not evaluated for photocatalysis, because the good quality composite PAN/DMF/TiO_2 nanofibres synthesized were unsupported and thus cannot easily be separated from one another. The HRSEM showed that the decomposed electrospun supported TiO_2 nanofibres had no nanocomposites materializing on the surface of the support. The degree of degradation of the methylene blue was characterised using UV-vis for the qualitative and quantitative analysis of the MB degraded. The degradation of the organic solution was carried under radiation of UV light according to the procedure which was described in Section 3.13. The percentage removal of MB obtained after 30, 60 or 90 minutes of UV radiation is presented in Figure 4.28, 4.29, 4.30 and 4.31. The UV-vis instrument was calibrated using 15 ppm, 25 ppm, 50 ppm and 75 ppm MB standards and the calibration curve is presented in Figure 4.27.

In Figure 4.28 the sample that was carbonized at 300 °C for 1 h holding time is presented and the photocatalysis degradation time applied is 30 min. The presented data is normalized to 0.3 g of deposited TiO_2 nanocrystals on the substrate based on Table 4.8 - 4.11 results.

The obtained supported PAN/DMF/TiO_2 nanocomposite have the highest photocatalytic activity to the degradation of methylene blue solution compared with the hallow nanofibres synthesised by (Zhang et al, 2008), because of their unique crystal structural orientation and high surface area. The present supported PAN/DMF/TiO_2 nanocomposite has removed 96.02 ± 0.0054 % of MB after 30 min degradation time in the presence of the 0.3 g supported TiO_2 nanocrystals decomposed at 50 °C/min up to 400 °C with a holding temperature of 2 h at 400 °C. This present degradation data is the better than the degradation data reported

in literature as the literature still reports the MB percentage removal below 80 % (Zhang et al, 2008).

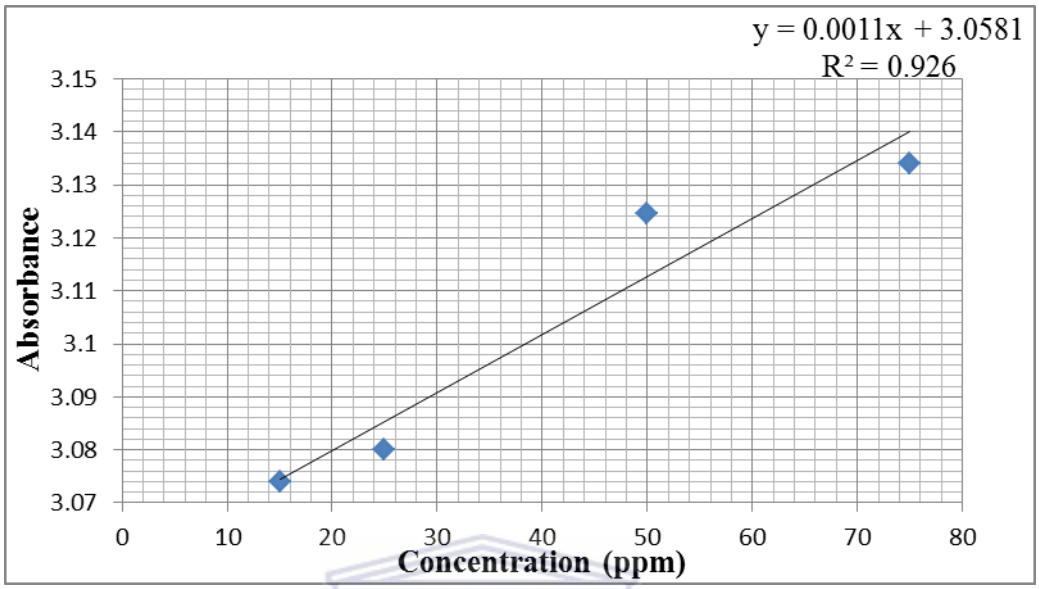

Figure 4.27: Methylene blue calibration curve (UV vis)

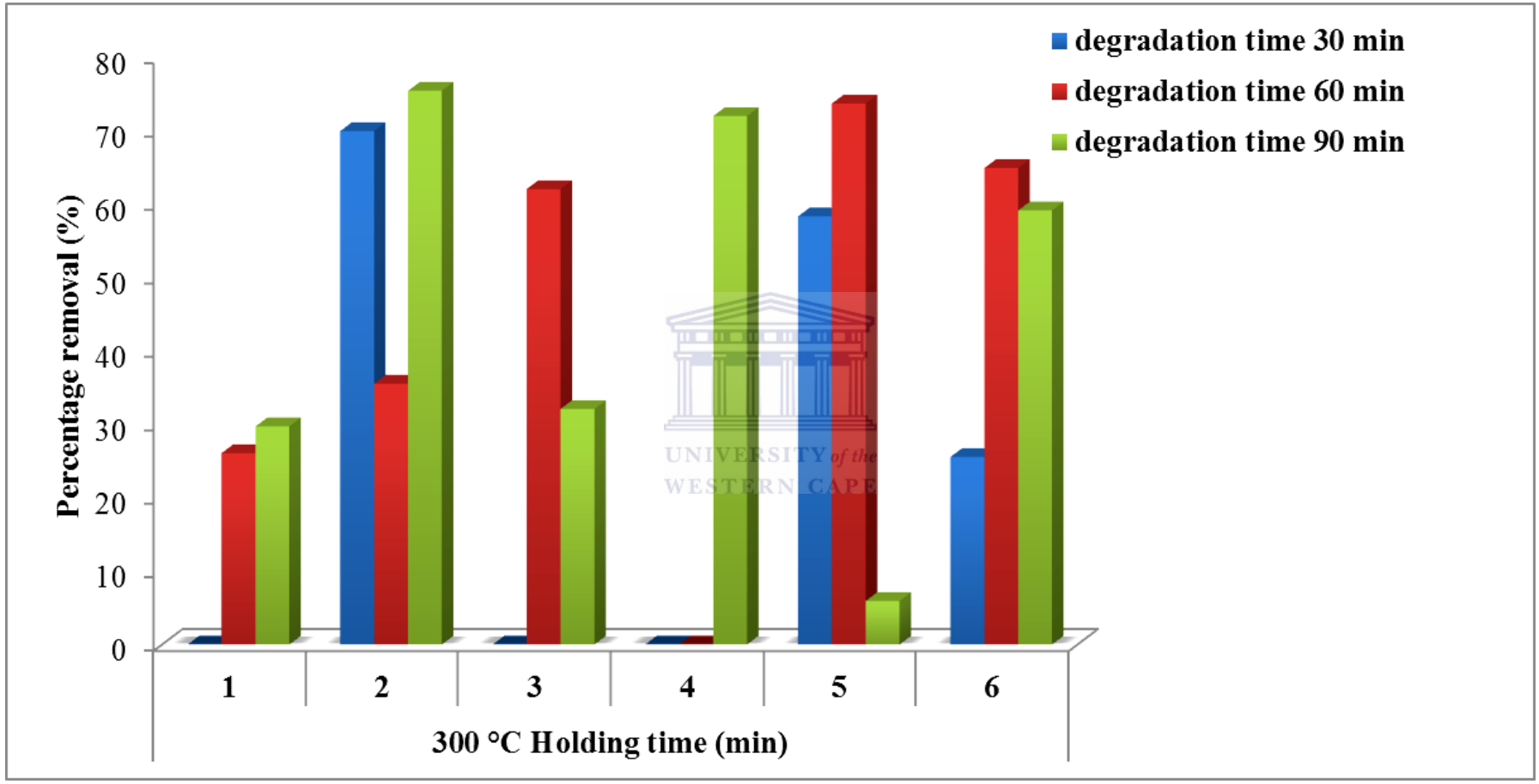

Figure 4.28: Degradation of MB for (TT4.1)

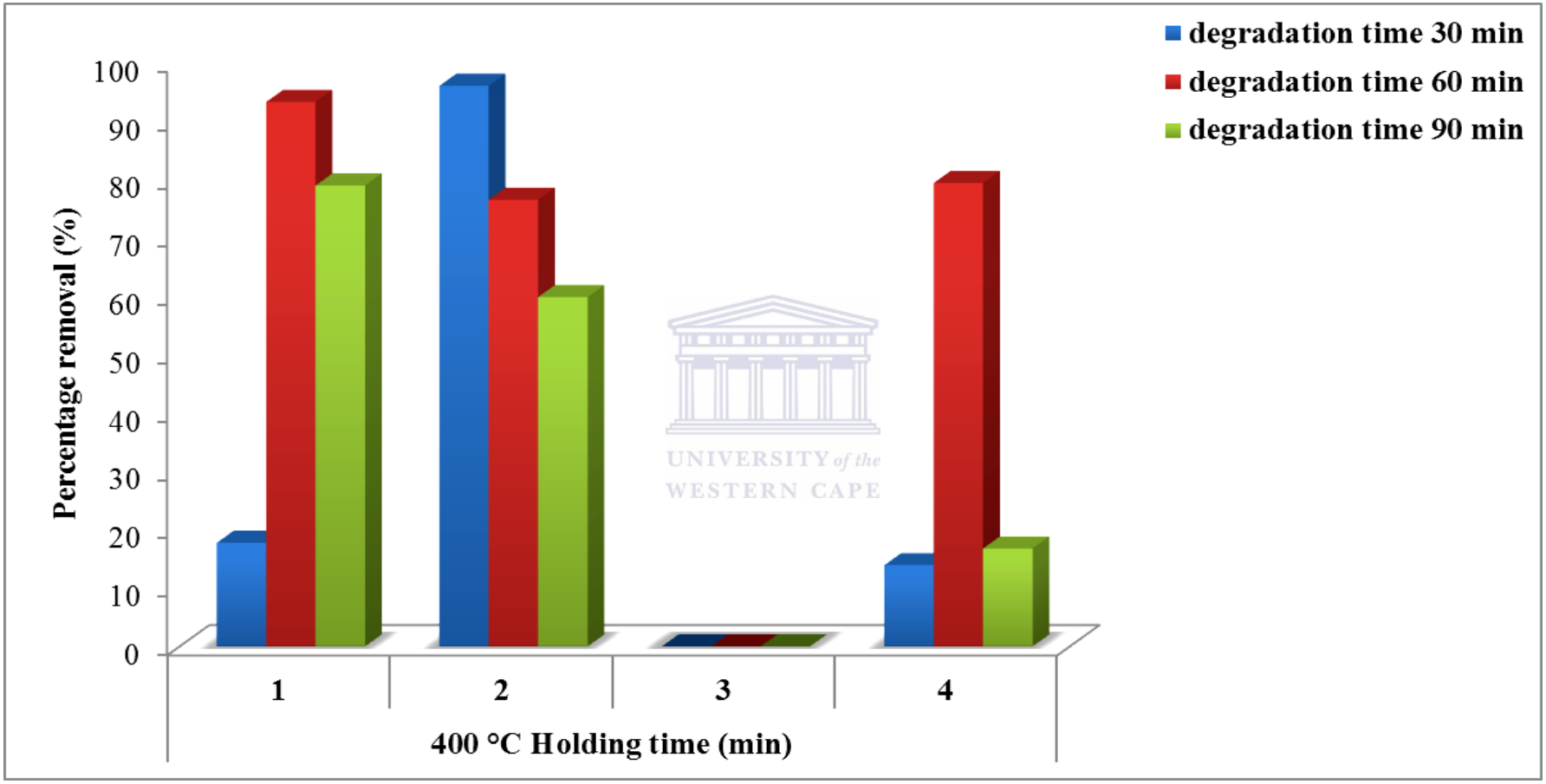

Figure 4.29: Degradation of MB for (TT4.2)

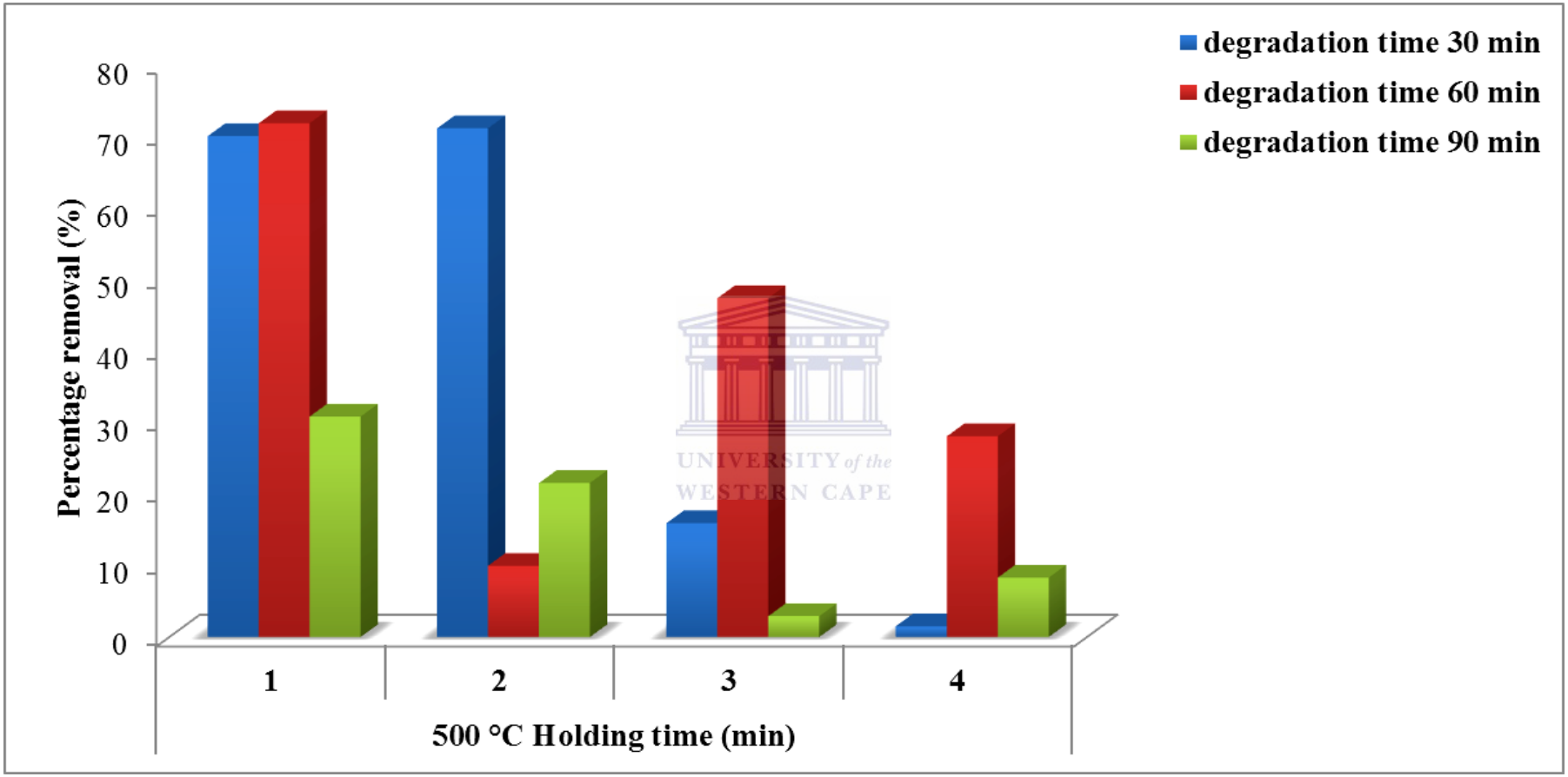

Figure 4.30: Degradation of MB for (TT4.3)

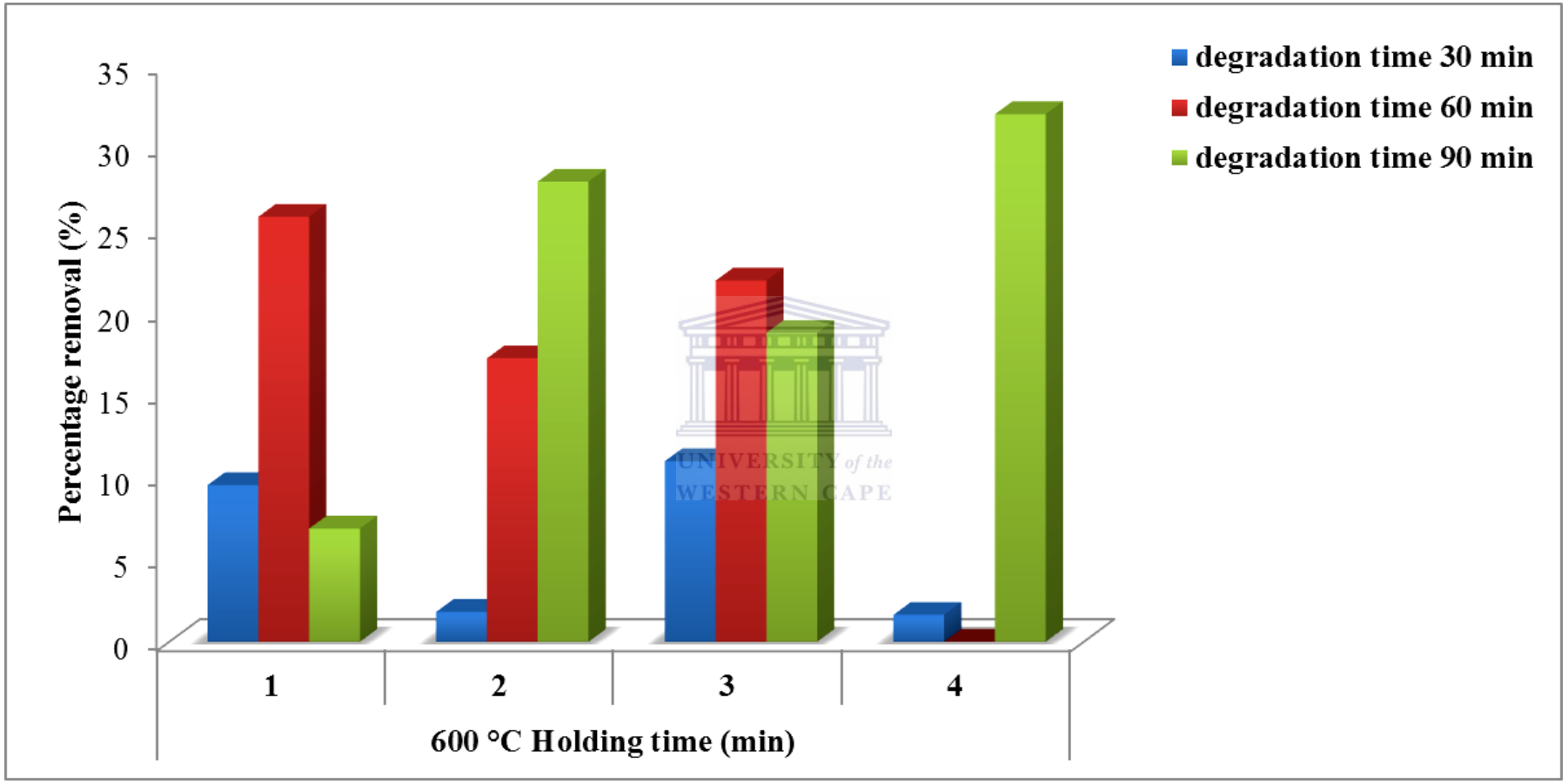

Figure 4.31: Degradation of MB for (TT4.4)

Figure 4.28 shows that for the composite samples treated at 300 °C (TT4.1) the MB degradation worked well as percentage removal ranged between 75.4 – 58.3%. In Figure 4.29 for the samples treated at 400 °C (TT4.2) the percentage removal for the MB degradation ranged between 96 – 59.8%. In Figure 4.30 the intermediate MB degradation was between 71.8 – 28 % for the samples treated at 500 °C (TT4.3). Also in Figure 4.31 for the samples treated at 600 °C (TT4.4) the percentage removal of MB was low and ranged between 32 – 6.9. The linear trend for each set of temperature, holding time and MB degradation time intervals are presented in Appendix four. All experiments were repeated three times and results are average.

The highest percentage MB removal obtained was 96 % after 30 min degradation time in the presence of the 0.3 g supported TiO_2 nanocrystals decomposed at 400 °C for 2 h (TT2.2). Figure 4.28 shows that all the supported TiO_2 nanocrystals possessed photocatalytic activity at various degradation time intervals except for the supported TiO_2 nanocrystals decomposed at 400 °C for 3 h which did not degrade MB. Even though all the immobilised TiO_2 nanocrystals possessed photocatalytic activity the supported TiO_2 nanocrystals decomposed at 400 °C for 2 h gave the highest degradation percentage ± 100 % and at the lowest degradation time interval of 30 min.

The variability of the UV vis results was due to the stirring of the supported PAN/DMF/TiO_2 nanocomposite that may have resulted in damaging the nanocomposite. This photocatalytic experimental setup was not optimized, thus the random movement of the catalyst means that the sample was not exposed to constant UV flux.

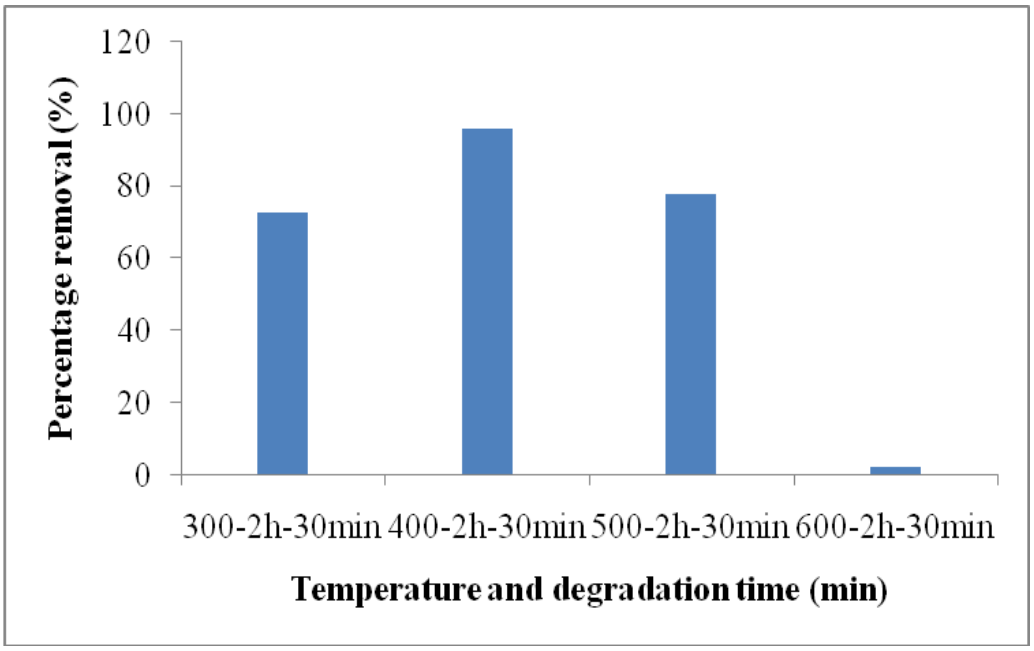

Figure 4.32: Comparison of percentage removal of MB after 30 min using the carbonized supported TiO_2 nanocrystals prepared at either TT4.1B, TT4.2B, TT4.3B and TT4.4B.

Figure 4.32 shows the % removal trend that increased to an optimum with an increase in catalyst treatment temperature at 400 °C and decreased again after 400 °C for the degradation of MB at 30 min using the carbonized TT4.1B, TT4.2B, TT4.3B and TT4.4B. The photocatalytic trends observed show that the composite crystal morphology obtained at 400 °C for 2h had the highedt active surface area as could be seen also from HRSEM.

Summary

In this study the photocatalytic activity of the supported TiO_2 nanocrystals was developed with high activity for organics degradation. The approach to overcoming the obstacles of powder form TiO_2 was to immobilise the TiO_2 nanocrystals on supporting material, via sol gel coating. The following attempts were made such as:

- The PAN/DMF/TiO_2 sol gel solutions were prepared using different methods and titanium precursors. The optimum sol gel formulation prepared from 8 % (PAN/DMF) sol solution and titanium precursor was prepared using 6 g of the 99 % pure $TiCl_4$ which was mixed with 50 mL of 8 % (PAN/DMF) solution. The manual sol gel coating of 8 % PAN/DMF/TiO_2 onto a stainless steel mesh support overcome the obstacle of depositing the sol gel solution.

- The stainless steel mesh coated with sol gel solution was decomposed using various heating profiles to immobilize the TiO_2 nanocrystals on the stainless steel mesh and the optimization of the decomposition procedure was carried out.

- The thermal decomposition method to grow TiO_2 nanocrystals on a stainless steel mesh surface was introduced and implemented, whereby the 8 % (PAN/DMF/TiO_2) sol gel coated stainless steel mesh was decomposed. In the case of 300 °C the holding time at temperature was expanded to 5 h as well as 6 h to check the morphology of the crystalline form. The morphology of the supported anatase phase TiO_2 nanocrystals were polycrystalline and agglomerated. It was found that 300 °C was too low a temperature to prepare well developed composite nanocrystallite anatase structure, whereas 400 °C proved to be a suitable temperature higher temperatures proved to cause inhomogeneous coatings.

The deposited mass loading of the supported TiO_2 nanocrystals decomposed at 300 °C and 500 °C were not reproducible. The mass percent loading of the TiO_2 composite decomposed at 300 °C was higher than the mass loading decomposed at 400 °C as the polymer was not fully degraded. The samples with the TiO_2 mass

loading decomposed at 500 °C varied between 10 - 14 mass percent loading. At 600 °C there was a constant linear increase of the mass percent loading and this may be due to oxide formation on the support.

The degree of coating of the stainless steel support with nanocrystalline anatase photocatalysts was not sufficient and nonuniform in cases where samples were prepared at 300 °C particulars when the temperature was held longer up to 6 h, and also at 500 °C where the 8 % (PAN/DMF/TiO_2) sol gel coating was thicker in certain areas and at 600 °C where the temperature was too high and caused cracking and inhomogeneous coatings.

The XRD characterisation technique identified the crystalline phase of the TiO_2 nanocrystals formed on the metal support, and confirmed that anatase was the only crystalline phase prepared under all applied conditions. The crystallite size was estimated from the Debye–Scherrer equation using the XRD line broadening of the anatase (101) plane diffraction peak. The crystallite size increases as the temperature increases, but surprisingly there is no correlation between the crystallite percentage and the degradation percentage. This may be due to the inhomogeneous nature of the crystallite structure.

The HRSEM characterization technique was used to determine the morphology of the supported TiO_2 nanocrystals formed at the various decomposition temperatures. Different morphologies of the supported TiO_2 anatase nanocrystals were observed depending upon the calcination in air temperatures applied. The HRSEM and SAED showed polycrystalline morphologies of the supported TiO_2 nanocrystals with different shapes of crystal structures. The supported TiO_2 nanocrystals prepared at 300 °C were characterized by three dimensional hexagonal shaped prismatic crystal structures with different diameter size as the holding time was changed. All the HRSEM images of samples prepared at temperatures above 300 °C demonstrated the formation of aggregated anatase TiO_2 polycrystalline composites with high surface areas, with the most uniform crystal morphology achieved at 400 °C for 2 h.

The FTIR characterization technique was used to confirm the functional groups of the TiO_2 with the spectral data of the supported TiO_2 nanocrystals. The peaks observed between 1440 and 1457 cm^{-1} corresponded to the Ti-O-Ti vibration which was compared with pure TiO_2 at 1400 cm^{-1}. The characteristic peaks 1737 - 1751, 1440 -1457, and 1217 -1218 cm^{-1} were attributed to the C=O, C=C and C-N stretching vibrations and these carbon bands are thought to contribute to the good adhesion of nanocrystals to the support. Therefore FTIR results confirmed that the supported TiO_2 nanocrystals had been synthesised and have adhesion due to carbon moeities remaining during the thermal degradation of precursor organic PAN.

CHAPTER FIVE: CONCLUSION AND RECOMMENDATION

5 Conclusion and Recommendations

5.1 Conclusion

This chapter gives the summary of the significant findings of this thesis and conclusions of the results presented in the previous chapters. Recommendations for further research on some aspects are outlined.

The successful anatase phase crystal formation was achieved by the sol gel solution prepared by mixing 3 g of the Polyacrylonitrile (PAN) and 34.5 g of N, N-dimethylformamide (DMF) making up 37.5 g of PAN/DMF, which was further added to 6 g of 99 % concentrated $TiCl_4$ used as the Ti precursor; making up the 8 % (PAN/DMF/TiO_2) sol gel solution in a sealed vessel.

Good quality composite PAN/DMF/TiO_2 nanofibres were synthesized from the 8 % PAN/DMF/TiO_2 sol gel solution with a 7.77 atomic % Ti content but the TiO_2 fibres were unsupported and thus not suitable for ease of separation. TiO_2 nanocomposites were successfully fabricated by coating the support with the Ti-precursor/polymer mixture solution 8 % (PAN/DMF/TiO_2), followed by decomposition at high temperatures for enhancing the adhesion of PAN/DMF/TiO_2 nanocrystals to the substrates.

The preparation of the nanocomposites, TiO_2 nanocrystal supported on the stainless steel mesh, by a coating technique was achieved. The XRD patterns has demonstrated that TiO_2 crystallizes above 300 °C in the of anatase form, which phase remarkably remained stable up to 600 °C. The stabilization of this TiO_2 phase in composite form is due to the nanometric size of the crystals immobilized onto the stainless steel mesh. The crystalline phase and morphology of the nanocomposites are supported by XRD and SEM analyses, which has shown homogeneous and monodisperse distribution of nodular anatase nanocrystals

(crystal size 17.3 nm) onto stainless steel mesh for the sample calcined in air at 400 °C for 2 h. The anatase nanocrystals are thermally stable, smaller than 20 nm, well dispersed and immobilized on the surface of stainless steel mesh.

The various supported anatase nanocomposites were successfully made and it was possible to tailor the crystal size depending on the processing conditions such as the heating temperature and holding time. The XRD and SEM characterization elucidated the crystallinity and morphology of the prepeared nanocomposites. The TiO_2 anatase phase changed the crystal structural morphology and the surface area with the change in temperature and holding time.

The HRSEM showed that the heating time and temperature had a substantial impact on the morphology of the supported TiO_2 nanocrystals and the result of equidimensional structures at 400 °C, hexagonal morphology at 300 °C and inhomogeneous (500 °C – 600 °C). The uniform degree of anatase coating on the stainless steel mesh was inhomogenious but sufficient for the stainless steel mesh piece.

The high surface area supported TiO_2 nanocomposites with high activity for organics degradation were achieved. The photocatalytic degradation of methylene blue over the supported TiO_2 nanocrystals was carried out and UV-vis was used to characterize the degree of degradation of the MB. The findings of this research are that the supported TiO_2 nanocrystals possessed obvious photocatalytic activity at various degradation time intervals. Of all the immobilised TiO_2 nanocrystals prepared that possessed photocatalytic activity, the supported TiO_2 nanocrystals (decomposed at 400 °C for 2 h), showed the highest degradation activity of 96 % after 30 min degradation time in the presence of the 0.3 g supported TiO_2 nanocrystals that were decomposed at 50 °C/min up to 400 °C with a holding temperature of 2 h at 400 °C in air. This work contributes to the preservation of water by efficient treatment of organic pollutants in waste waters with a new composite photocatalyst.

CHAPTER FIVE: CONCLUSION AND RECOMMENDATIONS

5.2 Recommendations

Based on the analysis and conclusions of the study, a number of recommendations regarding future research are as follows:

- This study has proved that the TiO_2 nanocrystals prepared from the PAN 8 % (PAN/DMF/TiO_2) sol gel solution could be tailored by varying decomposition temperature to form different crystal structures. The further investigation of the enhanced TiO_2 nanocrystals needs to be studied.

- The use of a Ti-mesh instead of stainless steel mesh as the supporting material may enhance the photodegradation of the supported TiO_2 nanocrystals.

- The spray coating of the 8 % (PAN/DMF/TiO_2) sol gel solution onto the supporting material needs to be implemented so as to ensure the uniform and systematic loading of the sol gel solution onto the substrate, avoiding the cracks on the deposited sample.

- The porosity and the surface area of the supported TiO_2 nanocrystals must be determined.

REFERENCES

Ahmad A., Awan G. H. & Aziz S. (2008), "Synthesis and applications of TiO_2 nanoparticles", *Pakistan Engineering Congress;* 676, 403 – 412.

Amethyst Galleries (2012), galleries.com web services (Accessed 21 May 2012)

Asahi R., Morikawa T., Ohwaki T., Aoki K. & Taga Y. (2001), "Visible-Light Photocatalysis in Nitrogen-Doped Titanium Oxides", *Central R&D Laboratories;* 293, 480-1192.

Barthel J. & Thust A. (2010), "Aberration measurement in HRTEM: Implementation and diagnostic use of numerical procedures for the highly precise recognition of diffractogram patterns", *Ultramicroscopy;* 111, 27 – 46.

Bessergenev V. G., Pereira R. J. F., Mateus M. C., Khmelinskii I. V., Vasconcelos D. A., Nicula R., Burkel E., Botelho do Rego A. M. & Saprykin A. I. (2005), "Study of physical and photocatalytic properties of titanium dioxide thin films prepared from complex precursors by chemical vapour deposition", *Science @ direct;* 503, 29 – 39.

Blake D. M., Maness P. C., Huang Z., Wolfrum E. J. & Huang J. (1999), "Application of the photocatalytic chemistry of titanium dioxide to disinfection and the killing of cancer cells", *Separation and Purification Methods;* 28, 1 - 50.

Brinker C. J., Frye G. C., Hurd A. J. & Ashley C. S. (1991), "Fundamentals Of Sol-Gel Dip Coating", *Thin Solid Films;* 201, 97 - 108.

Cˇerna M., Vesely M. & Dzik P. (2011), "Physical and chemical properties of titanium dioxide printed layers", *Catal.;* 161, 97 – 104.

Carmine T. (2009), "Mesoporous oxide of zirconium", *Patents Archive;* 17, 381.

REFERENCES

Chen I. H., Wang C. C. & Chen C. Y. (2009), "Fabrication and characterization of magnetic cobalt ferrite/polyacrylonitrile and cobalt ferrite/carbon nanofibers by electrospinning", *Science Direct;* 48, 604 – 611.

Chen X. & Mao S. S. (2007), "Titanium dioxide nanomaterials: synthesis, properties, modifications, and applications", *Chemical Reviews;* 107, 2891 – 2959.

Choi K. J. & Hong S. W. (2011), "Preparation of TiO_2 nanofibers immobilized on quartz substrate by electrospinning for photocatalytic degradation of ranitidine", *Research on Chemical Intermediates;* 38, 1161–1169.

Choi W. (2006), "Pure and modified TiO_2 photocatalysts and their environmental applications", *Catalysis Surveys from Asia;* 10, 16 – 28.

Chuangchote S., Jitputti J., Sagawa T. & Yoshikawa S. (2009), "Photocatalytic activity for hydrogen evolution of electrospun TiO_2 nanofibe", *Applied Materials & Interfaces;* 1, 1140–1143.

Cristallo G., Roncari E., Rinaldo A. & Trifirò F. (2001), "Study of anatase-rutile transition phase in monolithic catalyst V_2O_5/TiO_2 and V_2O_5-WO_3/TiO_2", *Applied Catalysis A;* 209, 249 - 256.

Cullity, B.D. & Stock, S.R. (2001), "Elements of X-ray Diffraction", 3rd Edition Prentice Hall.

Doh S. J., Kim C., Lee S. G., Lee S. J. & Kim H. (2007), "Development of photocatalytic TiO_2 nanofibers by electrospinning and its application to degradation of dye pollutants", *Journal of Hazardous Materials;* 154, 118–127.

Dutrow B. L. &, Clark C. M. (2012), "Integrating research and education: Geochemical Instrumentation and Analysis: Techniques X-ray Powder Diffraction (XRD)", http:///www. MSDS and instrumentation/Instrumentation/XRD.html (accessed on 21 March 2013).

REFERENCES

Dzenis Y. A. (2004), “Spinning continuous fibers for nanotechnology”, *Science*; 304, 1917-1919.

Egertton, R.F. (2005), "Physical principles of electron microscopy: An introduction to TEM, SEM and AEM", *Springe;*, USA.

Fujishima A., Hashimoto K. & Watanabe T. (1999). “TiO_2 Photocatalysis Fundaments and Applications”, BKC Inc, 174.

Goodge J. (2013), “Integrating research and education: Geochemical Instrumentation and Analysis: Techniques X-ray Powder Diffraction (XRD)”, http:///www. MSDS and instrumentation/Instrumentation/EDS.html (accessed on 21 March 2013).

Hackeyley V. A. & Ferraris C. F. (2001), “The use of nomenclature in dispersion science & technology”, available at: http://libcloud.s3.amazonaws.com/93/5a/1/2746/NMI-report-XRD-anatase.pdf (accessed 8 May 2013).

Herrmann J. M., Houas A., Lachheb H., Ksibi M., Elaloui E. & Guillard C. (2001), “Photocatalytic degradation pathway of methylene blue in water”, *Applied Catalysis B: Environmental*; 31, 145 – 157.

Hoefelmeyer J. D., Koodali R., Sereda G., Engebretson D., Puszynski J., Swiatkiewicz J., Fong H., Ahrenkiel P. & Shende R. (2011), “USD Catalysis Group for Alternative Energy”, *DOE Hydrogen and Fuel Cells Program ;* 11, 164 – 169.

Hoffmann M. R., Martin S. T., Choi W. & Bahnemann D. W. (1995), “Environmental Applications of Semiconductor Photocatalysis”, *Chemical Reviews;* 95, 6.

Holler F. J., Skoog D. A. & Crouch S. R. (2007), “Principles of Instrumental Analysis”, *International Student edition;* 6th edition 259 – 266.

http://www.pipeflow.co.uk/public/articles/Viscosity_And_Density_Units_And_Formula.pdf (Accessed on 27 July 2013)

Hu G., Meng X., Feng X., Ding Y., Zhang S. & Yang M. (2007), "Anatase TiO_2 nanoparticles/carbon nanotubes nanofibres: preparation, characterization and photocatalytic properties", *Journal of Materials Science;* 42, 7162 – 7170.

Huang Z. M., Zhang Y. Z., Kotaki M. & Ramakrishna S. (2003), "A review on polymer nanofibers by electrospinning and their applications in nanocomposites", *Composites Science and Technology;* 63, 2223 – 2253.

Kanjwal M. A., Barakat N. A. M., Sheikh F. A., Baek W., Khil M. S. & Kim H. Y. (2010), "Effects of silver content and morphology on the catalytic activity of silver-grafted titanium oxide nanostructure", *Fibers and Polymers;* 11, 700 - 709.

Karunakaran C., Anilkumar P. & Gomathisankar P. (2011), "Photoproduction of iodine with nanoparticulate semiconductors and insulators", *Chemistry Central Journal;* available at: http://openi.nlm.nih.gov/detailedresult.php?img=3141621_1752-153X-5-31-1&req=4 (accessed 21 February 2013)

Le N. T. T., Nagata H., Aihara M., Takahashi A., Okamoto T., Shimohata T., Mawatari K., Kinouchi Y., Akutagawa M. & Haraguchi M. (2011), "Applied and environmental microbiology, additional effects of silver nanoparticles on bactericidal efficiency depend on calcination temperature and dip-coating speed", *American Society for Microbiology;* 77, 5629–5634.

Lee C. B. (2009), "Influence of $TiCl_4$ treatment on dye-sensitized solar cell with electrospun TiO_2 nanofibers", *Journal of Future Fusion Technology;* 1, 43 – 46.

Lee D. Y., Cho J. E., Lee M. H., Cho N. I. & Song Y. S. (2008), "Insertion of a TiO_2 buffer layer for the fixation of electrospun TiO_2 nanofibers on glass substrates", *Korean Physical Society;* 55, 84 – 88.

REFERENCES

Lezere (2011), http://monographs.iarc.fr/ENG/Monographs/vol93/mono937.pdf (accessed 28 March 2012)

Li G., Li L., Boerio-Goates J., Brian F. & Woodfield J. (2005), "High purity anatase TiO_2 nanocrystals: Near room-Temperature synthesis, grain growth kinetics, and surface hydration chemistry", *Journal of the American Chemical Society;* 127, 8659 – 8666.

Li J., Zheng L., Li L., Xian Y. & Jin L. (2006), "Fabrication of TiO_2/Ti electrode by laser-assisted anodic oxidation and its application on photoelectrocatalytic degradation of methylene blue", *Journal of Hazadous Materials;* 139, 72 – 78.

Lim J. I., Yu B., Woo K. M. & Lee Y. K. (2008), "Immobilization of TiO_2 nanofibers on titanium plates for implant applications", *Applied Surface Science;* 255, 2456 – 2460.

Lin Y. P., Chen Y. Y., Lee Y. C. & Chen-Yang Y. W. (2011), "Synthesis of mesoporousanatase TiO_2 nanofibers by electrospinning with room temperature ionic liquid and its application on dye-sensitized solar cells", *Ceramic Society;* 89, 1861.

Litovchenko G. D. & Girshgorn V. M. (2004), "Study of the interaction of polyacrylonitrile with solvents according to IR absorption spectra", *UDC;* 535, 34.

López-Chuken U. J. (2012), "Hydroponics and Environmental Clean-Up" *A Standard Methodology for Plant Biological Researches*; 181-199.

Macwan D. P., Dave P. N. & Chaturvedi S. (2011), "A review on nano-TiO_2 sol–gel type syntheses and its applications", *Journal of Materials Science;* 46, 3669 – 3686.

Martinez T., Bertron A., Ringot E. & Escadeillas G. (2011), "Degradation of NO using photocatalytic coatings applied to different substrates", *Elsevier;* 46, 1808 - 1816.

REFERENCES

Mehranpour H., Askari M. & Ghamsari M. S. (2011), "Nucleation and Growth of TiO_2 Nanoparticles", *Nanomaterials*; 3-26.

Mishra S. and Ahrenkiel S. P. (2011), "Synthesis and characterization of electrospun nanocomposite TiO_2 nanofibers with Ag nanoparticles for photocatalysis applications", *Journal of Nanomaterials;* 1, 1 - 6.

Munekwa, S. & Ferrara J. D. 1998, "Imaging plates as detectors for x-ray diffraction", *The Rigaku Journal; 5,* 2.

Nagaveni K., Hegde M. S., Ravishankar N., Subbanna G. N. & Madras G. (2004), "Synthesis and structure of nanocrystalline TiO_2 with lower band gap showing high photocatalytic activity", *Langmuir; 20,* 2900 – 2907.

Nakane K. & Ogata N. (2010), "Photocatalyst Nanofibers Obtained by Calcination of Organic-Inorganic Hybrids", *Nanofibres;* 2-214-228.

Nakane K., Yasuda K., Ogihara T., Ogata N. & Yamaguchi S. (2007), "Formation of poly(vinyl alcohol)-titanium lactate hybrid nanofibers and properties of TiO_2 nanofibers obtained by calcination of the hybrids", *Journal of Applied Polymer Science;* 104, 1232 – 1235.

Ochanda F. O., Rajukada S & Barnett M. R. (2012), "Controlled Synthesis of TiO_2 Hierarchical Nanofibre Structures via Electrospinning and Solvothermal Processes: Photocatalytic Activity for Degradation of Methylene Blue", *Nanomaterials and Nanotechnology;* 2, 1 – 9.

Ojha S.S. (2007), "Fabrication and characterization of novel single and bicomponentelectrospunnanofibrous mats", *Raleigh;* 40, 997.

Park J. Y., Hwang K. J., Lee J. W. & Lee I. H. (2011), "Fabrication and characterization of electrospun Ag doped TiO_2 nanofibers for photocatalytic reaction", *Journal of Materials Science;* 46, 7240 – 7246.

REFERENCES

Podbielska H. & Ulatowska-Jarza A. 2005, "Sol-gel technology for biomedical engineering", *Bulletin of the Polish Academy of Sciences Technical Sciences;* 53, 261 - 271.

Prairie M. R., Evans L. R., Stange B. M. &Marlinez S. L. (1993), "An investigation of TiO_2 photocatalysis for the treatment of water contaminated with metals and organic chemicals", *Environmental Science & Technology; 27,* 1776 – 1782.

Prasai B., Cai B., Underwood M. K., Lewis J. P. & Drabold D. A. (2012), "Properties of amorphous and crystalline titanium dioxide from first principles", *Journal of Materials Science;* 47, 7515 – 7521.

Radich, J. G. & Kamat, P. V. (2013), "Making Graphene Holey**.** Gold-Nanoparticle-Mediated Hydroxyl Radical Attack on Reduced Graphene Oxide", *ACS Nano;* 7, 5546 – 5557.

Riley M., Borja J., Gill W. N. & Plawsky J. (2010), "Development of integrated photocatalytic systems", *Chemical Engineering and Processing*; 46, 781.

Saravanan L., Kumar R. M., Pandurangan A. & Jayavel R. (2010), "Synthesis and photophysical studies of PVP capped Titania Nanostrips for photocatalytic applications", *Optoelectronics and Advanced Materials – Rapid Communications;* 4, 1676 – 1680.

Shrivastava V. S. (2012), "Photocatalytic degradation of Methylene blue dye and Chromium metal from wastewater using nanocrystalline TiO_2 Semiconductor", *Archives of Applied Science Research;* 4, 1244 - 1254.

Stamate M. & Lazar G. (2007), "Application of titanium dioxide photocatalysis to create self-cleaning materials", *Romanian Technical Sciences Academy;* 3, 280 - 285.

Swapp S. (2013), "Integrating Research and Education:Geochemical Instrumentation and Analysis:Techniques Scanning Electron Microscopy (SEM)",

REFERENCES

http:///www. MSDS and instrumentation/Instrumentation/SEM.html (accessed on 21 March 2013).

Tang J., Redl F., Zhu Y., Siegrist T., Brus L. E., & Steigerwald M. L. (2005), "An organometallic synthesis of TiO_2 nanoparticles", *Nano Letters;* 5, 543 - 548.

Tavakoli A., Sohrabi M. & Kargari A. (2007), "A Review of methods for synthesis of nanostructured metals with emphasis on iron compounds. Institute of chemistry", *Slovak Academy of Sciences;* 61, 151 - 170.

Titanium Dioxide (TiO_2) Photocatalysis in Concrete http://pavemaintenance.wikispaces.com/TiO2+Photocatalys+-+Shannon (accessed on 27 July 2013)

Walter B., Heukelbach J., Fengler G., Worth C., Hengge U. & Feldmeier H. (2011), "Comparison of Dermoscopy, Skin Scraping, and the Adhesive Tape Test for the Diagnosis of Scabies in a Resource-Poor Setting", Arch Dermatol; 147, 468 – 473.

Wang C., Shao C., Zhang X. & Liu Y. (2009), "SnO_2 nanostructures-TiO_2 nanofibers heterostructures: controlled fabrication and high photocatalytic properties", *Inorganic Chemistry;* 48, 7261 – 7268.

Watthanaarun J., Pavarajarn V. & Supaphol P. (2005), "Titanium (IV) oxide nanofibers by combined sol–gel and electrospinning techniques: preliminary report on effects of preparation conditions and secondary metal dopant", *Science and Technology of Advanced Materials;* 6, 240–245.

Yu H., Irie H. & Hashimoto K. (2010), "Conduction band energy level control of titanium dioxide: toward an efficient visible-light-sensitive photocatalyst", *Jacs communications;* 132, 6898 – 6899.

Zalay O. C., Bardakjian B. L. (2008), "Mapped clock oscillators as ring devices and their application to neuronal electrical rhythms", *Trans Neural Syst Rehabil Eng;* 16, 233 – 244.

REFERENCES

Zhang J., Xu Q., L, M., Feng Z., & Li C. (2009). "UV raman spectroscopic study on TiO_2. II. Effect of nanoparticle size on the outer/Inner phase transformations", *The Journal of Physical Chemistry C;* 113, 1698 – 1704.

Zhang T., Ge L., Wang X. & Gu Z. (2008), "Porous TiO_2 containing multilayer nanofibers with enhanced photocatalytic activity", *Polymer;* 49, 2898 – 2902.

Zhang W., Zhao J., Liu Z., Liu Z. & Fu Z. (2010), "Influence of TiO2 Buffer on Structure and Optical Properties of ZnO Film on Si(100) Substrate", *Materials Transactions*; 51, 1064 – 1066.